

2023-03-09

Flying and Handling Qualities of Small-Scale Supersonic Uncrewed Aerial Vehicles

Durante, Benjamin Joseph

Durante, B. J. (2023). Flying and handling qualities of small-scale supersonic uncrewed aerial vehicles (Master's thesis, University of Calgary, Calgary, Canada). Retrieved from <https://prism.ucalgary.ca>.
<http://hdl.handle.net/1880/115925>

Downloaded from PRISM Repository, University of Calgary

UNIVERSITY OF CALGARY

Flying and Handling Qualities of Small-Scale Supersonic Uncrewed Aerial Vehicles

by

Benjamin Joseph Durante

A THESIS

SUBMITTED TO THE FACULTY OF GRADUATE STUDIES
IN PARTIAL FULFILMENT OF THE REQUIREMENTS FOR THE
DEGREE OF MASTER OF SCIENCE

GRADUATE PROGRAM IN MECHANICAL ENGINEERING

CALGARY, ALBERTA

MARCH, 2023

© Benjamin Joseph Durante 2023

Abstract

The development of large-scale supersonic aircraft has always been challenging as numerous problems exist in control, aerodynamics, handling, propulsion, and structural design. The difficulty of these problems increases when designing small-scale supersonic aircraft, and their successful development has remained elusive. In this thesis the flying and handling qualities of a Small-scale Supersonic Uncrewed Aerial Vehicle (SSUAV) are analyzed with the purpose to facilitate future SSUAV design and experimental testing. For this goal, the flying qualities of an experimental Multipurpose Uncrewed Fixed-wing Advanced Supersonic Aircraft (MUFASA) SSUAV under development at the University of Calgary are assessed. Aerodynamic coefficient data is obtained, and a Newtonian mathematical model is created to facilitate the simulation and evaluation of the MUFASA SSUAV. The flying qualities of the MUFASA SSUAV are evaluated against existing crewed aircraft standards. Specifically the Froude scaling method is used as it provides a way to quantitatively compare small-scale vehicles to existing full-scale vehicle standards. The results obtained show that the handling characteristics of the MUFASA SSUAV are acceptable at transonic cruise conditions, however, the aircraft is laterally unstable. A continuous handling quality evaluation was proposed and implemented across the SSUAV's flight regime providing observations that were unknown in the literature. The results highlight that the mean handling qualities of the targeted SSUAV range from acceptable to controllable in the supersonic flight regime and acceptable in the subsonic regime. Finally, a modified MUFASA SSUAV was compared to other small-scale UAVs as well as full-scale supersonic aircraft where it exhibited much higher roll-rates, leading to the conclusion that SSUAVs pose unique handling quality challenges that need to be addressed.

Preface

Portions of this work have been published in the AIAA Aviation 2022 Forum.

Acknowledgements

I would first like to acknowledge and thank my parents for their support during this degree, and my entire life for that matter. The importance of my family's love cannot be overstated and I am extremely grateful for it. I would also like to extend my appreciation to my friends and girlfriend who continually offered support, encouragement, or an ear, whenever each was required.

This graduate experience would not have been as fulfilling without the great people working in the AERO-CORE lab. Their enthusiasm, determination, and knowledge have been a highlight of my time in graduate school. I look forward to seeing what everyone accomplishes and reminiscing about our time as labmates together.

Finally I would like to thank my supervisors Dr. Alex Ramirez-Serrano and Dr. Craig Johansen for their support and encouragement while completing this research.

Table of Contents

Abstract	ii
Preface	iii
Acknowledgements	iv
Table of Contents	v
List of Figures and Illustrations	vii
List of Tables	ix
List of Symbols, Abbreviations and Nomenclature	xi
1 Introduction	1
1.1 MUFASA Project Background	4
2 Literature Review	7
2.1 Flying Quality Assessment	7
2.1.1 Piloted Flying Quality History	9
2.1.2 UAV Flying Qualities	16
2.2 Small-Scale Uncrewed Aerial Vehicles	19
2.2.1 Small-Scale Supersonic Uncrewed Aerial Vehicle Concepts	19
2.2.2 High-Speed Small-Scale Uncrewed Aerial Vehicles	23
2.3 Summary and Areas of Improvement	24
3 Research Overview	26
3.1 Problem Statement	26
3.2 Proposed Solution Overview	27
3.2.1 Assumptions	31
3.2.2 Constraints	32
4 Flight Dynamics Mathematical Model	34
4.1 Coordinate Systems	34
4.2 Kinematics and Dynamics	38
4.3 Forces and Moments	40

4.3.1	Control Surfaces	40
4.3.2	Aerodynamic Forces and Moments	42
4.3.3	Nondimensional Aerodynamic Coefficients	45
4.3.4	Propulsion Forces and Moments	47
4.3.5	Gravitational Forces	48
4.4	Mathematical Model Summary	49
4.5	Mathematical Model Discretization	51
4.5.1	Model Trimming	51
4.5.2	Model Linearization	52
4.5.3	Flying Quality Parameters	53
5	Flight Dynamics Simulation	56
5.1	Simulation Structure	56
5.1.1	Actuator Dynamics	58
5.1.2	Environmental Modelling	58
5.1.3	Aerodynamic Forces	59
5.1.4	Model Kinematics and Dynamics	60
5.1.5	FlightGear	60
6	Results	62
6.1	Model Verification	62
6.1.1	CFD Case Verification	63
6.1.2	Transient Aircraft Response to Elevon Deflection	64
6.1.3	Flying Quality Parameter Verification	66
6.2	MUFASA SSUAV Physical Overview	67
6.2.1	MUFASA Aerodynamic Overview	68
6.2.2	MUFASA Actuator Overview	70
6.3	Flying Qualities	71
6.4	Flight Regime Flying Qualities	74
6.5	Aerodynamic Stability	81
6.6	Handling Qualities Time Response Comparison	85
7	Conclusions	94
7.1	Recommendations and Future Work	95
7.1.1	UAV Flying Qualities	95
7.1.2	SSUAV Development	96
	Bibliography	99
	A MUFASA A Aerodynamic Coefficients	121
	B Trance Constants	127

List of Figures and Illustrations

1.1	Examples of proposed supersonic transport concepts.	2
1.2	MUFASA A.2 airframe design.	6
2.1	Examples of general static and dynamic responses.	9
2.2	Flying quality standards development since inception in 1954.	10
2.3	Supersonic UAV gliders (not to scale).	20
2.4	Air breathing SSUAV concept drawings (not to scale).	22
2.5	High-speed small-scale UAV concepts and prototypes.	23
3.1	Proposed solution architecture.	29
4.1	NED inertial, vehicle and body frames of reference on the MUFASA UAV. .	35
4.2	Wind, stability and body frames of reference.	37
4.3	MUFASA axes of motion.	38
4.4	MUFASA's control surface sign convention.	41
4.5	MUFASA free body diagram.	42
4.6	MUFASA surface mesh and domain.	47
4.7	Flying quality parameter identification. Poles obtained for MUFASA during flight at a speed of $50 \frac{m}{s}$, and an altitude of 4km.	54
5.1	MUFASA Simulink simulation implementation.	57
5.2	FlightGear visualization of the MUFASA model.	61
6.1	MUFASA UAV coefficient of drag mesh convergence study at Mach 1.05, based on the procedure by Eça and Hoekstra (2014).	63
6.2	MUFASA aerodynamic body frame force and moment changes with respect to time in response to a single elevon deflection.	65
6.3	MUFASA side profile key dimensions.	68
6.4	MUFASA top profile key dimensions.	69
6.5	MUFASA Mach number contour at Mach 1.1 freestream conditions.	70
6.6	Proportionally scaled MUFASA and SR-71.	72
6.7	Scaled MUFASA longitudinal short period flying qualities evaluated against the MIL-STD-1797A standard class III, phase C requirements.	75
6.8	Scaled MUFASA flight regime mean handling quality level with a potential flight trajectory overlaid.	77
6.9	Scaled MUFASA flight regime mean handling qualities with aerodynamic co- efficient evaluation Mach numbers overlaid.	78

6.10	Scaled MUFASA flight regime mean handling qualities with dynamic pressure contour lines overlaid.	79
6.11	Scaled MUFASA-M flight regime mean handling quality level with potential trajectory overlaid.	83
6.12	Scaled MUFASA-M flight regime mean handling qualities with aerodynamic coefficient evaluation Mach numbers overlaid.	84
6.13	Drawings of aircraft modeled in the handling comparison study (not to scale).	86
6.14	MUFASA-M, Trance, and SR-71 inverse time constant modal response comparison.	88
6.15	Aircraft response following a 0.1° aileron deflection at 2s.	89
6.16	Aircraft response following a 0.1° elevator deflection at 2s.	90
6.17	Aircraft attitude acceleration response following a 0.1° deflection at 2s. . . .	90
6.18	Normalized aircraft attitude rate response following a 0.1° deflection at 2s. .	92
A.1	MUFASA lift aerodynamic coefficients.	124
A.2	MUFASA drag aerodynamic coefficients.	124
A.3	MUFASA pitch aerodynamic coefficients.	125
A.4	MUFASA sideforce aerodynamic coefficients.	125
A.5	MUFASA roll aerodynamic coefficients.	126
A.6	MUFASA yaw aerodynamic coefficients.	126

List of Tables

1.1	MUFASA project aircraft iteration scheme, adapted from Durante et al. (2022).	5
2.1	Comparison of conventional and slender aircraft inertias, adapted from Rech and Leyman (1980).	8
2.2	MIL-STD-1797A standard aircraft classification example and general weight requirements (Department of Defense, 2004).	12
2.3	MIL-STD-1797A standard flight phase examples (Department of Defense, 2004).	13
2.4	Summary of the MIL-STD-1797A flying quality requirements for a class III aircraft in phase C flight (Department of Defense, 2004).	14
2.5	Froude scaling factors for scaled models ($n < 1$), adapted from Klyde et al. (2020a).	18
4.1	Aerodynamic analysis software tools used to determine the aerodynamic coefficients of interest.	46
4.2	Far-field mesh size scaling parameters based on the aircraft geometry evaluated.	47
5.1	Simulation parameters.	57
6.1	F-4 aircraft flying quality parameter comparison between Heffley and Jewell (1972), Roskam (2001), and the Discrete model procedure presented in Section 4.5.	67
6.2	MUFASA physical characteristics.	68
6.3	MUFASA actuator characteristics.	72
6.4	MUFASA SSUAV cruise flying and handling qualities when scaled to the size of an SR-71.	73
6.5	Adapted flying quality requirements for a class III aircraft in phase C flight.	76
6.6	MUFASA-M SSUAV cruise flying and handling qualities when scaled to the size of an SR-71.	82
6.7	Cruise conditions of various aircraft.	89
A.1	MUFASA A.2 control surface dependant partial derivative coefficients.	122
A.2	MUFASA A.2 angular rate dependant partial derivative coefficients.	122
A.3	MUFASA A.2 nominal, AOA, and sideslip dependant partial derivative coefficients.	123

B.1	Trance modelled characteristics.	127
B.2	Trance control surface dependant partial derivative coefficients.	128
B.3	Trance angular rate dependant partial derivative coefficients.	128
B.4	Trance nominal partial derivative coefficients.	128
B.5	Trance AOA and sideslip dependant partial derivative coefficients.	128

List of Symbols, Abbreviations and Nomenclature

Abbreviation	Definition
ACC	Aerodynamic Coefficient Centre
AOA	Angle Of Attack
BVLOS	Beyond Visual Line Of Sight
CFD	Computational Fluid Dynamics
CG	Centre of Gravity
DOF	Degrees Of Freedom
EC	Engine Centre
FAA	Federal Aviation Administration
FAI	Fédération Aéronautique Internationale
HQTE	Handling Quality Test Elements
MAC	Mean Aerodynamic Chord
MTE	Mission Task Elements
MUFASA	Multipurpose Uncrewed Fixed-wing Advanced Supersonic Aircraft
MUFASA-M	Modified MUFASA
NED	North-East-Down
NASA	National Aeronautics and Space Administration
NATO	North Atlantic Treaty Organization
SSUAV	Small-scale Supersonic Uncrewed Aerial Vehicle
UAV	Uncrewed Aerial Vehicle

Symbol	Definition
A	State space state matrix
A_{long}	Longitudinal state space state matrix
A_{lat}	Lateral state space state matrix
a	Speed of sound
B	State space input matrix
b	Wingspan
C_D	Drag coefficient
C_F	Skin friction coefficient
C_l	Roll coefficient

C_L	Lift coefficient
C_m	Pitch coefficient
C_n	Yaw coefficient
C_T	Thrust coefficient
C_Y	Lateral coefficient
$c()$	Shorthand for cosine
c_{mean}	Mean aerodynamic chord
F_{aero}	Aerodynamic forces along the body axes
F_D	Force of drag
F_g	Force of gravity
F_L	Force of lift
F_T	Force of engine thrust
F_Y	Force of sideslip
g	Gravitational acceleration
h	Altitude
I_{xx}, I_{yy}, I_{zz}	Aircraft moments of inertia about the body axes x, y, z
I_{xz}	Aircraft product of inertia about the body xz -axis
J	Similarity matrix
k_0	Zero velocity thrust coefficient
k_1	Engine velocity dependence
L	Body length
M	Mach number
M_L	Roll moment
M_M	Pitch moment
M_N	Yaw moment
M_{aero}	Aerodynamic moments about the body axes
M_T	Moment due to engine thrust
m	Mass
n	Scaling factor
P, Q, R	Aircraft angular velocity about the body axes x, y, z
R_b^v	Rotation matrix from the body to vehicle coordinate frame
R_v^b	Rotation matrix from the vehicle to body coordinate frame
R_w^b	Rotation matrix from the wind to body coordinate frame
$R_x(\phi), R_y(\theta), R_z(\psi)$	Intermediary rotation matrices from the vehicle to body frame
$R_s^b(\alpha), R_w^s(\beta)$	Intermediary rotation matrices from the wind to body frame
Re	Reynolds number
r_{ACC}	Aerodynamic coefficient centre position
r_{CG}	Centre of gravity position
r_{EC}	Engine position
S	Wing planform area
S_{wet}	Wetted planform area
s	Laplace symbol
$s()$	Shorthand for sine
T	Time Constant
T_{ph_2}	Phugoid mode time-to-double pitch angle

T_{s_2}	Spiral mode time-to-double bank angle
t	Temperature
U, V, W	Aircraft translational velocity along the body axes x, y, z
\bar{u}	Control input vector
V_a	Airspeed
V_{in}	Inertial speed
V_w	Wind speed
x, y, z	Cartesian coordinate axes
\bar{x}	State vector

Greek Symbol

Definition

α	Angle of attack
β	Angle of sideslip
γ	Climb angle
δ_a	Aileron deflection angle
δ_e	Elevator deflection angle
δ_{pte}	Port elevon deflection angle
δ_{ptvs}	Port vertical stabilator deflection angle
δ_{sbe}	Starboard elevon deflection angle
δ_{sbvs}	Starboard vertical stabilator deflection angle
δ_r	Rudder deflection angle
δ_T	Throttle position setting between 0 and 1
ζ	Damping ratio
θ	Pitch angle
$\Lambda_N, \Lambda_E, \Lambda_D$	Position North, East, and down in the global coordinate frame
ρ	Air density
σ	Ratio of air density between flight condition and sea level
τ_p	Phase delay
$\Phi_{2\omega_{180^\circ}}$	Phase angle at twice the frequency at -180° phase angle
ϕ	Roll angle
ψ	Yaw angle
ω	Natural frequency
ω_{180°	Frequency at -180° phase angle
$\frac{n}{\alpha}$	Load factor sensitivity
$\frac{1}{T_{\theta_2}}$	Largest stable zero in the pitch-elevator transfer function

Subscript

Definition

0	Nominal coefficient
b	Body coordinate frame
dr	Dutch-Roll mode
d	Desired value

i	Inertial coordinate frame
P	Coefficient as a function of vehicle roll rate
ph	Phugoid mode
Q	Coefficient as a function of vehicle pitch rate
R	Coefficient as a function of vehicle yaw rate
r	Roll mode
s	Stability coordinate frame
sp	Spiral mode
v	Vehicle coordinate frame
w	Wind coordinate frame

Greek Subscript

Definition

α	Coefficient as a function of angle of attack
α^2	Coefficient as a function of the square of angle of attack
β	Coefficient as a function of angle of sideslip
δ_a	Coefficient as a function of aileron deflection angle
δ_e	Coefficient as a function of elevator deflection angle
δ_e^2	Coefficient as a function of the square of elevator deflection angle
δ_r	Coefficient as a function of rudder deflection angle

Superscript

Definition

$\bar{\square}$	Variable vector
$\dot{\square}$	Variable derivative with respect to time
$\hat{\square}$	Normalized variable

Chapter 1

Introduction

Small-scale Supersonic Uncrewed Aerial Vehicles (SSUAVs) have the potential to revolutionize high-speed research and civil transportation. Since the retirement of the Concorde in 2003, there have been no vehicles capable of facilitating supersonic civil transportation (Candel, 2004; Luckring et al., 2017). However, due to a desire for faster aerial transatlantic transportation there has been renewed interest in supersonic civil transportation (Sun and Smith, 2017). Supersonic business jets are expected to pioneer the next era in supersonic civil transportation (Sun and Smith, 2017). To facilitate this market trend, a handful of companies and diverse academic research teams are developing new prototype vehicles to explore supersonic technology with examples presented in Fig. 1.1 (National Aeronautics and Space Administration, 2022; Sheetz, 2020; Sun and Smith, 2020). However, multiple technological hurdles exist for commercial supersonic aviation to be realized including boom minimization, propulsion, environmental sustainability, and economic sustainability (Candel, 2004; Sun and Smith, 2017). In addition, the cost of developing supersonic prototypes, let alone final vehicles, is large and exposes companies to the risk of financial failure (Reed, 2021; Sheetz, 2021). Typical commercial aircraft carry a production cost of \$1500 per pound, irrespective of development costs (Department of Defense, 2002).

A potential solution to high development costs may be found in small-scale Uncrewed



(a) Aerion AS2, adapted from Aerion Supersonic (2021).



(b) BOOM Overture, adapted from Boom Technology (2022).



(c) Spike S-512, adapted from Spike Aerospace (2022).



(d) Lockheed Martin supersonic concept, adapted from Lockheed Martin (2016).



(e) Virgin Galactic's Supersonic Concept, adapted from Virgin Galactic (2020).



(f) Exosonic supersonic concept, adapted from Exosonic (2022).

Figure 1.1: Examples of proposed supersonic transport concepts.

Aerial Vehicles (UAVs) as they can benefit commercial supersonic transportation development due to their lower cost, rapid development cycles, and shorter times from concept to testing (Cai et al., 2014; Hassanalian and Abdelkefi, 2017; Stöcker et al., 2017). While previously only used to mimic large-scale aircraft, small-scale UAVs are now increasingly used as low-cost technology testing platforms (Sobron et al., 2021). SSUAVs are suitable vehicles to be used as standalone, low-cost experimental platforms for high-speed research into aerodynamics, novel intake systems, as well as numerous other components that are critical aspects in supersonic flight (Eckstrom and Peele, 1975). In addition to being potential high-speed test-beds, SSUAVs have also been considered as potential platforms for diverse tasks including rapid reconnaissance in security and disaster situations (Department of Defense, 2002; Hildmann and Kovacs, 2019; Shakhathreh et al., 2019). Unfortunately there are no known successful test flights of an air-breathing SSUAV in the open literature (Dalman et al., 2021; McCrink and Gregory, 2021; Walter and Starkey, 2012).

The Multipurpose Uncrewed Fixed-wing Advanced Supersonic Aircraft (MUFASA) project at the University of Calgary is a joint effort between the University of Calgary and Atlantis

Research Labs Inc. to develop a fixed-wing SSUAV. One of the project’s goals is to utilize the SSUAV to perform high-speed testing of advanced propulsion and intake technologies. Based on the project’s description (Durante et al., 2022), the MUFASA SSUAV has the potential to be an inexpensive alternative to traditional high-speed aircraft research methods. However, due to their novelty within the open literature, there are many open questions about SSUAVs related to aerodynamic simulation validity (Stoldt et al., 2021), optimal sizing (Dalman et al., 2021), and controllability (Burnashev and Zbrutsky, 2019; Wienke, 2011). The work presented in this thesis document is in support of the MUFASA supersonic aircraft development, specifically to enable effective flight of such aircraft (which has not yet been achieved).

In order to ensure successful flight of MUFASA, the vehicle must be analyzed in simulated environments and its flying qualities determined. Aircraft flying qualities are defined as the measurement of a vehicle’s dynamic response to a control command (Klyde et al., 2018). Research on the flying qualities of typical crewed aircraft exists to ensure the application of new technology enhances the operation of the aircraft to accomplish a desired mission (Greene et al., 2014). Understanding a vehicle’s flying and handling quality behaviour is imperative prior to control system implementation (Stevens et al., 2015). Crewed aircraft have a well defined standard, MIL-STD-1797 (Department of Defense, 2004), that is followed throughout their control system development (Harris and Stanford, 2018; Kim et al., 2020; Loschke, 2003). UAVs have historically had mishaps, defined as events causing damage or injury (Department of Defense, 2011), at one to two orders of magnitude the rate of crewed military aircraft per 100,000 hours (Department of Defense, 2009). One potential reason for the high UAV mishap rate is a lack of dedicated standards to evaluate UAV flying qualities prior to experimental testing, let alone SSUAV flying qualities. As the development of a standard for UAV flying qualities is ongoing (Klyde et al., 2020a), the work described in this thesis document investigates whether SSUAV’s pose unique flying quality challenges that differ in response from previously noted crewed or uncrewed vehicles. In an attempt to reach

such a goal the three main objectives of the present work are:

1. Perform a full system description of the MUFASA SSUAV by obtaining its complete aerodynamic behaviour.
2. Evaluate the MUFASA SSUAV flying qualities against current crewed aircraft standards.
3. Compare the MUFASA SSUAV handling qualities against small-scale UAVs and full-scale supersonic aircraft.

This thesis first provides a detailed background of crewed flying quality standards, the current state of UAV flying qualities research, and an overview of existing SSUAV projects in Chapter 2. An overview of the research problem and solution approach are presented in Chapter 3. To facilitate analysis of the MUFASA SSUAV, Chapter 4 details the mathematical model formulated, while Chapter 5 describes the structure of the simulation framework implemented. The flying and handling qualities of the MUFASA SSUAV are evaluated in Chapter 6. A novel flying quality evaluation method and response comparison method are proposed and evaluated. SSUAV results are then compared to other full-scale supersonic aircraft and small-scale UAVs. A summary of the findings generated as part of this work and suggested future areas of research for SSUAV development is provided in Chapter 7.

1.1 MUFASA Project Background

Due to the complexities associated with the development of SSUAVs, multiple MUFASA iterations are under concurrent development to address different challenges. Current MUFASA iterations are presented in Table 1.1.

The letter designation (A or B) of each MUFASA iteration (see Table 1.1) indicates the aerodynamic profile of the UAV. For example, “MUFASA A” is the aerodynamic shape seen in Fig. 1.2. “MUFASA A” is the initial aerodynamic shape evaluated by Dalman

Table 1.1: MUFASA project aircraft iteration scheme, adapted from Durante et al. (2022).

Version	Description
MUFASA A	Aerodynamic shape evaluated for scaling and feasibility
MUFASA A.1	0.62-scale low-speed demonstrator, 2.5kg maximum
MUFASA A.2	1.0-scale, aluminum airframe, 25kg maximum
MUFASA A.3	1.6-scale (approx.), composite airframe (future work)
MUFASA B	Aerodynamic shape optimized for performance (future work)
MUFASA B.1	1.0-scale, carbon fibre airframe (future work)

et al. (2021) in SUAVE, a software tool developed by MacDonald et al. (2017) to analyze unconventional aircraft configurations. MUFASA B is a new aerodynamic concept profile optimized for minimal drag. Each numeric sub-designation in Table 1.1 refers to a different scale or construction method of the aerodynamic profile indicated by the letter designation. The MUFASA version used in this work is “MUFASA A.2” which was first evaluated by Dalman et al. (2021), and is illustrated in Fig. 1.2.

MUFASA A.2, herein referred to as just MUFASA, is a 2.087m long delta-wing UAV with a pitot-intake and a wingspan of 1.070m. The aircraft uses an aluminum spar construction technique, is designed to weigh less than 25kg, and predicted to have a cruise range of 5km (Dalman, 2021). MUFASA has four independently operated control surfaces consisting of a pair of elevons and vertical stabilators (Fig. 1.2). The aircraft is symmetric about its longitudinal plane, with one control surface type on each side. The wing trailing edge elevons provide roll and pitch control. Forward of the trailing edge and inboard of the elevons are the vertical stabilators to provide yaw control.

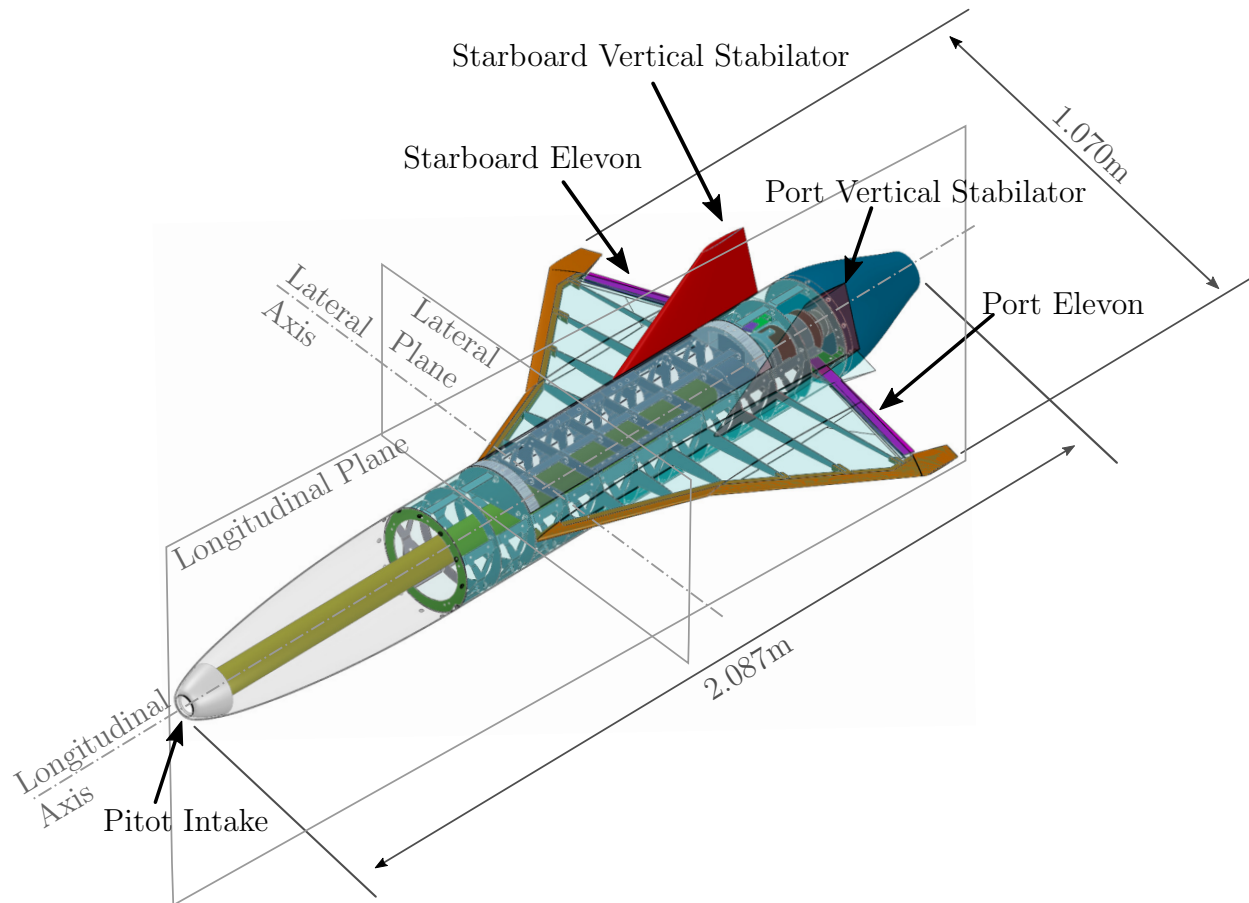


Figure 1.2: MUFASA A.2 airframe design.

Chapter 2

Literature Review

In this chapter a brief overview of the subjects relevant to this present work is provided. A history of crewed flying quality standards is presented along with the current state of UAV flying quality assessment methods. The current state of SSUAV projects and research, as well as high-speed UAVs are also presented.

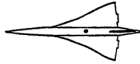
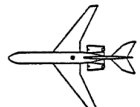

2.1 Flying Quality Assessment

A significant challenge facing autonomous supersonic aircraft development is formulating a control system that is applicable throughout the flight regime including takeoff, climb, subsonic / transonic / supersonic cruise, descent, and landing. One of the challenges is that in each flight regime, the operating (e.g. aerodynamic) conditions vary, causing a constant control command to illicit a different response. Furthermore, the aerodynamic conditions experienced by an SSUAV within diverse flight regimes are not fully known and neither are their effects on the aircraft (Nelson et al., 2022). Within the available literature, each SSUAV research team has implemented different control systems (Burnashev and Zbrutsky, 2019; Langston et al., 2016; Wienke, 2011), however, none have explicitly explored the unique challenges associated with enabling a small-scale UAV to achieve supersonic flight.

Full-scale supersonic aircraft pose unique control and handling challenges due to their

varying aerodynamic behaviour with speed, and their inertial properties (Candel, 2004; Collard, 1991; McMaster and Schenkt, 1974; Morgan, 1972; Steer and Cook, 1999; Vicroy et al., 2018). Lateral control, defined as rotation about the longitudinal axis of the aircraft (seen in Fig. 1.2), has proven complex in full-scale supersonic aircraft due to low roll inertia. When compared to the pitch and yaw inertia, low roll inertia is a common trait of typical slender supersonic delta-wing designs as employed by the aircraft presented in Fig. 1.1 (Candel, 2004; Collard, 1991; Rech and Leyman, 1980; Steer and Cook, 1999). A low roll inertia ratio compared to pitch and yaw is not present in other aircraft such as subsonic conventional wing or swept-wing aircraft. A comparison of conventional subsonic and supersonic aircraft roll, pitch, and yaw inertia ratios are presented in Table 2.1.

Table 2.1: Comparison of conventional and slender aircraft inertias, adapted from Rech and Leyman (1980).

Aircraft Type	Inertia Ratios			Aircraft Shape
	Roll	Pitch	Yaw	
Supersonic delta-wing	1	7	8	
Subsonic swept-wing	1	3-5	4-5	
Subsonic conventional wing	1	1	2	

When comparing roll and pitch inertia ratios for delta-wing aircraft (Table 2.1) it is observed that the roll inertia is roughly seven times smaller than the pitch inertia. The ratio between roll and pitch inertia for subsonic and conventional aircraft is closer to one. A large difference in inertia ratio indicates an aircraft is much more sensitive to motion in one axis than another, complicating control and reducing handling qualities (Candel, 2004; Collard, 1991; Rech and Leyman, 1980; Steer and Cook, 1999). Small-scale UAVs also pose unique control and handling quality challenges due to their low overall inertia (Foster and Bowman,

2005). Previous work has indicated low inertia leads to sensitivity and handling quality degradation, particularly in the lateral plane (Mohamed et al., 2014; Panta et al., 2018). The flying qualities of a small-scale UAV travelling at supersonic speeds with a delta-wing profile (Table 2.1) are still not documented and remain an open research question.

2.1.1 Piloted Flying Quality History

An implemented control law can only be deemed satisfactory if a set of design requirements or performance criteria is available (Stevens et al., 2015). The most basic performance criteria involves evaluating an aircraft’s static and dynamic stability as positive, neutral, or negative. Static stability is the tendency of an aircraft to return to its original equilibrium state following a disturbance (Cook, 2012). Static stability is determined by evaluating an aircraft’s nondimensional aerodynamic coefficients. Dynamic stability describes the transient response of an aircraft following a disturbance (Cook, 2012). Illustrations of static and dynamic responses are presented in Fig. 2.1.

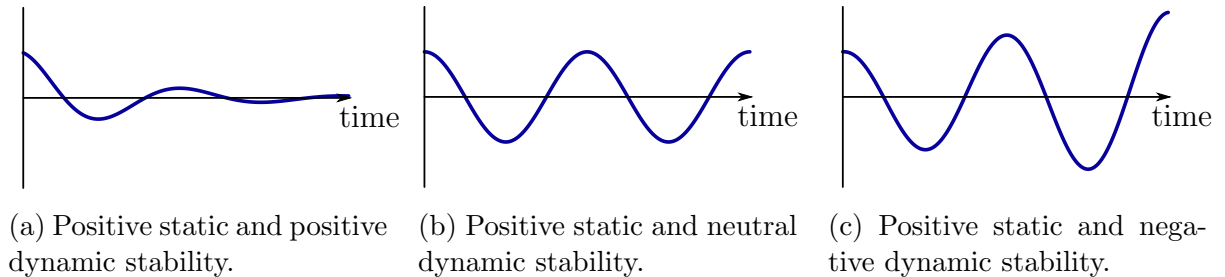


Figure 2.1: Examples of general static and dynamic responses.

Beyond assessing an aircraft’s qualitative static and dynamic stability, quantitative flying quality design specifications for typical large-scale fixed-wing aircraft have been developed which are “intended to assure flying qualities that provide adequate mission performance and flight safety regardless of design implementation or flight control system mechanization,” (p. 1) based on the MIL-STD-1797A standard developed by the United States Department of Defense (1980). The specifications evaluating a fixed-wing aircraft’s flying and handling qualities have existed since the initial release of MIL-F-8785 in the 1950s (refer to Fig. 2.2).

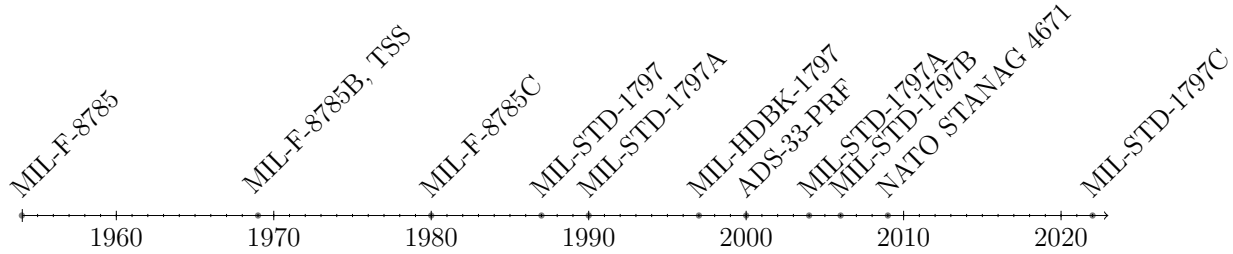


Figure 2.2: Flying quality standards development since inception in 1954.

Within the available literature the terms “*flying*” and “*handling*” qualities have different yet similar definitions. Flying qualities include analytical and empirical parameters that are measured from the open-loop aircraft system. The open-loop aircraft system is absent of computer or pilot control inputs, allowing for the vehicle’s inherent dynamic response to be evaluated. Handling qualities on the other hand describe how easily and precisely a pilot can perform a desired task. Taken together, “flying qualities criteria are measures by which one attempts to quantify the handling qualities of an airplane,” (Klyde et al., 2018, p. 3). Explicit flying quality specifications were initially detailed by military standard MIL-F-8785, created by the United States Military Department of Defense in 1954. MIL-F-8785 was subsequently updated to MIL-F-8785B and MIL-F-8785C which included pilot flight path control requirements (Weissman, 1966) and equivalent airplane definitions (Mitchell et al., 2004), respectively. While MIL-F-8785 attempted to cover all piloted aircraft, no specific considerations were detailed for supersonic aircraft. Therefore, when the supersonic Concorde aircraft was developed, to facilitate its certification, the Air Registration Board of England and the Secr tariat G n ral a l’Aviation Civile of France developed the Technical Supersonic Standard (TSS) (Air Registration Board and Secr tariat G n ral a l’Aviation Civile, 1969). The TSS requirements are based on evaluating the probability of a specific flight condition or mechanical failure occurring. A comparison by Wanner and Carlson (1972) between the TSS and military standard MIL-F-8785B indicated that the TSS and MIL-F-8785B were equivalent in intent and goals, with MIL-F-8785B being more stringent and broadly applicable. While the TSS is sufficient for commercial certification procedures, the

TSS relies on statistical analysis and is overly complicated when compared to MIL-F-8785B (Snyder, 1976). Piloted flying quality standards continued to be developed (Fig. 2.2) with the MIL-STD-1797 standard superseding the MIL-F-8785C standard. Due to the perceived unquantifiableness of flying qualities in the late 1990s, the first standard revision (MIL-STD-1797A) briefly became a handbook (MIL-HDBK-1797) to be used for guidance only and not as a specification document (Department of Defense, 1997, 2004). In ambivalence to the new designation, industry, academia, and the Department of Defense itself still relied and used MIL-HDBK-1797 as a standard, causing it to be reinstated as MIL-STD-1797A seven years after it was demoted to a handbook (Department of Defense, 1997, 2004). The MIL-STD-1797 standard has continued to be updated with the latest published revision being the MIL-STD-1797B standard in 2006, which is a limited-distribution document only accessible by the United States Department of Defense (Klyde et al., 2020a). Also not designated for public release is the proposed MIL-STD-1797C standard which is a new document revision set to include additional high-speed flying quality criteria (Mitchell et al., 2020).

Flying and handling quality standards have not been updated very frequently since the year 2000 (Mitchell et al., 2020). Despite numerous updates to the standards described above, multiple standardization issues with flying and handling quality evaluations still exist. One major deficiency of current flying quality specifications is that passing (meeting) all criteria does not necessarily indicate that the aircraft has good handling characteristics (Mitchell et al., 1994). This deficiency is the reason why qualitative pilot feedback is still the backbone of the Federal Aviation Administration (FAA) aircraft certification process (Klyde et al., 2018). Another deficiency of current flying quality specifications is their reliance on subjective decisions and qualitative feedback. Certain aspects of the MIL-STD-1797A standard such as aircraft classification are intentionally subjective to allow applicability to a very wide range of fixed-wing aircraft. Aircraft handling qualities are evaluated qualitatively by pilots and quantitatively rated using the Cooper-Harper Handling Qualities Rating scale (Cooper and Harper, 1969; Harper and Cooper, 1986). The Cooper-Harper rating allows for

a pass/fail aircraft criteria based on the quantification of a pilot’s opinion.

As it is still not possible to precisely specify design criteria for control systems intended to modify aircraft dynamics (Stevens et al., 2015), multiple flying quality evaluation methods are applied in practice. Vehicle flying qualities are quantitatively evaluated by analyzing one or all of the following qualities: an aircraft’s modal response, bandwidth frequency, time delay, control anticipation parameter, or mission task element performance based on the flight testing requirements. The MIL-STD-1797A standard classifies aircraft into one of four categories (Department of Defense, 2004):

- I. Small, light aircraft,
- II. Medium weight, low-to-medium manoeuvrability aircraft,
- III. Large, heavy, low-to-medium manoeuvrability aircraft, and
- IV. High-manoevrability aircraft.

The aircraft classification requirements are intentionally left vague by the military standard to allow for the broadest level of applicability, however, this leaves them very subjective (Meyer and Husband, 1990). Example aircraft that would fit into each classification as detailed by the military standard are presented in Table 2.2. The MIL-STD-1797A standard indicates that aircraft should be classified using a combination of intended aircraft use and weight (Department of Defense, 2004).

Table 2.2: MIL-STD-1797A standard aircraft classification example and general weight requirements (Department of Defense, 2004).

Class	Example Aircraft Types	Example Aircraft	Weight (lbs)
I	Light utility, primary trainer	Cessna 172	1000-13000
II	Light transport, tactical bomber	U-2s	6500-130000
III	Heavy transport, heavy bomber, patrol	SR-71	65000+
IV	Fighter-interceptor	F-35	1000+

Each aircraft is then evaluated in one of three flight phases (Department of Defense, 2004):

- A. Nonterminal flight requiring rapid manoeuvring and precise flight-path control,
- B. Nonterminal flight requiring gradual manoeuvring without precise flight-path control,
and
- C. Terminal flight requiring gradual manoeuvring and accurate flight-path control.

The aircraft flight phase classification are also intentionally left vague for the broadest level of applicability, however, example scenarios for each flight phase are presented in Table 2.3.

Table 2.3: MIL-STD-1797A standard flight phase examples (Department of Defense, 2004).

Phase	Flight Scenario Example
A	Combat, reconnaissance, close formation flying, in-flight refueling
B	Climb, cruise, loiter, descent
C	Takeoff, approach, landing

Using the above classification and flight phases, each aircraft’s handling quality level is rated between one and three where each level implies the following (Department of Defense, 2004):

- Level 1: Satisfactory - Flying qualities clearly adequate for the mission Flight Phase. Desired performance is achievable with no more than minimal pilot compensation.
- Level 2: Acceptable - Flying qualities adequate to accomplish the mission Flight Phase, but some increase in pilot workload or degradation in mission effectiveness, or both, exists.
- Level 3: Controllable - Flying qualities such that the aircraft can be controlled in the context of the mission Flight Phase, even though pilot workload is excessive or mission effectiveness is inadequate, or both.

The aircraft’s flying qualities (i.e., damping, natural frequency, and time constant) are numerically evaluated to determine its handling quality level. The longitudinal response is characterized by two modes: short period, and long period (also known as phugoid). Three

modes categorize the lateral response: roll subsidence, Dutch-Roll, and spiral divergence. The damping ratio (ζ), natural frequency (ω), and time constant (T) associated with each aerodynamic modal response are determined and compared to multiple inequalities set by the military standards to determine the flying qualities level of each mode (Department of Defense, 2004). The time constant is computed from the damping ratio and natural frequency using Eq. 2.1 (Saeed, 2008).

$$T = \frac{1}{\zeta\omega} \quad (2.1)$$

An example of the military specification handling level breakdown is shown in Table 2.4, which relates the aircraft modal responses to handling level for a class III, phase C aircraft, such as a high-speed North American XB-70 “Valkyrie” (Berry and Powers, 1970) or Lockheed SR-71 “Blackbird” (Cox and Jackson, 1997). Subscript sp, ph, dr, and r represent short period, phugoid, Dutch-Roll, and roll subsidence modes, respectively. Subscript ph₂ and s₂ represent the time for the aircraft phugoid and spiral mode to double in amplitude, respectively. The phugoid mode time-to-double is determined via Eq. 2.2 (Stevens et al., 2015), with the spiral mode time-to-double following an equivalent procedure.

Table 2.4: Summary of the MIL-STD-1797A flying quality requirements for a class III aircraft in phase C flight (Department of Defense, 2004).

Mode	Handling		
	Level 1	Level 2	Level 3
Short Period	$0.35 \leq \zeta_{sp} \leq 1.3$	$0.25 \leq \zeta_{sp} \leq 2.0$	$\zeta_{sp} \geq 0.15$
Phugoid	$\zeta_{ph} \geq 0.04$	$\zeta_{ph} \geq 0$	$T_{ph_2} \geq 55 \text{ s}$
	$\zeta_{dr} \geq 0.08$	$\zeta_{dr} \geq 0.02$	$\zeta_{dr} \geq 0$
Dutch-Roll	$\zeta_{dr}\omega_{dr} \geq 0.10 \frac{\text{rad}}{\text{s}}$	$\zeta_{dr}\omega_{dr} \geq 0.05 \frac{\text{rad}}{\text{s}}$	—
	$\omega_{dr} \geq 0.4 \frac{\text{rad}}{\text{s}}$	$\omega_{dr} \geq 0.4 \frac{\text{rad}}{\text{s}}$	$\omega_{dr} \geq 0.4 \frac{\text{rad}}{\text{s}}$
Roll Subsidence	$T_r \leq 1.4 \text{ s}$	$T_r \leq 3.0 \text{ s}$	$T_r \leq 10.0 \text{ s}$
Spiral	$T_{s_2} \geq 12.0 \text{ s}$	$T_{s_2} \geq 8 \text{ s}$	$T_{s_2} \geq 4 \text{ s}$

$$T_{\text{ph}_2} = \frac{\ln(2)}{|\zeta_{\text{ph}}|\omega_{\text{ph}}} \quad (2.2)$$

While these inequalities are framed as hard rules, exceptions and caveats do exist. As an example, with regards to roll subsidence and Dutch-Roll, any damping ratio less than 0.3 is considered too easily excitable, and if precise attitude control is required damping should be no less than 0.7 at a minimum (Klyde et al., 2020a).

Bandwidth and phase delay analysis are another method currently used to quantify aircraft flying qualities. The bandwidth frequency denotes the highest frequency a pilot can still double the input gain without inducing instability, while phase delay denotes how quickly instability occurs at frequencies above the bandwidth frequency. Restated quantitatively, bandwidth is the frequency at which the aircraft's phase margin is 45° or gain margin 6dB, whichever is lower (Department of Defense, 2004). Phase delay represents how fast attitude/control inputs degrade at high frequencies as represented by Eq. 2.3 (Department of Defense, 2004), where τ_p , ω_{180° , and $\Phi_{2\omega_{180^\circ}}$ represent the phase delay, frequency at -180° phase angle, and phase angle at twice the frequency at -180° phase angle, respectively. Bandwidth analysis requires continuous closed-loop control of the aircraft to facilitate flying quality evaluation (Klyde et al., 2018).

$$\tau_p = \frac{-(\Phi_{2\omega_{180^\circ}} + 180^\circ)}{\left(\frac{180^\circ}{\pi}\right)(2\omega_{180^\circ})} \quad (2.3)$$

Bandwidth analysis is also used to evaluate other aspects of flying qualities such as pilot-induced oscillations (Mandal and Gu, 2016).

To complement the MIL-STD-1797 standard, other methods do exist. Mission Task Element (MTE) analysis is the procedure of evaluating an aircraft's ability to perform set tasks deemed essential for its mission. Currently, this flying quality evaluation metric has only been standardized for rotorcraft under standard ADS-33-PRF (presented in Fig. 2.2) (Department of Defense, 2000). Klyde et al. (2020b) proposed integrating MTEs into current

fixed-wing flying quality evaluations, among other things to evaluate new fly-by-wire systems, and renaming them Handling Quality Test Elements (HQTEs). The purpose of HQTEs is similar to MTEs, having the goal to classify the test(s) an aircraft must perform and then compare the obtained results to the proper bandwidth requirements (Klyde et al., 2020b).

It must be noted that only the most commonly cited methods for evaluating fixed-wing aircraft flying qualities are presented here. Standards not scoped for fixed-wing aircraft flying qualities, or proposed methods with no follow-up publications have been omitted for brevity. The most promising proposed closed-loop flying quality analysis methods involve combining MTEs and bandwidth analysis (Klyde et al., 2018). Recent flying quality procedures explore how MTEs could be applied to FAA fixed-wing certification to provide greater granularity to how good/bad an aircraft flies (Klyde et al., 2020b). While MTEs and bandwidth analysis show potential to be the definitive flying quality analysis metrics, further research is required. It should be kept in mind that while achieving adequate flying quality performance does entail minimal pilot control effort, it does not necessarily equate to adequate aircraft handling for FAA certification (Klyde et al., 2020b).

2.1.2 UAV Flying Qualities

Despite the available standards and procedures for crewed aircraft, no flying quality standards are available for fixed-wing UAV systems (Cotting, 2010b; Mitchell et al., 2004). The lack of flying quality criteria for UAVs is one of the most critical issues limiting UAV development (Cotting, 2010b; Mitchell et al., 2004), as current crewed flying quality standards have limited relevance to UAVs (Cotting, 2010a). Early research on remote piloted vehicles explored the application of MIL-F-8785B, however, it was determined that additional flying quality data from a range of remote piloted vehicles was required to evaluate applicability and no resolution was obtained (Prosser and Wiler, 1976). Of all the fixed-wing flying quality standards available for crewed aircraft since 1954 (Fig. 2.2) only the North Atlantic Treaty Organization (NATO) STANAG 4671 is specifically scoped to include UAVs (North Atlantic

Treaty Organization, 2019). NATO STANAG 4671 is designed to evaluate UAV airworthiness to allow the operation of UAVs across NATO member states. However, the NATO STANAG 4671 has a slightly different scope such as placing emphasis on the communication protocols between the UAV and its ground control station, and does not provide quantitative flying quality criteria. As noted by Klyde et al. (2018), “because of the wide variety of UAV types (e.g. fixed-wing, rotary-wing variants, ducted-fans, airships, etc.) and vehicle size from micro vehicles to large units such as the Global Hawk with a wingspan similar to a Boeing 737, there cannot be a one-size-fits-all set of flying quality requirements” (P. 10). UAV classification to facilitate flying quality evaluation is ongoing with preliminary work by Cotting (2009) suggesting UAVs may be classifiable based on Reynold’s number and weight, however, a more comprehensive review is required. The biggest challenge impeding the development of a rigorous UAV handling quality standard is the lack of a database combining mission data, test data, flight lessons learned and pilot/controller experiences (Greene et al., 2014; Holmberg et al., 2008). Following a review of crewed aircraft standards, it is evident that a UAV specific standard is required for UAV handling, likely based upon the methodology of Mission Oriented Requirements (Cotting, 2010a; Holmberg et al., 2008; Mitchell et al., 1994). As a result, multiple methods have been proposed to quantify UAV flying qualities, however, widespread adoption of a rigorous UAV flying qualities standard has not been yet realized (Cotting, 2010b; Klyde et al., 2020a).

Current UAVs are evaluated against the MIL-F-8785C or MIL-STD-1797A standard documents (Holmberg et al., 2008). Previous work has indicated the importance of modal response characteristics, specifically natural frequency and damping ratio, in predicting an aircraft’s handling and controllability characteristics (Stevens et al., 2015). A lower damping ratio has been found to lead to poor gust rejection in UAVs (Bertolin et al., 2022). High frequencies combined with minimal damping can make control impossible (Stevens et al., 2015), hence there is a need to understand UAV behaviour prior to controller development. One limitation of the available military handling quality standards is that they were created

before the prevalence of UAVs, and as a result only designed to evaluate crewed aircraft. Crewed aircraft are in general larger and heavier than typical UAVs (Hassanalian and Abdelkefi, 2017), and thus behave differently than UAVs (Bogos and Stroe, 2012; Mohamed et al., 2014). While much discussion exists, there are currently no equivalent recognized standards for quantifying UAV handling qualities (Capello et al., 2012; Cotting, 2010b; Foster and Bowman, 2005; Klyde et al., 2020a; Williams, 2003). In the absence of a recognized standard for UAV handling qualities, Froude scaling is often used to scale-up UAV parameters for evaluation using crewed aircraft standards (Burk and Wilson, 1975; Foster and Bowman, 2005; Klyde et al., 2020a). Froude scaling is a method to scale aircraft parameters in a way that maintains the ratio between inertial-to-gravitational and aerodynamic-to-gravitational forces (Mettler et al., 1999; Wolowicz and Bowman, 1979). As a result, Froude scaling typically involves changing specific aircraft parameters by previously determined ratios based on a scaling factor n (Burk and Wilson, 1975). Certain Froude scaled parameters (e.g., mass and moment of inertia) are also scaled using the ratio between air density at the large scale flight condition and sea level, σ (Burk and Wilson, 1975). A list of Froude scaling relationships typically used are shown in Table 2.5.

Table 2.5: Froude scaling factors for scaled models ($n < 1$), adapted from Klyde et al. (2020a).

Property	Scaling Factor
Length	n
Area	n^2
Mass	n^3/σ
Moment of Inertia	n^5/σ
Linear Velocity	$n^{1/2}$
Time	$n^{1/2}$

Previous work by Klyde et al. (2020a), has indicated that Froude scaling is currently the best way to facilitate the evaluation of a UAV’s handling characteristics using MIL-STD-1797A prior to flight testing.

2.2 Small-Scale Uncrewed Aerial Vehicles

As there exist multiple definitions for what constitutes a UAV (Cai et al., 2014; Franke, 2014, 2018; Gupta et al., 2013; Hassanalian and Abdelkefi, 2017) the following definition will be used in this thesis:

An airborne vehicle which does not carry a human operator, which may be piloted remotely, follow a pre-programmed flight path, fly autonomously, or a combination of all three. It is designed to be recoverable and carries a lethal or non-lethal payload. Nonrecoverable vehicles and projectiles such as ballistic vehicles, cruise missiles, and artillery projectiles are not considered UAVs. (Franke, 2014, p. 54)

Furthermore, even though UAVs have existed since at least 1917 (Mills, 2019) in the form of a simple remote controlled vehicle, UAV classification is still an open research issue (Stansbury et al., 2015). Multiple classifications exist categorizing UAVs by size, weight, or energy, leaving the definition of a small-scale UAV open to interpretation (Gupta et al., 2013; Hassanalian and Abdelkefi, 2017; North Atlantic Treaty Organization, 2016). Thus, to resolve such aspects there is a tendency to use the United States Department of Defense (2002) definitions and classify a small-scale UAV as weighing less than 100kg and having a wingspan no greater than three metres. To not conflate the design philosophies of small and micro UAVs, vehicles with a maximum energy of less than 66J are classified as micro-scale UAVs (North Atlantic Treaty Organization, 2016). Presented in the following sections is a summary on the current state of the art of SSUAVs and high-speed small-scale UAVs.

2.2.1 Small-Scale Supersonic Uncrewed Aerial Vehicle Concepts

In the open literature, a handful of developmental research programs have investigated the feasibility and implementation of an air-breathing SSUAV demonstrator. The National Experimental Supersonic Transport (NEXST) program run by the Japanese Aerospace Exploration Agency from 1997 until 2006 used rocket-launched supersonic gliders to investigate

technology for supersonic aircraft (Iwamiya, 2002; Machida et al., 2007; Yoshida et al., 2002). Due to numerous challenges, diverse concept aircraft (e.g. NEXST-2) were never flown and eventually the research focus shifted to sonic boom minimization (Yoshida, 2009). The Drop test for Simplified Evaluation of Non-symmetrically Distributed sonic boom (D-SEND) program carried on the new research focus with balloon launched gliders from 2010 until 2015. The new focus culminated in the D-SEND#2 UAV which achieved speeds greater than Mach 2 (Kawaguchi et al., 2017). Both NEXST and D-SEND programs were deemed successful as they obtained experimental supersonic flight results (Kawaguchi et al., 2017; Murakami et al., 2008). Images of the flight tested supersonic gliders are shown in Fig. 2.3. Both the NEXST and D-SEND experimental vehicles were unpowered gliders, thus limiting flight time.



(a) NEXST-1, adapted from Yoshida et al. (2002).



(b) D-SEND#2, adapted from the Japan Aerospace Exploration Agency (2012).

Figure 2.3: Supersonic UAV gliders (not to scale).

Limited supersonic flight time is a shortcoming that the Muroran Institute of Technology aimed to address with their Ohwashi program, a self-powered air-breathing UAV designed for supersonic flight testing of high-speed technologies (Mizobata et al., 2005) (Fig. 2.4a). Multiple iterations of the UAV have been documented, however, the only known flight test conducted reached a maximum speed of 58m/s (Mizobata et al., 2014), corresponding to a speed of approximately Mach 0.17. As of 2019 the program was ongoing with work focusing on redesigning the airframe and testing control options (Ueba et al., 2021; Yamazaki et al., 2019). During the same time period as the Ohwashi program, research teams in Brazil and

the United States worked on similar research programs related to SSUAVs. Researchers in Brazil proposed the Pohox SSUAV as a way to test a multi-cycle engine being developed by Gabaldo et al. (2016) (Barbosa et al., 2014). The conceptual design called for the Pohox to be a 7kg SSUAV with a wingspan of 0.44m and a maximum speed of slightly below Mach 2.0 at an altitude of 20km (Fig. 2.4b). Due to the lack of recent publications, the Pohox program appears to have been terminated. In the United States researchers at the University of Colorado-Boulder focused on developing the Graduate Organization Jet Engine Technology Team (GOJETT) to facilitate research into miniature gas-turbine engines, sonic-boom minimization, and thrust vectoring studies (Walter and Starkey, 2012). The goal of the GOJETT aircraft (Fig. 2.4c) was to break the Fédération Aéronautique Internationale (FAI) World Speed record for a sub 50kg vehicle. Due to the lack of recent publications, the GOJETT program appears to have been terminated without any successful flights documented. In contrast to the GOJETT program, researchers at the University of Washington focused on a Research-UAV program (R-UAV) to better understand low speed behaviours of supersonic aircraft with experimental SSUAVs (Livne and Nelson, 2012; Livne, 2017). As of 2022 the R-UAV program is ongoing, with results being contributed to the newly introduced National Aeronautics and Space Administration (NASA) Supersonic Configurations At Low Speed (SCALOS) Program (Nelson et al., 2022). Supersonic aircraft designs have previously experienced difficulty with low speed and high Angle Of Attack (AOA) landing approach flight (Bertolin et al., 2022). As a result, the SCALOS program was introduced into the literature in 2022 seeking to better understand what design features elicit certain aircraft responses. The SCALOS goal is to parameterize low speed supersonic aircraft handling qualities by combining data from Computational Fluid Dynamics (CFD), water tunnel tests, and wind tunnel tests (Magee et al., 2022). It is worth noting that while the SCALOS and the University of Washington experimental UAVs have supersonic profiles, they are subsonic representations of full-scale aircraft and are not designed to investigate the intricacies of SSUAVs at high-speed. More recently, in 2020 “*Project Boom*” was conceived with the goal

of developing a transonic UAV (Jacob et al., 2021) (Fig. 2.4d). As of the time of this writing, the project is in its early conceptual design and prototyping phases (Jacob et al., 2021). A spin-off of Project Boom is “*The Mach Initiative*” which started in 2022 and is currently working to develop a sub-25kg supersonic UAV (The Mach Initiative, 2023) (Fig. 2.4e). In 2019 the MUFASA program was initiated at the University of Calgary, Canada, as an early conceptual design for testing novel engines and high-speed research (Fig. 2.4f). Some of the early MUFASA work has been reported by Dalman et al. (2021) and Durante et al. (2022). Preliminary vehicle size optimization has been performed to find the size of vehicle required for various mission requirements (Dalman et al., 2021). The MUFASA program is ongoing, extending prior work by others including previously proposed air-breathing SSUAV concepts shown in Fig. 2.4. However, with no known successful test flights of an air-breathing SSUAV in the open literature, many research questions still exist (Dalman et al., 2021; McCrink and Gregory, 2021; Walter and Starkey, 2012), which are being addressed within the context of the MUFASA program.

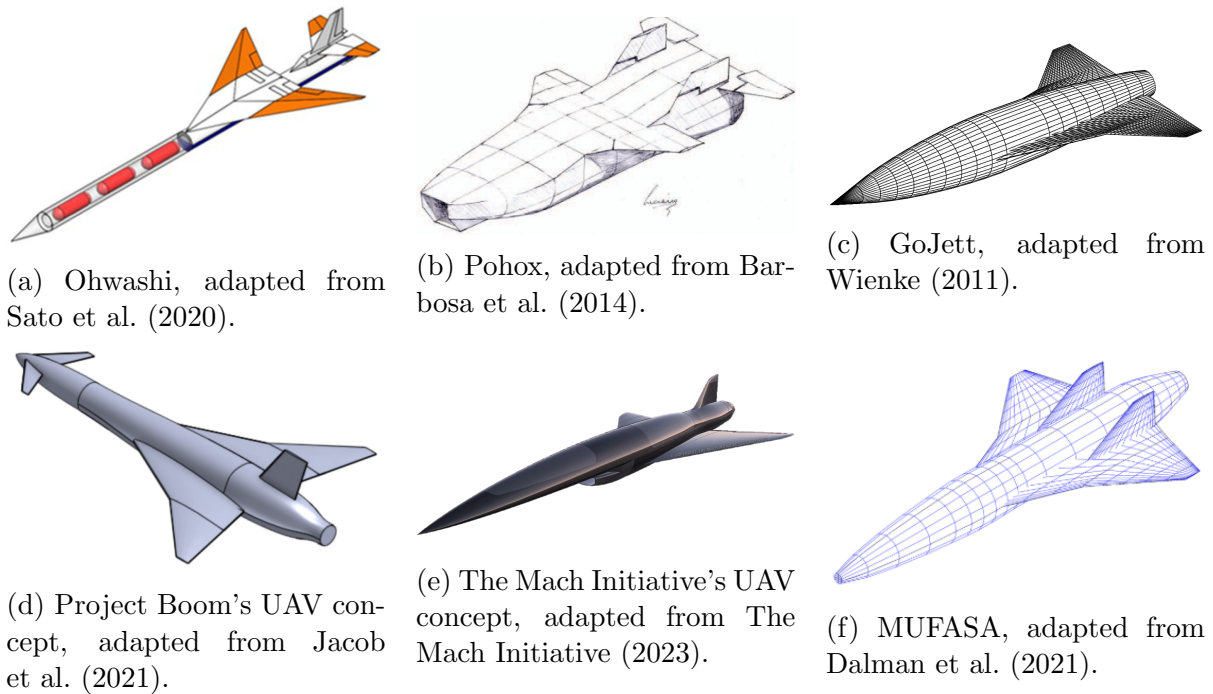
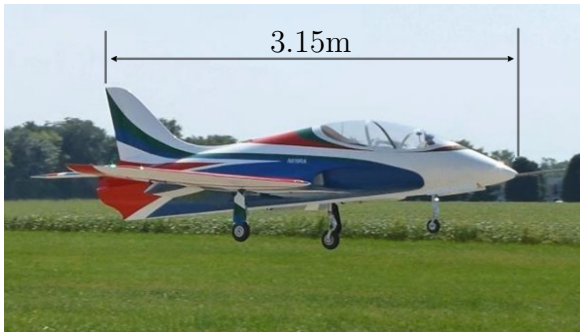


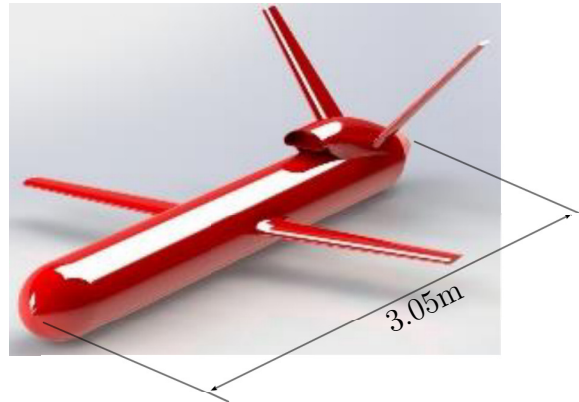
Figure 2.4: Air breathing SSUAV concept drawings (not to scale).

2.2.2 High-Speed Small-Scale Uncrewed Aerial Vehicles

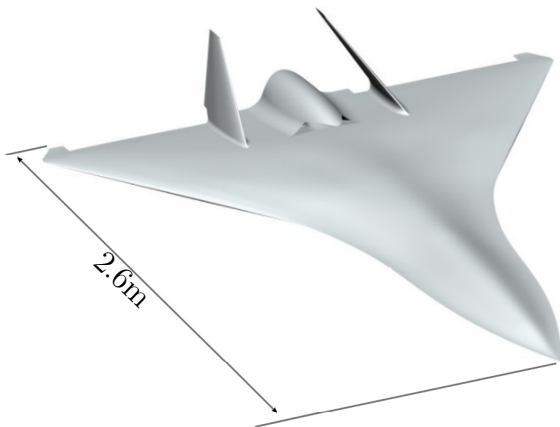
High-speed small-scale UAV proposals have previously been undertaken, with some even facilitating test flights. Work by McCrink and Gregory (2021) investigated the feasibility of high-speed small-scale Beyond Visual Line Of Sight (BVLOS) flight using a SkyMaster Avanti XXL aircraft with a wingspan of 2.48m (Fig. 2.5a). Such work aimed to achieve the FAI World Speed record for a 5kg to 50kg vehicle, the same record the GoJett team was after (Walter and Starkey, 2012). The group was ultimately successful in setting the FAI speed record with a speed of 147.20mph (i.e., $65.8 \frac{\text{m}}{\text{s}}$), or approximately Mach 0.19 (McCrink and Gregory, 2021).



(a) SkyMaster Avanti XXL, adapted from McCrink and Gregory (2021).



(b) HS-UAV, adapted from Hussain et al. (2019).



(c) Target drone concept, adapted from Ozyetis and Alemdaroglu (2014).



(d) Trance, adapted from Guinness World Records (2017).

Figure 2.5: High-speed small-scale UAV concepts and prototypes.

The literature for high-speed small-scale UAVs capable of speeds above Mach 0.5 is significantly less. Two notable academic high-speed small-scale UAVs are the HS-UAV developed by Hussain et al. (2019) and a target drone developed by Ozyetis and Alemdaroglu (2014) shown in Figs. 2.5b and 2.5c, respectively. The HS-UAV proposed by Hussain et al. (2019) is a rocket launched UAV that uses a turbojet to achieve a maximum speed of Mach 0.6. The HS-UAV has a wingspan of 1.65m and a preliminary stability analysis suggested the vehicle is stable (Hussain et al., 2019). Work by Ozyetis and Alemdaroglu (2014) used an optimization process leading to the 1.8m wingspan, double-delta wing planform UAV capable of cruise at Mach 0.5. Although a proof-of-concept half-scale demonstration flight was flown, limited results have been reported in the literature (Ozyetis and Alemdaroglu, 2014). Due to a lack of publications from these and other authors it is unclear if either the HS-UAV or the target drone program have developed further. A notable high-speed small-scale UAV developed outside of an academic or industrial setting is the Trance remote piloted UAV created by N. Herbrich (personal communication, February 9, 2022) (see Fig. 2.5d). The Trance aircraft has a wingspan of 1.04m and a takeoff weight of 7.5kg. Using a similar engine as McCrink and Gregory (2021), Trance set the 2017 Guinness World Record for the fastest remote-controlled jet-powered model aircraft with a speed of 749km/h, or approximately Mach 0.61 (Guinness World Records, 2017).

2.3 Summary and Areas of Improvement

As described above, only a handful of research and developmental programs worldwide have or are attempting to develop self-powered air-breathing SSUAVs. Such a goal remains elusive, and there are still multiple technological hurdles that must be overcome. One such challenge is ensuring that the aircraft’s flying qualities are sufficient enough to ensure safe control operation needed for mission success. There are multiple standardized methods to evaluate crewed vehicle flying qualities, however, UAV flying qualities standard development is in its

infancy, and is at the same place as crewed standards were in the 1950's (Cotting, 2010b). With the further proliferation of UAVs, a UAV specific flying quality standard is needed to reduce the high mishap rate associated with these aircraft (Department of Defense, 2009; Greene et al., 2014). In the absence of a UAV flight database to facilitate a fixed-wing UAV specific flying quality standard, UAVs have been evaluated against current crewed standards by scaling via Froude scaling. Due to their novelty SSUAV's have been largely absent from control and flying quality reviews (Hassanalian and Abdelkefi, 2017; Michailidis et al., 2020). A comprehensive overview of SSUAV flying qualities has yet to be addressed in the literature. There is currently no metric to guide SSUAV design, regulate this vehicle type, or maximize the chance of safe and successful mission success.

Chapter 3

Research Overview

SSUAVs have the potential to revolutionize high-speed research by offering a cost-effective way to obtain high-speed experimental data (Eckstrom and Peele, 1975; Mizobata et al., 2014; Walter and Starkey, 2012). However, a variety of open problems related to UAV flying qualities and SSUAV development exist. This chapter details the challenges of SSUAV development derived from the summary provided in Chapter 2. These challenges are refined into a concise problem statement that this thesis seeks to solve. A description of the proposed solution is provided along with the associated assumptions and constraints.

3.1 Problem Statement

The next era in supersonic civil transportation is coming with multiple supersonic aircraft concepts proposed for development (Sun and Smith, 2017). Unfortunately, supersonic prototype aircraft are very expensive and the financial risk of development to companies is large (Reed, 2021; Sheetz, 2021). An alternative to full-scale prototype aircraft development is an SSUAV. Small-scale UAVs are now increasingly used as low-cost technology testing platforms (Sobron et al., 2021), and developing an SSUAV would greatly reduce the costs of supersonic aircraft development. A handful of developmental research programs have investigated the feasibility of an SSUAV demonstrator, however, only six programs (Ohwashi, MUFASA,

SCALOS, R-UAV, Project Boom, and The Mach Initiative) are ongoing according to recent publications (Durante et al., 2022; Jacob et al., 2021; Nelson et al., 2022; The Mach Initiative, 2023; Ueba et al., 2021). One reason for the lack of a functioning SSUAV is that the aerodynamic conditions experienced by an SSUAV and the control required remain undetermined (Nelson et al., 2022). Whether SSUAVs pose unique handling quality challenges is an open research question that requires further study. Different SSUAV control strategies have been implemented (Burnashev and Zbrutsky, 2019; Langston et al., 2016; Ueba et al., 2021; Wienke, 2011), however, due to the absence of a standardized performance criteria, none of the control laws can be deemed reliably satisfactory (Stevens et al., 2015). Unfortunately, fixed-wing UAV flying quality performance standards are nonexistent (Klyde et al., 2020a), with UAV flying quality research still in its infancy (Cotting, 2010b; Klyde et al., 2020a). To facilitate UAV flying quality standard development, flying quality data from multiple aircraft types must be generated (Greene et al., 2014; Holmberg et al., 2008). In order to facilitate the inclusion of SSUAVs in future UAV flying quality standards, SSUAV flying quality data must be generated. A comprehensive overview of SSUAV flying qualities has yet to be addressed in the literature and is critical for SSUAV development. Therefore, the following problem needs to be addressed:

Develop mechanisms to assess SSUAV flying qualities and whether such aircraft pose unique handling quality challenges.

3.2 Proposed Solution Overview

To develop a solution to the problem statement in Section 3.1, the problem is broken down into four interrelated tasks focused on developing:

1. A flight dynamics mathematical model,
2. A flight dynamics simulation,

3. Vehicle parameter identification, and
4. Flying quality analysis.

The first and second tasks will define the six-Degree-Of-Freedom (6-DOF) motion and simulation environment that the SSUAV experiences. The third task will obtain SSUAV physical and aerodynamic data from physical models and CFD, respectively. The fourth task will evaluate the SSUAV flying quality data by using the Froude scaling flying quality parameters and comparing the results to the MIL-STD-1797A standard, along with a novel modification of the MIL-STD-1797A standard proposed in this thesis. The fourth task will also evaluate control surface perturbation responses from the SSUAV for a novel comparison to full-scale supersonic aircraft and small-scale UAVs. Combined together, these tasks will obtain simulated SSUAV flying quality data and determine if SSUAVs pose unique handling quality challenges. A schematic diagram of the proposed solution is presented in Fig. 3.1. The four tasks above are broken into smaller sub-tasks and represented by blocks shaded orange, blue, green, and red, respectively. The contributions of this thesis work are indicated by parallelograms in Fig. 3.1 and are elaborated in the following paragraphs. All blocks are also used to form three interrelated groups which together aim to solve the problem statement (Section 3.1):

- Flight Dynamics Mathematical Model,
- Flight Dynamics Simulation, and
- Results.

The first task (orange blocks in Fig. 3.1) consists of procedures that makeup the flight dynamics mathematical model. The aircraft motion will be defined by combining coordinate systems, kinematic and dynamic equations, aerodynamic forces, and propulsion and gravity forces. The resulting mathematical model will be implemented into a simulation program and into a mathematical model discretization block (Fig. 3.1) which evaluates the flying

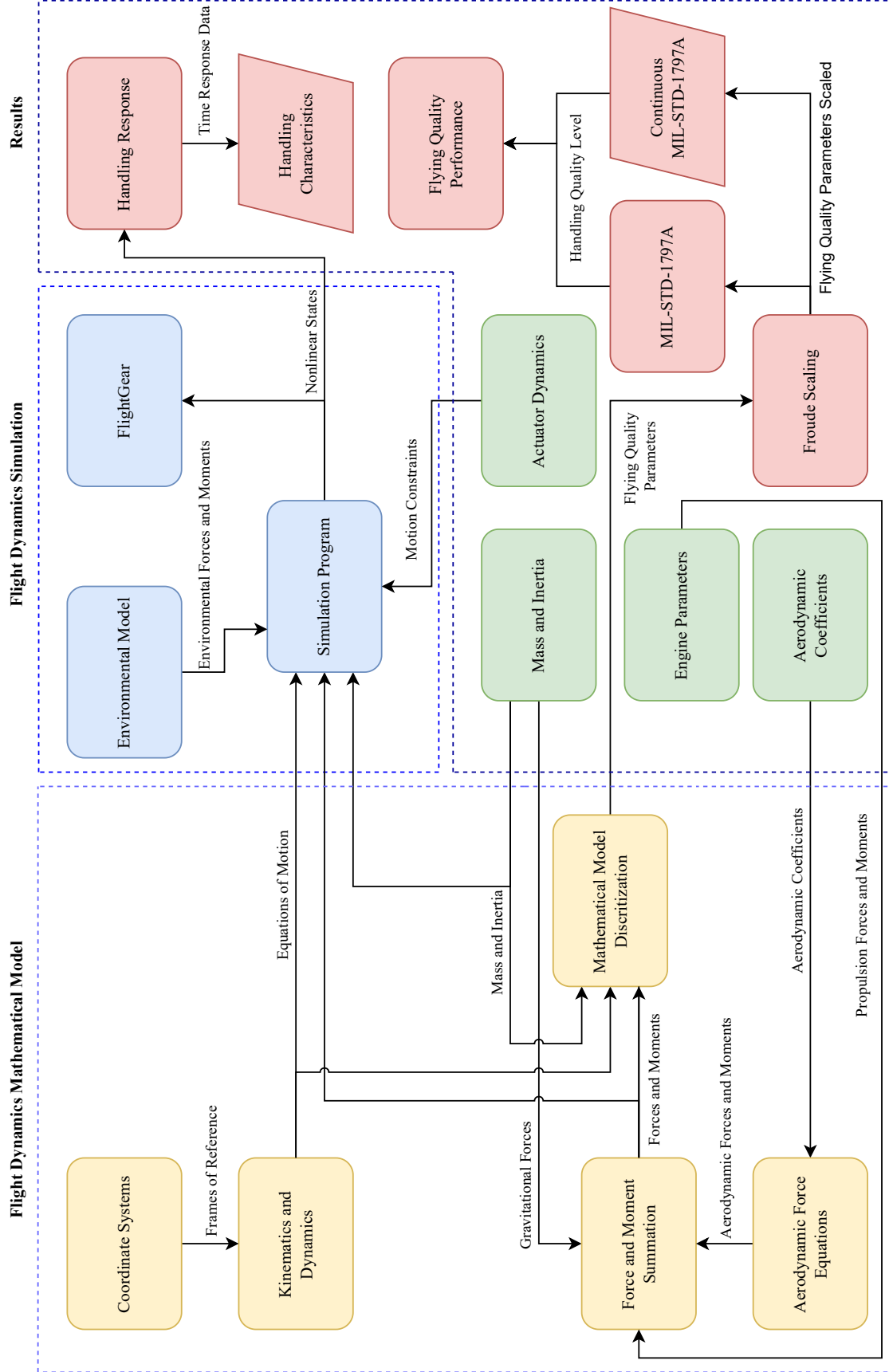


Figure 3.1: Proposed solution architecture.

quality parameters of the aircraft. These aspects will be presented in Chapter 4, “Flight Dynamics Mathematical Model”.

The second task (blue blocks in Fig. 3.1) focuses on the methods used to facilitate a flight dynamics simulation. For this, a process will be developed to incorporate actuator motion constraints and an environmental model to simulate the motion of the nonlinear 6-DOF vehicle at discrete time steps. A time series of the vehicle’s state (velocity, attitude, angular velocity, and position) will be outputted and used as an input to the handling response block and the FlightGear real time visualization block (Fig. 3.1). These aspects will be presented in Chapter 5, entitled: Flight Dynamics Simulation.

The third task (green blocks in Fig. 3.1) presents the vehicle parameters required. Information about the engine parameters, mass, inertia, aerodynamic coefficients, and actuator dynamics will be compiled and organized for inclusion into a model for the MUFASA SSUAV. Thus, all of these vehicles parameters will be specific to the aircraft being analyzed. In the absence of aerodynamic coefficient data, aerodynamic coefficients will be obtained by combining low and high fidelity CFD. The engine parameters, mass, inertia, and aerodynamic coefficients will be used to calculate the forces used to propel and disturb the UAV. These parameters will be supplied into the flight dynamics mathematical model blocks (Fig. 3.1). The actuator dynamics parameters will define motion constraints used by the flight dynamics simulation blocks. These aspects will be presented in Chapter 6, “Results”.

The final task (red blocks in Fig. 3.1) consists of flying and handling response analysis mechanisms and represent the main contribution of this thesis. Vehicle flying quality parameters are calculated from the mathematical model discretization block. A Froude scaling procedure will be applied to the flying quality parameters so that the scaled MUFASA SSUAV cruise values are comparable against the MIL-STD-1797A standard. To provide greater flying quality performance insight, a novel evaluation criteria will be proposed. This novel evaluation criteria will be a continuous modification of criteria set out in the MIL-STD-1797A standard. The MIL-STD-1797A and novel developed continuous MIL-STD-

1797A blocks (Fig. 3.1) will output the computed handling quality levels that will indicate the SSUAV’s flying quality performance data both at cruise conditions and throughout the SSUAV’s flight regime. A mechanism to simulate and evaluate vehicle handling response parameters from a time series representation of the vehicle’s nonlinear state will also be developed. The vehicle’s nonlinear state will be perturbed in the handling response block (Fig. 3.1) and its time series state response collected. By performing this procedure on the MUFASA SSUAV, a small-scale UAV, high-speed small-scale UAVs, and large-scale supersonic aircraft, a collection of response handling characteristics will be determined. This novel comparison between full-scale supersonic aircraft, small-scale UAVs, and an SSUAV will be used to assess whether SSUAVs pose unique handling quality challenges. These aspects will be presented in Chapter 6, “Results”.

The aforementioned mechanisms will allow for the flying and handling quality evaluation of the current MUFASA SSUAV, along with subsequent SSUAV iterations. The mechanism procedures developed will act to guide SSUAV design, inform future standards and regulations, and maximize the chance of safe and successful SSUAV mission success.

3.2.1 Assumptions

To reduce the problems complexity, yet still develop practical results, the proposed solution incorporates the following assumptions:

Assumption 1: It will be assumed that the aircraft is equipped with sensors that provide accurate and precise information about the vehicle’s state (i.e., attitude and velocity). These sensors are assumed to provide the vehicle state at the required frequency.

Assumption 2: It will be assumed that a position control algorithm ensures that commanded and achieved actuator deflections are identical in magnitude and direction.

Assumption 3: It will be assumed that the MUFASA SSUAV is capable of achieving supersonic flight speeds at the current weight and wingspan specified.

3.2.2 Constraints

To reduce the complexities associated with the proposed solution the following five constraints will be used:

Constraint 1: The aircraft physical structure will be constrained to be perfectly rigid.

This constraint eliminates aeroelastic effects such as aerodynamic flutter. A rigid airframe is a common constraint (Beard and McLain, 2012; Stevens et al., 2015), and has been applied to supersonic aircraft (Mcmaster and Schenkt, 1974; Moes and Iliff, 2002; Steer, 2004), and SSUAV concepts (Langston et al., 2016; Ninomiya et al., 2018; Wienke, 2011).

Constraint 2: Aerodynamic coefficients will be constrained to follow the principle of superposition via the component build-up method. The component build-up method is a common aerodynamic coefficient constraint (Beard and McLain, 2012). The method is applicable from subsonic to hypersonic flight speeds provided aerodynamic coefficients are determined at each Mach number (Stevens et al., 2015). Aircraft modelling via the component build-up method has successfully been applied in practice on aircraft such as the supersonic X-34 spaceplane (Pamadi et al., 2001) and the Tupolev TU-144LL supersonic transport aircraft (Lensi, 2000).

Constraint 3: The aircraft flight conditions analyzed will be constrained to cruise conditions and in the absence of environmental disturbances. Takeoff

and landing flight regimes, along with aircraft ground aerodynamic interactions such as ground effect, will not be considered.

Constraint 4: Aircraft control surfaces will be considered to be rigid with actuators that are infinitely powerful when deflected. This constraint will eliminate control surface flutter which is common with high-speed aircraft (Yang et al., 2017; Mai et al., 2019) and thus facilitate the current work.

Constraint 5: Vehicle mass and inertia are constrained to be constant as data collection will be performed over brief time intervals of steady-level flight. That is, fuel consumption will not be considered. Gravity will also be held constant as magnitude variation, such as due to altitude changes, is constrained to be negligible (Moritz, 1980).

Chapter 4

Flight Dynamics Mathematical Model

This chapter details the dynamic formulations used to simulate, control, and analyze the MUFASA SSUAV. As an experimental version of MUFASA capable of supersonic speeds does not yet exist, a mathematical model using current airframe design and aerodynamic coefficients was used to facilitate initial aircraft flying and response quality analysis.

4.1 Coordinate Systems

For the modeling process, the standard fixed flat Earth model as presented in Stevens et al. (2015) was chosen. This model uses a North-East-Down (NED) *inertial* coordinate frame where the North and East axis align with their cardinal direction namesakes while down points in the direction of gravity with the origin at sea-level. The NED inertial coordinate frame is represented by the three axes x_{in} , y_{in} , and z_{in} , respectively as shown in Fig. 4.1. As the UAV moves about the fixed flat earth model it is assigned its own coordinate system known as the *vehicle* frame (denoted by subscript v). This vehicle frame of reference is located at the UAV's Centre of Gravity (CG), but aligned with the axis of the inertial frame. Within this thesis the vehicle frame coordinates are represented by the axes x_v , y_v , z_v , and are used to evaluate the translational movements of the UAV. In order to account for the UAV's orientation, a *body* frame of reference (denoted by subscript b) is defined by

the axes x_b , y_b , and z_b . The body frame is used to account for the UAV's orientation about the vehicle frame. The UAV's orientation is defined by the Euler angles for roll (ϕ), pitch (θ), and yaw (ψ) which follow the right-hand rule for direction about each's respective axis and shown in Fig. 4.1 (Beard and McLain, 2012; Duke et al., 1994; Stevens et al., 2015). The body frame of reference moves with respect to the vehicle's frame of reference as the vehicle rolls, pitches, and/or yaws.

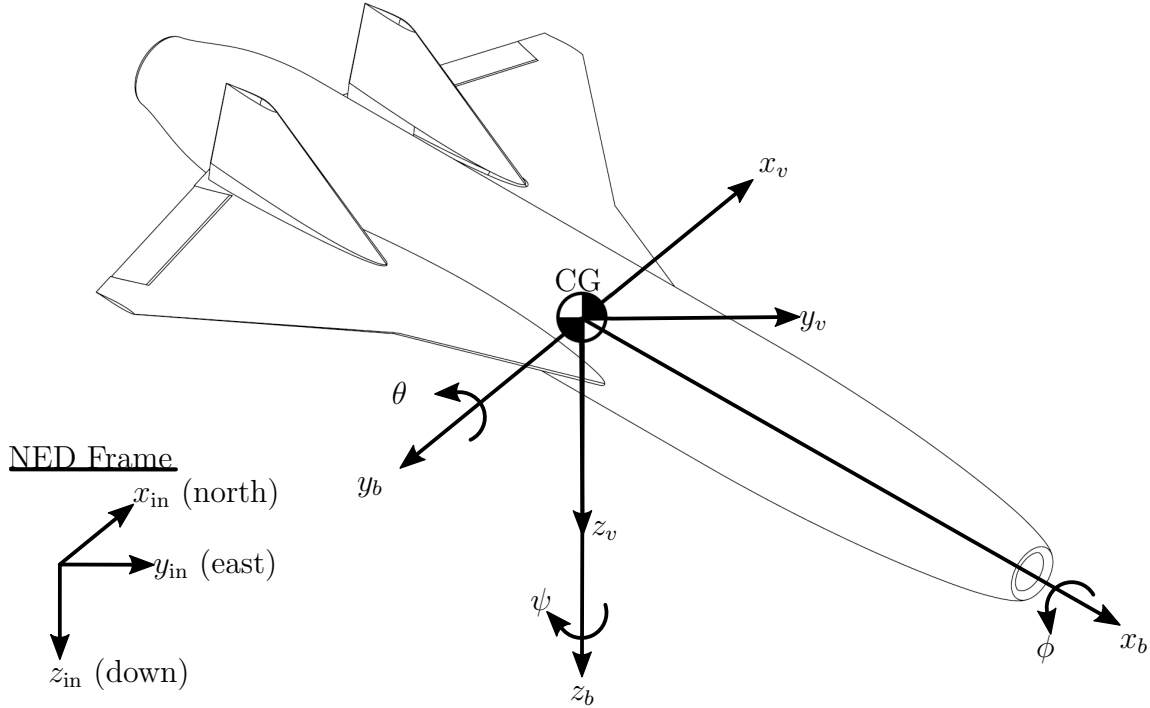


Figure 4.1: NED inertial, vehicle and body frames of reference on the MUFASA UAV.

Figure 4.1 depicts the inertial, vehicle and body coordinate frames used to define the UAV's location and orientation. The rotational transformation from the vehicle frame to the body frame of reference is denoted by $R_{\text{vehicle}}^{\text{body}}$, presented in Eq. 4.1 (Stevens et al., 2015) where cosine and sine of a variable are represented by $c()$ and $s()$, respectively. The vehicle to body rotation matrix, denoted by R_v^b is a 3-2-1 rotation system represented by intermediary roll (ϕ), pitch (θ), and yaw (ψ) rotations $R_x(\phi)$, $R_y(\theta)$, and $R_z(\psi)$, respectively.

A more robust rotational notation is quaternions as they are not susceptible to singu-

larities at high angles of attack (Beard and McLain, 2012). This robustness comes at the cost of additional implementation and linearization complexity when compared to Euler angles (Wienke, 2011). The use of quaternions was deemed unnecessary in the context of this thesis as the MUFASA flight regime does not include high angle of attack flight or flight manoeuvres where the aircraft might move through gimbal lock configurations.

$$\begin{aligned}
R_{\text{vehicle}}^{\text{body}} &= R_v^b = R_x(\phi)R_y(\theta)R_z(\psi) \\
&= \begin{bmatrix} 1 & 0 & 0 \\ 0 & \cos(\phi) & \sin(\phi) \\ 0 & -\sin(\phi) & \cos(\phi) \end{bmatrix} \begin{bmatrix} \cos(\theta) & 0 & -\sin(\theta) \\ 0 & 1 & 0 \\ \sin(\theta) & 0 & \cos(\theta) \end{bmatrix} \begin{bmatrix} \cos(\psi) & \sin(\psi) & 0 \\ -\sin(\psi) & \cos(\psi) & 0 \\ 0 & 0 & 1 \end{bmatrix} \\
&= \begin{bmatrix} c(\psi)c(\theta) & s(\psi)c(\theta) & -s(\theta) \\ c(\psi)s(\phi)s(\theta) - c(\phi)s(\psi) & s(\phi)s(\psi)s(\theta) + c(\phi)c(\psi) & c(\theta)s(\phi) \\ c(\phi)c(\psi)s(\theta) + s(\phi)s(\psi) & c(\phi)s(\psi)s(\theta) - c(\psi)s(\phi) & c(\phi)c(\theta) \end{bmatrix} \quad (4.1)
\end{aligned}$$

Aerodynamic forces are generated on the UAV as its airframe moves through the air surrounding it. The velocity of the aircraft relative to the surrounding air is denoted as the airspeed vector (\bar{V}_a). The magnitude of the airspeed vector is referred to as airspeed (V_a), and is defined by Eq 4.2 from Stevens et al. (2015):

$$V_a = \|\bar{V}_{in} - \bar{V}_w\| \quad (4.2)$$

where V_{in} is the inertial translational velocity of the aircraft with respect to the body frame and V_w is the velocity of the surrounding wind with respect to the body frame. Two other frames of reference are introduced to relate the UAV to the airspeed vector: the *stability* and the *wind* frames. The difference in orientation between the body frame, (x_b, y_b, z_b) , and the stability frame denoted by subscript s , (x_s, y_s, z_s) , is called the AOA represented by α . Similarly, the difference in angle between the stability frame and the wind frame

denoted by subscript w , (x_w, y_w, z_w) , is called the sideslip angle represented by β . A visual representation of these coordinate frames is presented in Figure 4.2. The transformation from the wind frame to the body frame of reference is denoted by $R_{\text{wind}}^{\text{body}}$ as shown in Eq. 4.3 (Beard and McLain, 2012) which for simplicity is also denoted as R_w^b . The R_w^b matrix is a rotation system represented by rotations about the stability z -axis ($R_w^s(\beta)$) and body y -axis ($R_s^b(\alpha)$) (Beard and McLain, 2012).

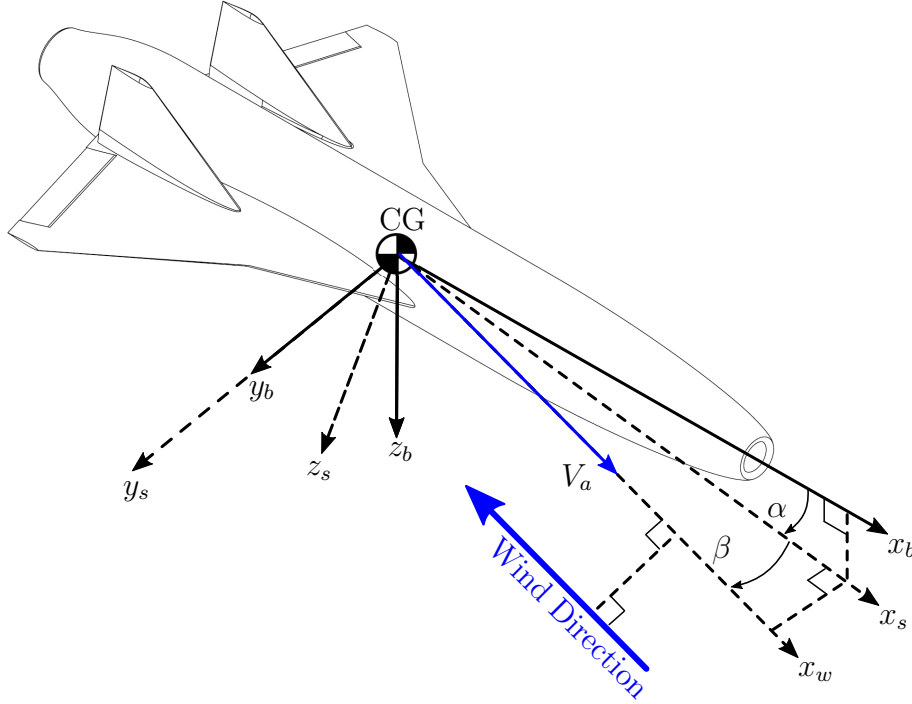


Figure 4.2: Wind, stability and body frames of reference.

$$\begin{aligned}
 R_{\text{wind}}^{\text{body}} &= R_w^b = R_s^b(\alpha) R_w^s(\beta) \\
 &= \begin{bmatrix} \cos(\alpha) & 0 & -\sin(\alpha) \\ 0 & 1 & 0 \\ \sin(\alpha) & 0 & \cos(\alpha) \end{bmatrix} \begin{bmatrix} \cos(\beta) & -\sin(\beta) & 0 \\ \sin(\beta) & \cos(\beta) & 0 \\ 0 & 0 & 1 \end{bmatrix} \\
 &= \begin{bmatrix} \cos(\beta) \cos(\alpha) & -\sin(\beta) \cos(\alpha) & -\sin(\alpha) \\ \sin(\beta) & \cos(\beta) & 0 \\ \cos(\beta) \sin(\alpha) & -\sin(\beta) \sin(\alpha) & \cos(\alpha) \end{bmatrix}
 \end{aligned} \tag{4.3}$$

4.2 Kinematics and Dynamics

The kinematics and dynamics of MUFASA were modelled considering the aircraft as a 6-DOF rigid dynamic system in accordance with Newtonian practices (Beard and McLain, 2012; Stevens et al., 2015). While work by Guimarães et al. (2022) indicates aeroelastic models are better suited for supersonic vehicle design, the models are significantly more complex and are best employed during the detailed design engineering phase. The aircraft velocity was defined by six variables: three translational velocities (U , V , W) and three rotational velocities (P , Q , R) defined with respect to the UAV's body frame as shown in Fig. 4.3. The corresponding translational and rotational speed mathematical formulas are shown in Eqs. 4.4 and 4.5 (Stevens et al., 2015), respectively.

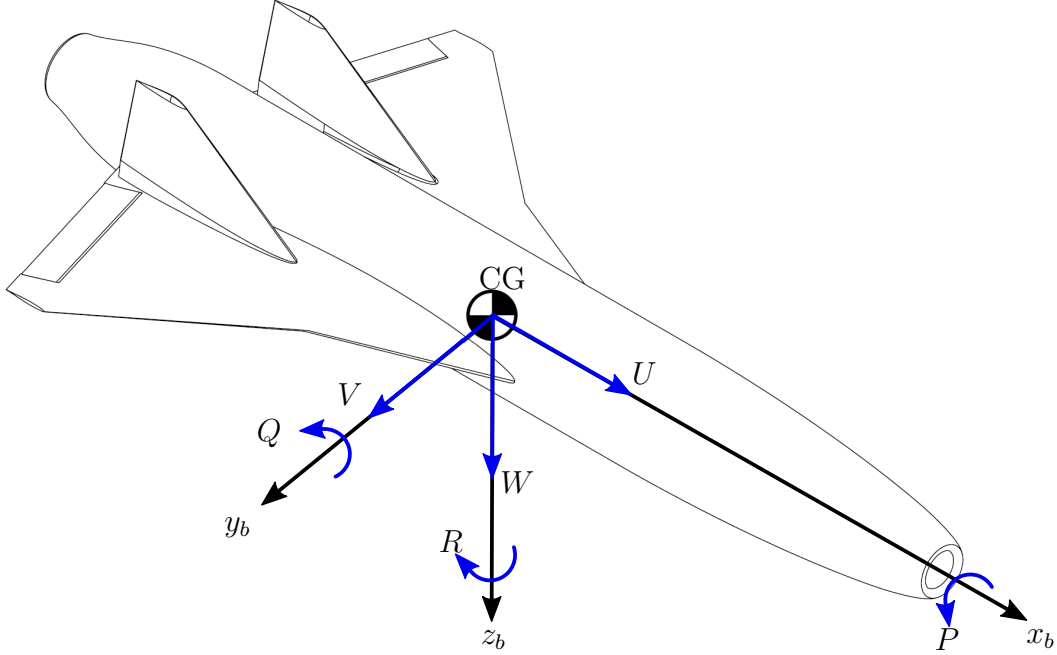


Figure 4.3: MUFASA axes of motion.

$$\begin{bmatrix} \dot{U} \\ \dot{V} \\ \dot{W} \end{bmatrix} = \frac{1}{m} (\bar{F}_g + \bar{F}_T + \bar{F}_{\text{aero}}) - \begin{bmatrix} P \\ Q \\ R \end{bmatrix} \times \begin{bmatrix} U \\ V \\ W \end{bmatrix} \quad (4.4)$$

The terms m , $\dot{\square}$, \bar{F}_g , \bar{F}_T , and \bar{F}_{aero} in Eq. 4.4 represent the mass, the variable time derivatives, and the force vectors due to gravity, thrust, and aerodynamic interactions, respectively.

$$\begin{bmatrix} \dot{P} \\ \dot{Q} \\ \dot{R} \end{bmatrix} = \begin{bmatrix} I_{xx} & 0 & I_{xz} \\ 0 & I_{yy} & 0 \\ I_{xz} & 0 & I_{zz} \end{bmatrix}^{-1} \left((\bar{M}_T + \bar{M}_{\text{aero}}) - \begin{bmatrix} 0 & -R & Q \\ R & 0 & -P \\ -Q & P & 0 \end{bmatrix} \begin{bmatrix} I_{xx} & 0 & I_{xz} \\ 0 & I_{yy} & 0 \\ I_{xz} & 0 & I_{zz} \end{bmatrix} \begin{bmatrix} P \\ Q \\ R \end{bmatrix} \right) \quad (4.5)$$

The terms \bar{M}_T , \bar{M}_{aero} , I_{xx} , I_{yy} , I_{zz} , and I_{xz} in Eq. 4.5 represent the moment vectors due to the thrust forces and the aerodynamic interactions applied to the aircraft, the aircraft's inertias about the x_b , y_b , and z_b axes (Fig. 4.1), and the product of inertia about the x_b and z_b axes, respectively. The mathematical formulations used to calculate \bar{M}_T and \bar{M}_{aero} will be described in Section 4.3. The changing angular orientation of the vehicle with respect to the vehicle frame is calculated from Euler angles and angular rates as represented in Eq. 4.6 from Stevens et al. (2015). In turn, the position of the vehicle, defined with respect to the inertial NED frame, is represented by Λ_N , Λ_E , and Λ_D . The change in position with time is calculated via Eq. 4.7 from Stevens et al. (2015), where R_b^v is the rotation matrix from the body frame to the vehicle frame. It should be noted that a vehicle's vertical position is also described as its altitude (h) which is represented by negative values of Λ_D (as the inertial frame of reference is positioned at sea level).

$$\begin{bmatrix} \dot{\phi} \\ \dot{\theta} \\ \dot{\psi} \end{bmatrix} = \frac{1}{\cos(\theta)} \begin{bmatrix} \cos(\theta) & \sin(\phi) \sin(\theta) & \cos(\phi) \sin(\theta) \\ 0 & \cos(\phi) \cos(\theta) & -\sin(\phi) \cos(\theta) \\ 0 & \sin(\phi) & \cos(\phi) \end{bmatrix} \begin{bmatrix} P \\ Q \\ R \end{bmatrix} \quad (4.6)$$

$$\begin{bmatrix} \dot{\Lambda}_N \\ \dot{\Lambda}_E \\ \dot{\Lambda}_D \end{bmatrix} = R_b^v \begin{bmatrix} U \\ V \\ W \end{bmatrix} \quad (4.7)$$

4.3 Forces and Moments

As the MUFASA airframe travels through the air it experiences forces and moments from aerodynamic sources. Furthermore, the forces and moments influencing the aircraft are also attributed to propulsive and gravitational forces. As this work's focus is on flight behaviour within open free spaces, ground aerodynamic interactions and the corresponding aerodynamic effects were not considered.

In terms of aerodynamic aspects, complex vortex flow fields due to shock wave interactions have a strong influence on control surface effectiveness and aircraft handling qualities (Sepulveda and Smith, 2017). Body and mechanical forces are in some way dependant on gravity and thrust forces as these act along the body frame of reference. Aerodynamic forces occur within the wind frame and include lift, drag, and sideforce. These aerodynamic forces are represented in the body frame by F_{L_b} , F_{D_b} , and F_{Y_b} , respectively. Propulsion moments originate from thrust generation while aerodynamic moment interactions are caused by control surface deflections and wind perturbations. Moments caused by aerodynamic forces about the roll, pitch, and yaw axis are herein represented by M_{L_b} , M_{M_b} , and M_{N_b} , respectively. These generalized aerodynamic forces (F_{L_b} , F_{D_b} , F_{Y_b}) and corresponding moments (M_{L_b} , M_{M_b} , M_{N_b}) act on the airframe and control surfaces, and are presented mathematically in Section 4.3.2. First though, the aircraft control surface deflections are defined in Section 4.3.1.

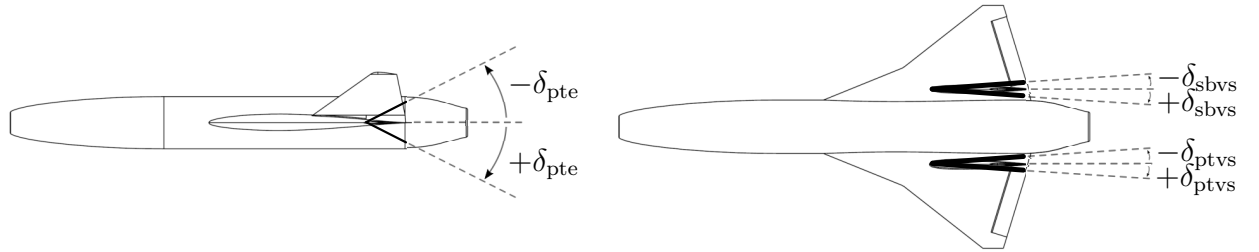
4.3.1 Control Surfaces

Due to MUFASA's delta-wing design, the elevon control surfaces shown in Fig. 1.2 simultaneously control the UAV's pitch and roll motion. In contrast to MUFASA's control surface configuration, typical fixed-wing aircraft incorporate elevator and aileron control surfaces which independently control the aircraft's pitch and roll motion respectively. In the case of the MUFASA aircraft it was important to decouple the elevon's longitudinal and lateral

aircraft dynamics. Elevon deflections are related to elevator and aileron deflections as per Eq. 4.8 (Beard and Mclain, 2012).

$$\begin{bmatrix} \delta_e \\ \delta_a \end{bmatrix} = \begin{bmatrix} 1 & 1 \\ -1 & 1 \end{bmatrix} \begin{bmatrix} \delta_{sbe} \\ \delta_{pte} \end{bmatrix} \quad (4.8)$$

Here δ_{sbe} and δ_{pte} represent the deflection angle of the starboard and port elevon respectively while δ_e and δ_a represent the deflection angle of an equivalent elevator and aileron setup, respectively. The UAV's yaw motion is controlled by the port and starboard vertical stabilators which are represented by δ_{ptvs} , and δ_{sbvs} , respectively. The sign convention adapted from Beard and Mclain (2012) associated with the elevon and vertical stabilator control surfaces is illustrated in Fig. 4.4.



(a) Elevon deflection. Both the starboard and port elevons follow the same sign convention.

(b) Vertical Stabilator deflection.

Figure 4.4: MUFASA's control surface sign convention.

For simplicity when computing the aerodynamic forces in Section 4.3.2, the vertical stabilator deflection angles are represented as a rudder deflection angle (δ_r). The relationship between the vertical stabilators and the rudder is represented by Eq. 4.9, a novel formulation proposed in this thesis document. The corresponding forces and moments generated by these control surfaces are computed using aerodynamic coefficients as described in Section 4.3.2.

$$\delta_r = \frac{\delta_{ptvs} + \delta_{sbvs}}{2} \quad (4.9)$$

The actuators of the aerodynamic control surfaces are modelled as a second-order transfer

function using Eq. 4.10 (Prasad B. and Pradeep, 2007):

$$\frac{\delta_{ptvs}}{\delta_{ptvs_d}} = \frac{(100)^2}{s^2 + 2\left(\frac{\sqrt{2}}{2}\right)(100)s + (100)^2} \quad (4.10)$$

where subscript d represents the desired variable value. The maximum deflection angle and deflection rate specific to MUFASA A.2 aerodynamic control surfaces are provided in Section 6.2.

4.3.2 Aerodynamic Forces and Moments

To mathematically represent the forces (e.g., \bar{F}_g , \bar{F}_T , and \bar{F}_{aero}) and moments (e.g., \bar{M}_T and \bar{M}_{aero}) that the SSUAV will experience during flight (Eqs. 4.4 and 4.5) a free body diagram of the MUFASA UAV showing the associated parameters that need to be considered is presented in Fig. 4.5.

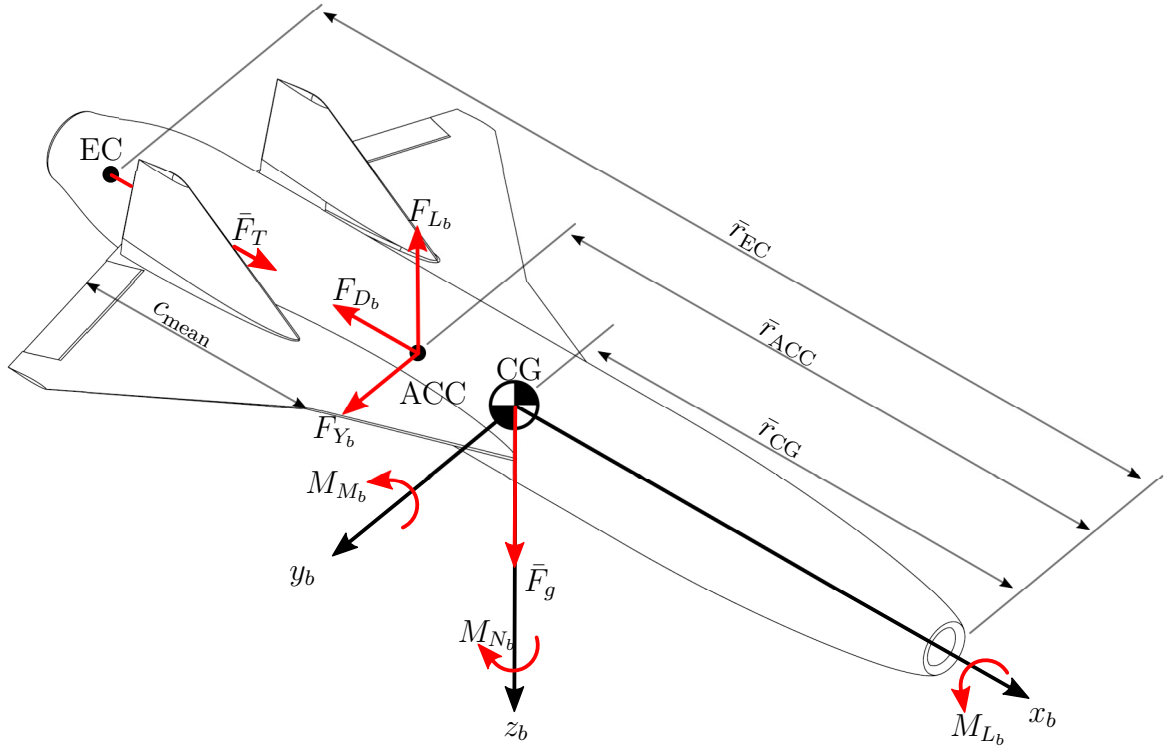


Figure 4.5: MUFASA free body diagram.

The aerodynamic forces (F_{L_b} , F_{Y_b} , F_{D_b}) and moments (M_{L_b} , M_{M_b} , M_{N_b}) are computed from nondimensional aerodynamic coefficients as denoted by Eqs. 4.11 and 4.12 (Stevens et al., 2015). Aerodynamic forces are computed via Eq. 4.11:

$$\bar{\mathbf{F}}_{\text{aero}} = \begin{bmatrix} F_{D_b} \\ F_{Y_b} \\ F_{L_b} \end{bmatrix} = \frac{1}{2} \rho V_a^2 S R_w^b \begin{bmatrix} -C_D \\ C_Y \\ -C_L \end{bmatrix} \quad (4.11)$$

where ρ , S , C_L , C_D and C_Y represent the air density, aircraft planform area, and the nondimensional aerodynamic coefficient of lift, drag, and sideforce force, respectively. In turn, the moments due to the control surface deflections and wind perturbations about the body frame are computed via Eq. 4.12:

$$\begin{bmatrix} M_{L_b} \\ M_{M_b} \\ M_{N_b} \end{bmatrix} = \frac{1}{2} \rho V_a^2 S c_{\text{mean}} \begin{bmatrix} C_l \\ C_m \\ C_n \end{bmatrix} \quad (4.12)$$

where c_{mean} , C_l , C_m and C_n represent the Mean Aerodynamic Chord (MAC) (see Fig. 4.5), and the nondimensional aerodynamic coefficient of roll, pitch, and yaw moment, respectively. Each of the corresponding three forces (F_{L_b} , F_{D_b} , F_{Y_b}) and moments (M_{L_b} , M_{M_b} , M_{N_b}) occur at one of three locations: i) the aircraft's CG, ii) the aircraft's Engine Centre (EC), or iii) the aircraft's Aerodynamic Coefficient Centre (ACC). The location of the CG, EC, and ACC with respect to the aircraft's body frame for the MUFASA UAV are represented by positional vectors \bar{r}_{CG} , \bar{r}_{EC} , and \bar{r}_{ACC} , respectively (Fig. 4.5). It must be noted that all such positional vectors originate at the tip of the aircraft's nose. The summation of all aerodynamic moments and forces are consolidated into $\bar{\mathbf{M}}_{\text{aero}}$ and computed via Eq. 4.13 (Stevens et al., 2015) where \times denotes a cross-product operation.

$$\bar{M}_{\text{aero}} = \begin{bmatrix} M_{L_b} \\ M_{M_b} \\ M_{N_b} \end{bmatrix} + \bar{F}_{\text{aero}} \times (\bar{r}_{\text{CG}} - \bar{r}_{\text{ACC}}) \quad (4.13)$$

Each of the six nondimensional aerodynamic coefficients (C_{\square}) in Eqs. 4.11 and 4.12 are a function of the aircraft's aerodynamic shape, airspeed velocity, angular rates, and control surface deflections. These dependencies are mathematically represented via the component build-up method as described in Beard and McLain (2012) and denoted by Eqs. 4.14 to 4.19:

$$C_L = C_{L_0} + C_{L_\alpha} \alpha + C_{L_Q} \frac{c_{\text{mean}}}{2V_a} Q + C_{L_{\delta_e}} \delta_e \quad (4.14)$$

$$C_D = C_{D_0} + C_{D_{\alpha^2}} \alpha^2 + C_{D_Q} \frac{c_{\text{mean}}}{2V_a} Q + C_{D_{\delta_e^2}} \delta_e^2 + C_F \quad (4.15)$$

$$C_m = C_{m_0} + C_{m_\alpha} \alpha + C_{m_Q} \frac{c_{\text{mean}}}{2V_a} Q + C_{m_{\delta_e}} \delta_e \quad (4.16)$$

$$C_Y = C_{Y_0} + C_{Y_\beta} \beta + C_{Y_P} \frac{c_{\text{mean}}}{2V_a} P + C_{Y_R} \frac{c_{\text{mean}}}{2V_a} R + C_{Y_{\delta_a}} \delta_a + C_{Y_{\delta_r}} \delta_r \quad (4.17)$$

$$C_l = C_{l_0} + C_{l_\beta} \beta + C_{l_P} \frac{c_{\text{mean}}}{2V_a} P + C_{l_R} \frac{c_{\text{mean}}}{2V_a} R + C_{l_{\delta_a}} \delta_a + C_{l_{\delta_r}} \delta_r \quad (4.18)$$

$$C_n = C_{n_0} + C_{n_\beta} \beta + C_{n_P} \frac{c_{\text{mean}}}{2V_a} P + C_{n_R} \frac{c_{\text{mean}}}{2V_a} R + C_{n_{\delta_a}} \delta_a + C_{n_{\delta_r}} \delta_r \quad (4.19)$$

where each of the six nondimensional aerodynamic coefficients is a function of its nominal value indicated by a subscript zero (C_{\square_0}), and a collection of partial derivatives indicated by their respective subscript ($C_{\square\square}$) (Beard and McLain, 2012). As a result, each of the six aerodynamic coefficients is treated as the sum of its partial derivatives with respect to certain variable combinations of interest. Such combinations and the corresponding variables of interest have been determined by previous work (Beard and McLain, 2012; Grauer and Morelli, 2015; Tyan et al., 2018). However, for such a method to be applicable to the MUFASA aircraft the mathematical representation of the drag component build-up method (Eq. 4.15) has been modified from Beard and McLain (2012). Drag is a significant parameter

when evaluating supersonic aircraft (Morgan, 1972), and a significant limiting factor for SSUAVs due to limited thrust generation options (Dalman et al., 2021). Due to nonlinearity observed the drag coefficient with respect to AOA ($C_{D_{\alpha^2}}$) and elevator deflection ($C_{D_{\delta_e^2}}$) were set as a function of AOA squared (α^2) and elevator deflection squared (δ_e^2), respectively to better model drag due to manoeuvres. The drag coefficient is also set as a function of the aircraft’s skin friction coefficient (C_F) as indicated via Eq. 4.20.

$$C_F = \frac{0.455}{(\log(Re))^{2.58}} (1 + 0.15M^2)^{-0.58 \frac{S_{\text{wet}}}{S}} \quad (4.20)$$

The terms Re , M , and S_{wet} in Eq. 4.20 represent the Reynolds number, Mach number, and the aircraft’s wetted surface area, respectively. As indicated by Dalman (2021), the source of Eq. 4.20 is unknown, however, it sees common use in industry. The skin friction coefficient is used to account for viscous effects not considered in the inviscid CFD method used to compute the required aerodynamic coefficients (Mavriplis et al., 2022).

4.3.3 Nondimensional Aerodynamic Coefficients

All of the 30 required aerodynamic coefficients needed to calculate forces and moments were acquired through the use of two open-source software programs, OpenVSP and SU2. Previous work has shown that both of these software are applicable and compatible for evaluating supersonic aircraft (Guillermo-Monedero, 2020; MacDonald et al., 2017; Tyan et al., 2018).

OpenVSP is a vortex-lattice method based software tool which provides aerodynamic coefficient data within the aircraft’s linear regime of flight (Mavriplis et al., 2022) via a submodule called VSPAERO (Tyan et al., 2018). An aircraft’s linear regime is defined as the flight region where aerodynamic coefficient partial derivatives are linear and excludes nonlinear effects such as aerodynamic stall (Mavriplis et al., 2022). SU2 is an open-source software suite for computational fluid dynamics analysis and design (Economou et al., 2016),

which has proven pivotal in high-speed aircraft design (Viviani et al., 2021). Compressible Euler finite volume CFD run in SU2 has been used to compute results across the flight regime of both supersonic aircraft and SSUAVs (Economon et al., 2016; Palacios et al., 2013; Stoldt et al., 2021). Previous work by Stoldt et al. (2021) and Dalman et al. (2021) has verified the use of SU2 compressible Euler for the aerodynamic analysis of supersonic delta-wing aircraft. Stoldt et al. (2021) determined SU2 is capable of modelling delta-wing aerodynamic vortices with an average disagreement from experiments of less than 4%. Meanwhile, Dalman et al. (2021) determined that SU2 compressible Euler is capable of modelling a delta-wing aircraft with a relative coefficient of drag error of 3.3% compared to Reynolds-averaged Navier-Stokes CFD. Note, SU2 (version 6.2.0) defines a positive sideslip angle as opposite to the convention presented in Fig. 4.2, necessitating a correction be applied to all sideslip coefficients (C_{\square_β}). While OpenVSP is capable of generating all the required aerodynamic coefficients, unlike SU2, it is not considered a high-fidelity solver and has larger relative error when compared to experiments (Dalman et al., 2021; MacDonald et al., 2017; Stoldt et al., 2021; Tyan et al., 2018). Due to its lower fidelity, OpenVSP is only used to obtain aerodynamic coefficients not readily outputted by SU2 (Tyan et al., 2018). The complete list of which of MUFASA’s aerodynamic coefficients were determined by which program is presented in Table 4.1.

Table 4.1: Aerodynamic analysis software tools used to determine the aerodynamic coefficients of interest.

Program	Coefficients Determined							
OpenVSP	C_{L_Q}	C_{D_Q}	C_{m_Q}	C_{Y_P}	C_{l_P}	C_{n_P}	C_{Y_R}	C_{l_R}
	C_{n_R}	$C_{L_{\delta e}}$	$C_{D_{\delta e 2}}$	$C_{m_{\delta e}}$	$C_{Y_{\delta a}}$	$C_{l_{\delta a}}$	$C_{n_{\delta a}}$	
SU2	C_{L_0}	C_{D_0}	C_{m_0}	C_{Y_0}	C_{l_0}	C_{n_0}	C_{L_α}	$C_{D_{\alpha^2}}$
	C_{m_α}	C_{Y_β}	C_{l_β}	C_{n_β}	$C_{Y_{\delta r}}$	$C_{l_{\delta r}}$	$C_{n_{\delta r}}$	

OpenVSP was used to generate surface meshes required to run SU2 compressible Euler finite volume CFD. Two meshes were generated, a mesh along the UAV’s surface (Fig. 4.6a) and another rectangular domain mesh (Fig. 4.6b) that bounds the simulation centred about the UAV (Fig. 4.6).

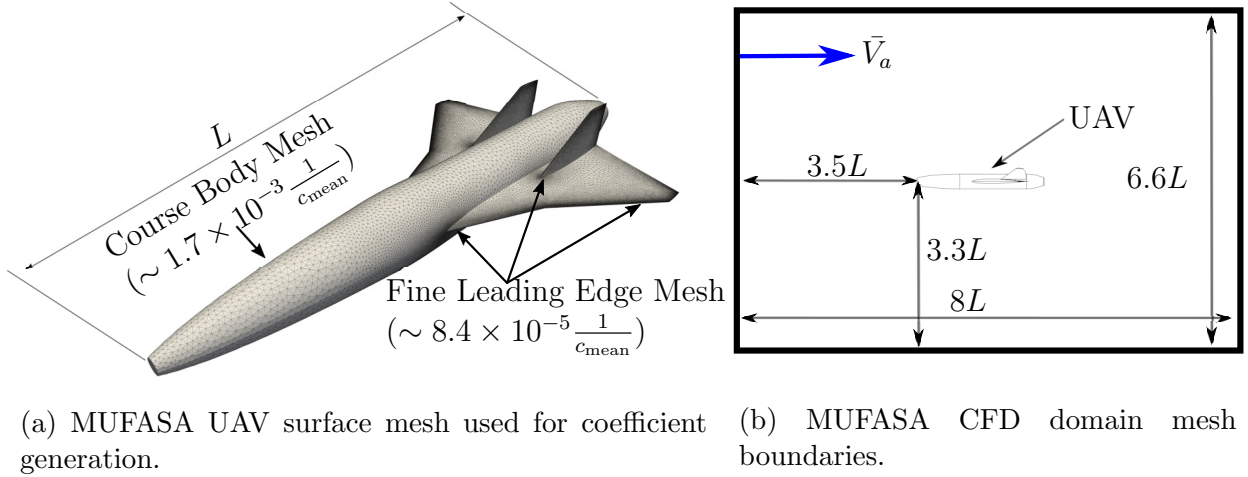


Figure 4.6: MUFASA surface mesh and domain.

An image of the OpenVSP UAV surface mesh used for aerodynamic coefficient generation is presented in Fig. 4.6a. Note that approximate mesh sizing values are normalized against the UAV's MAC. The domain mesh (Fig. 4.6b) was designed relative to MUFASA as per body length (L) scaling factors in Table 4.2. The software tool *Gmsh* (Geuzaine and Remacle, 2009) was then used to connect the two mesh surfaces and generate a full-volume mesh. This full-volume mesh consists of twenty-three million elements and is used by SU2 to model the environment surrounding the UAV.

Table 4.2: Far-field mesh size scaling parameters based on the aircraft geometry evaluated.

Dimension	UAV Axis	Body Length Scaling Factor
Length	x_b	8.0
Width	y_b	4.1
Height	z_b	6.6

4.3.4 Propulsion Forces and Moments

The thrust force is determined based on the engine model. As the physical design of a supersonic MUFASA UAV is ongoing, at the time of this writing the engine data for thermodynamic modelling is unavailable. However, in order to incorporate engine behaviour

as a function of speed and altitude, the thrust force and thrust coefficient are calculated using Eqs. 4.21 and 4.22 (Stengel, 2015), respectively which represent theoretical behaviour associated with a turbojet.

$$\bar{F}_T = C_T S \rho V_a^2 \frac{1}{2} \begin{bmatrix} 1 \\ 0 \\ 0 \end{bmatrix} \quad (4.21)$$

$$C_T = (k_0 + k_1 V_a^{-2}) \delta_T \quad (4.22)$$

The thrust coefficient (C_T) in Eq. 4.22 is a function of the maximum-throttle coefficient (k_0), velocity dependence coefficient (k_1), and throttle setting (δ_T). The maximum-throttle coefficient and velocity dependence coefficient are back-calculated based on the engine maximum static thrust. The throttle setting ranges from 0-1, representing no thrust to full throttle. The engine dynamics are modelled as a first-order system as seen in Eq. 4.23 (Gryte, 2015).

$$\frac{\delta_T}{\delta_{Td}} = \frac{1}{(0.2)s + 1} \quad (4.23)$$

The moment due to thrust is determined by the location of the engine in the body coordinate frame as per Eq. 4.24 (see Fig. 4.5). This equation allows for future simulation of internally or externally mounted engine configurations.

$$\bar{M}_T = \bar{F}_T \times (\bar{r}_{EC} - \bar{r}_{CG}) \quad (4.24)$$

4.3.5 Gravitational Forces

The SSUAV mass was treated as a point mass located at the aircraft's CG. As mentioned in Constraint 5 in Chapter 3, gravity (g) and the aircraft mass (m) were modelled as constants. The force due to gravity in the body frame requires a rotation from the vehicle frame (R_v^b),

and is represented by Eq. 4.25 (Stevens et al., 2015).

$$\bar{F}_g = R_v^b \begin{bmatrix} 0 \\ 0 \\ mg \end{bmatrix} \quad (4.25)$$

4.4 Mathematical Model Summary

Combining Sections 4.1 through to 4.3, a high level representation of the nonlinear UAV mathematics is represented by Eqs. 4.6, 4.7, 4.26, and 4.27. Complete aerodynamic forces and moments used in Eqs. 4.26 and 4.27 are compiled and computed via Eqs. 4.28 and 4.29.

The aircraft's state is defined by its state vector (\bar{x}) which represents the aircraft's velocity, angular rates, orientation angles, and position (shown below). The aircraft's control surfaces and throttle are defined by its control input vector (\bar{u}) which represents the aileron, elevator, port vertical stabilator, and starboard vertical stabilator deflection angles, along with the throttle setting (shown below). This nonlinear mathematical model can now be incorporated into a program to facilitate 6-DOF simulations.

$$\bar{x} = \begin{bmatrix} U \\ V \\ W \\ P \\ Q \\ R \\ \phi \\ \theta \\ \psi \\ \Lambda_N \\ \Lambda_E \\ \Lambda_D \end{bmatrix}$$

$$\bar{u} = \begin{bmatrix} \delta_a \\ \delta_e \\ \delta_{ptvs} \\ \delta_{sbvs} \\ \delta_T \end{bmatrix}$$

$$\begin{bmatrix} \dot{U} \\ \dot{V} \\ \dot{W} \end{bmatrix} = \frac{1}{m} \begin{pmatrix} \begin{bmatrix} 0 \\ R_v^b \\ 0 \end{bmatrix} mg \\ 0 + (k_0 + k_1 V_a^{-2}) \delta_T S \rho V_a^2 \frac{1}{2} \\ 0 \end{pmatrix} + \bar{F}_{\text{aero}} \begin{pmatrix} \begin{bmatrix} 1 \\ 0 \\ 0 \end{bmatrix} \\ \begin{bmatrix} P \\ Q \\ R \end{bmatrix} \times \\ \begin{bmatrix} U \\ V \\ W \end{bmatrix} \end{pmatrix} \quad (4.26)$$

$$\begin{bmatrix} \dot{P} \\ \dot{Q} \\ \dot{R} \end{bmatrix} = \begin{bmatrix} I_{xx} & 0 & I_{xz} \\ 0 & I_{yy} & 0 \\ I_{xz} & 0 & I_{zz} \end{bmatrix}^{-1} \left(\begin{pmatrix} \begin{bmatrix} 1 \\ 0 \\ 0 \end{bmatrix} \\ (k_0 + k_1 V_a^{-2}) \delta_T S \rho V_a^2 \frac{1}{2} \\ 0 \end{pmatrix} \times (\bar{r}_{\text{EC}} - \bar{r}_{\text{CG}}) + \bar{M}_{\text{aero}} \right) \quad (4.27)$$

$$\bar{F}_{\text{aero}} = \frac{1}{2} \rho V_a^2 S R_w^b \begin{bmatrix} - \left(C_{D_0} + C_{D_{\alpha^2}} \alpha^2 + C_{D_Q} \frac{c_{\text{mean}}}{2V_a} Q + C_{D_{\delta_e^2}} \delta_e^2 + \frac{0.455}{(\log(R_e))^{2.58}} (1 + 0.15M^2)^{-0.58} \frac{S_{\text{wet}}}{S} \right) \\ C_{Y_0} + C_{Y_\beta} \beta + C_{Y_P} \frac{c_{\text{mean}}}{2V_a} P + C_{Y_R} \frac{c_{\text{mean}}}{2V_a} R + C_{Y_{\delta_a}} \delta_a + C_{Y_{\delta_r}} \delta_r \\ - \left(C_{L_0} + C_{L_\alpha} \alpha + C_{L_Q} \frac{c_{\text{mean}}}{2V_a} Q + C_{L_{\delta_e}} \delta_e \right) \end{bmatrix} \quad (4.28)$$

$$\bar{M}_{\text{aero}} = \frac{1}{2} \rho V_a^2 S C_{\text{mean}} \begin{bmatrix} C_{l_0} + C_{l_\beta} \beta + C_{l_P} \frac{c_{\text{mean}}}{2V_a} P + C_{l_R} \frac{c_{\text{mean}}}{2V_a} R + C_{l_{\delta_a}} \delta_a + C_{l_{\delta_r}} \delta_r \\ C_{m_0} + C_{m_\alpha} \alpha + C_{m_Q} \frac{c_{\text{mean}}}{2V_a} Q + C_{m_{\delta_e}} \delta_e \\ C_{n_0} + C_{n_\beta} \beta + C_{n_P} \frac{c_{\text{mean}}}{2V_a} P + C_{n_R} \frac{c_{\text{mean}}}{2V_a} R + C_{n_{\delta_a}} \delta_a + C_{n_{\delta_r}} \delta_r \end{bmatrix} + \bar{F}_{\text{aero}} \times (\bar{r}_{\text{CG}} - \bar{r}_{\text{ACC}}) \quad (4.29)$$

4.5 Mathematical Model Discretization

To facilitate the flying quality parameter identification, the continuous nonlinear mathematical model shown in Eqs. 4.6, 4.7, 4.26, and 4.27 was evaluated at multiple flight conditions and discretized into multiple flight states. The flight states were initialized using trim conditions and then linearized to obtain a state-space representation of the MUFASA SSUAV. The linear state-space model was then used to identify flying quality parameters. These procedures are detailed in the following subsections.

4.5.1 Model Trimming

Trim conditions provide simulations with initial input conditions, aid in determining the limits of the flight regime, and allow for easy comparison between different model implementations (De Marco et al., 2007). A trim condition, or steady-state operating point, includes state and control variables that do not change with time. When searching for a trim condition the UAV's state vector (excluding the UAV's NED position) and control input vector derivatives were first initialized to zero. Motion constraints were applied to the control inputs to ensure the trim condition was realizable. The trim condition was specified by setting a desired airspeed, altitude, and climb angle (γ). Airspeed and altitude were set based on the trim point desired. In this work the climb angle was set to zero, effectively trimming the aircraft for steady-state straight-and-level flight. The climb angle is computed using Eq. 4.30 (Stevens et al., 2015), and is the angle relating an aircraft's vertical and horizontal velocity in the vehicle frame.

$$\gamma = \text{atan2} \left(-\dot{\Lambda}_D, \sqrt{\dot{\Lambda}_N^2 + \dot{\Lambda}_E^2} \right) \quad (4.30)$$

With the initial conditions and trim condition specified the MUFASA aircraft was trimmed using the MATLAB operating point optimization function *findop* (MathWorks, 2021c). Multiple trim conditions were generated throughout the SSUAV's flight regime to facilitate anal-

ysis in Chapter 6.

4.5.2 Model Linearization

In order to apply classical linear control and evaluation methods a linear model of the non-linear mathematical model of the aircraft was calculated (Beard and Mclain, 2012; Sebbane, 2015). A numerical linearization approach was used at a time step of 0.001s (Stevens et al., 2015; Wienke, 2011). The MATLAB *linearize* function was used to linearize the Simulink model block-by-block for an exact discretization in the time domain at the trim point specified. The *linearize* function obtains a linear equation using a Taylor series expansion. The partial derivatives of the resulting Jacobian's were resolved using the forward difference quotient (MathWorks, 2021b). The result was a nominal generic state-space matrix representation of the form seen in Eq. 4.31 (Stevens et al., 2015), where A represents the state matrix while B represents the input matrix.

$$\dot{\bar{x}} = A\bar{x} + B\bar{u} \quad (4.31)$$

State and input matrices were obtained for multiple trimmed operating conditions throughout the SSUAV's flight regime. An example state and input matrix describing MUFASA during steady-state, straight-and-level flight at a speed of $350\frac{\text{m}}{\text{s}}$, altitude of 4km, and climb angle of zero is shown below. The flight speed and altitude are MUFASA's approximate cruise conditions. The columns of the state and input matrices correspond to the state and control input vectors presented in Section 4.4. With regards to units within the state vector, base SI units were used, so for example all angles are measured in radians and all linear speeds in meters-per-second.

$$A = \begin{bmatrix} -0.3494 & 0 & 0.2302 & 0 & -5.3200 & 0 & 0 & -9.8088 & 0 & 0 & 0 & 0.0002 \\ 0 & -1.6314 & 0 & 5.8447 & 0 & -348.4194 & 9.8088 & 0 & 0 & 0 & 0 & 0 \\ -0.4333 & 0 & -13.9148 & 0 & 340.6196 & 0 & 0 & -0.1531 & 0 & 0 & 0 & 0.0015 \\ 0 & 0.2900 & 0 & -57.7856 & 0 & -7.2308 & 0 & 0 & 0 & 0 & 0 & 0 \\ -2.5685 & 0 & -76.1866 & 0 & -83.0839 & 0 & 0 & 0 & 0 & 0 & 0 & 0.0163 \\ 0 & 4.3996 & 0 & -2.5545 & 0 & -10.3648 & 0 & 0 & 0 & 0 & 0 & 0 \\ 0 & 0 & 0 & 1 & 0 & 0.0156 & 0 & 0 & 0 & 0 & 0 & 0 \\ 0 & 0 & 0 & 0 & 1 & 0 & 0 & 0 & 0 & 0 & 0 & 0 \\ 0 & 0 & 0 & 0 & 0 & 1.0001 & 0 & 0 & 0 & 0 & 0 & 0 \\ 0.9999 & 0 & 0.0156 & 0 & 0 & 0 & 0 & 0 & 0 & 0 & 0 & 0 \\ 0 & 1 & 0 & 0 & 0 & 0 & -5.4632 & 0 & 350 & 0 & 0 & 0 \\ -0.0156 & 0 & 0.9999 & 0 & 0 & 0 & 0 & -350 & 0 & 0 & 0 & 0 \end{bmatrix}$$

$$B = \begin{bmatrix} 0 & 11.8448 & 0 & 0 & 167.1692 \\ -156.9727 & 0 & 268.0861 & 268.0861 & 0 \\ 0 & -722.0763 & 0 & 0 & 0 \\ 18557.7717 & 0 & 18.5602 & 18.5602 & 0 \\ 0 & -8028.7151 & 0 & 0 & 0 \\ 1808.5112 & 0 & 1859.5868 & 1859.5868 & 0 \\ 0 & 0 & 0 & 0 & 0 \\ 0 & 0 & 0 & 0 & 0 \\ 0 & 0 & 0 & 0 & 0 \\ 0 & 0 & 0 & 0 & 0 \\ 0 & 0 & 0 & 0 & 0 \\ 0 & 0 & 0 & 0 & 0 \end{bmatrix}$$

4.5.3 Flying Quality Parameters

The response characteristic of each flying quality parameter, short period, phugoid, roll subsidence, Dutch-Roll, and spiral, were determined by manipulating the state matrix A and isolating longitudinal and lateral responses. A similarity matrix J was used to rearrange the state matrix into longitudinal and lateral modal responses, represented by A_{long} and A_{lat} , respectively. The formulation used to calculate the longitudinal and lateral state matrices is presented in Eq. 4.32 (Stevens et al., 2015).

$$J = \begin{bmatrix} 1 & 0 & 0 & 0 & 0 & 0 & 0 & 0 & 0 & 0 & 0 & 0 \\ 0 & 0 & 1 & 0 & 0 & 0 & 0 & 0 & 0 & 0 & 0 & 0 \\ 0 & 0 & 0 & 0 & 1 & 0 & 0 & 0 & 0 & 0 & 0 & 0 \\ 0 & 0 & 0 & 0 & 0 & 0 & 0 & 1 & 0 & 0 & 0 & 0 \\ 0 & 1 & 0 & 0 & 0 & 0 & 0 & 0 & 0 & 0 & 0 & 0 \\ 0 & 0 & 0 & 1 & 0 & 0 & 0 & 0 & 0 & 0 & 0 & 0 \\ 0 & 0 & 0 & 0 & 0 & 1 & 0 & 0 & 0 & 0 & 0 & 0 \\ 0 & 0 & 0 & 0 & 0 & 0 & 1 & 0 & 0 & 0 & 0 & 0 \\ 0 & 0 & 0 & 0 & 0 & 0 & 0 & 1 & 0 & 0 & 0 & 0 \\ 0 & 0 & 0 & 0 & 0 & 0 & 0 & 0 & 1 & 0 & 0 & 0 \\ 0 & 0 & 0 & 0 & 0 & 0 & 0 & 0 & 0 & 1 & 0 & 0 \\ 0 & 0 & 0 & 0 & 0 & 0 & 0 & 0 & 0 & 0 & 1 & 0 \end{bmatrix}$$

$$\begin{bmatrix} \begin{array}{c|cccc} & 0 & 0 & 0 & 0 \\ \hline A_{\text{long}} & 0 & 0 & 0 & 0 \\ & 0 & 0 & 0 & 0 \\ & 0 & 0 & 0 & 0 \\ & 0 & 0 & 0 & 0 \end{array} & & \\ \hline & & \begin{array}{c|cccc} & 0 & 0 & 0 & 0 \\ \hline & 0 & 0 & 0 & 0 \\ & 0 & 0 & 0 & 0 \\ & 0 & 0 & 0 & 0 \\ & 0 & 0 & 0 & 0 \end{array} & \\ \hline \begin{array}{c|cccc} 0 & 0 & 0 & 0 \\ \hline 0 & 0 & 0 & 0 \\ 0 & 0 & 0 & 0 \end{array} & & \end{bmatrix} = JAJ^{-1} \quad (4.32)$$

The eigenvalues of the longitudinal (A_{long}) and lateral (A_{lat}) state matrices were computed and assigned to their respective flying quality response. The eigenvalues and the flying qualities they represent are presented in Fig. 4.7 for MUFASA at a trim condition speed of $50 \frac{\text{m}}{\text{s}}$, and an altitude of 4km.

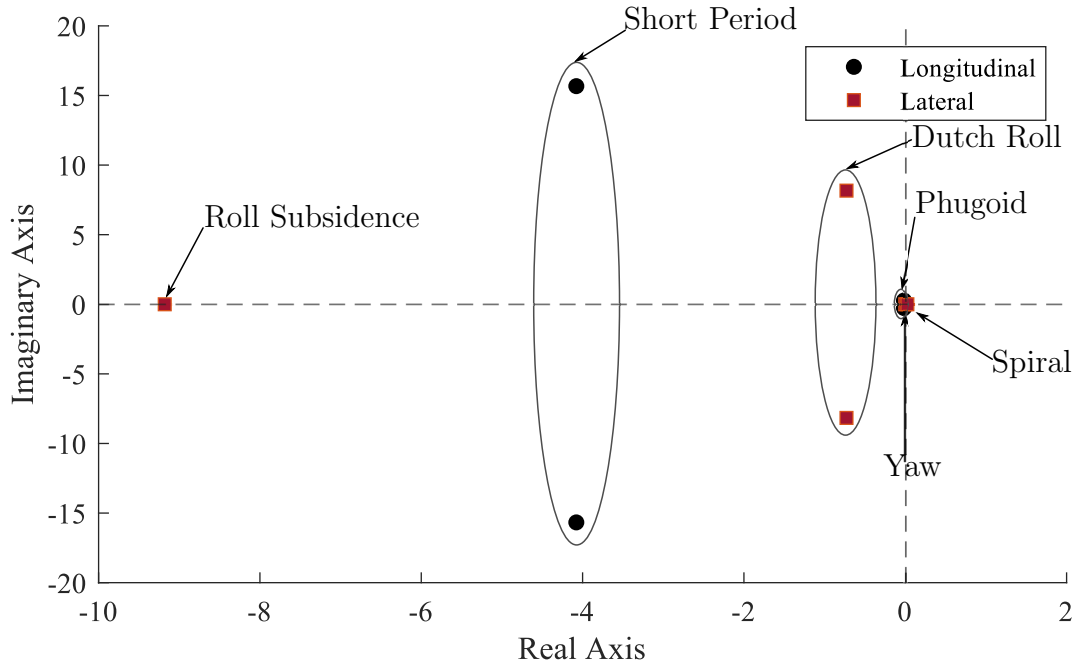


Figure 4.7: Flying quality parameter identification. Poles obtained for MUFASA during flight at a speed of $50 \frac{\text{m}}{\text{s}}$, and an altitude of 4km.

Longitudinal eigenvalues generally are two complex conjugate pairs, with the more negative real pair being the short period mode and the more positive real pair being the phugoid mode (labelled in Fig. 4.7). Complex conjugate pairs indicate an oscillatory modal response

of the mode they are associated to. If one longitudinal eigenvalue complex conjugate pair does not exist and both poles instead lie on the real axis, then that mode is critically damped and exhibits non-oscillatory behaviour. If both poles exist on the real axis in the left half plane, then the mode is stable and the more negative pole is used to calculate the modal properties. If both poles exist on the real axis, one in the left half plane and one in the right half plane, then the mode is unstable and the unstable positive pole is used to calculate the modal properties (Campos and Marques, 2021; Cook, 2012). All lateral eigenvalues occur on the real axis and are critically damped but for one complex conjugate pair which represents the Dutch-Roll mode (labelled in Fig. 4.7). The one eigenvalue at the origin is related to the yaw angle and does not represent any specific mode. Finally, the most negative and positive remaining lateral eigenvalues represent the roll subsidence and spiral mode respectively.

With all eigenvalues determined and assigned to their respective modal parameter, the flying qualities (natural frequency and damping ratio) of each eigenvalue were calculated. From the natural frequency and damping ratio the time constant and time-to-double was calculated for each mode using Eqs. 2.1 and 2.2, respectively. This procedure was applied to multiple steady-state conditions throughout MUFASA's flight regime to assess its flying qualities.

Chapter 5

Flight Dynamics Simulation

The mathematical model was implemented into the MATLAB & Simulink environment to facilitate simulations and data collection. The mathematical model simulation allows for analysis of MUFASA's flying qualities at trim conditions throughout its flight regime. The simulation structure is also generalized so the control perturbation response of different fixed-wing aircraft can be recorded and compared to facilitate comparative vehicle handling characteristics.

5.1 Simulation Structure

The simulation structure presented in Fig. 5.1 was developed to allow for the evaluation of fixed-wing aircraft (including supersonic and subsonic vehicles). By specifying the desired control inputs the vehicle's state was computed throughout its flight regime (shaded red hexagons in Fig. 5.1). All aircraft constants such as mass, inertia, motion constraints, and MAC are stored in a general *Constants* file (Fig. 5.1) which is distributed around the Simulink model. Tables 5.1, 6.2, and 6.3 provide a list of parameters used by the simulation to describe the environment and the MUFASA aircraft.

Aerodynamic coefficients listed in Table 4.1 are fed into Simulink as a constant 30-by-16 array organized by Mach number as presented in Appendix A, Tables A.1 to Table A.3. Inputting

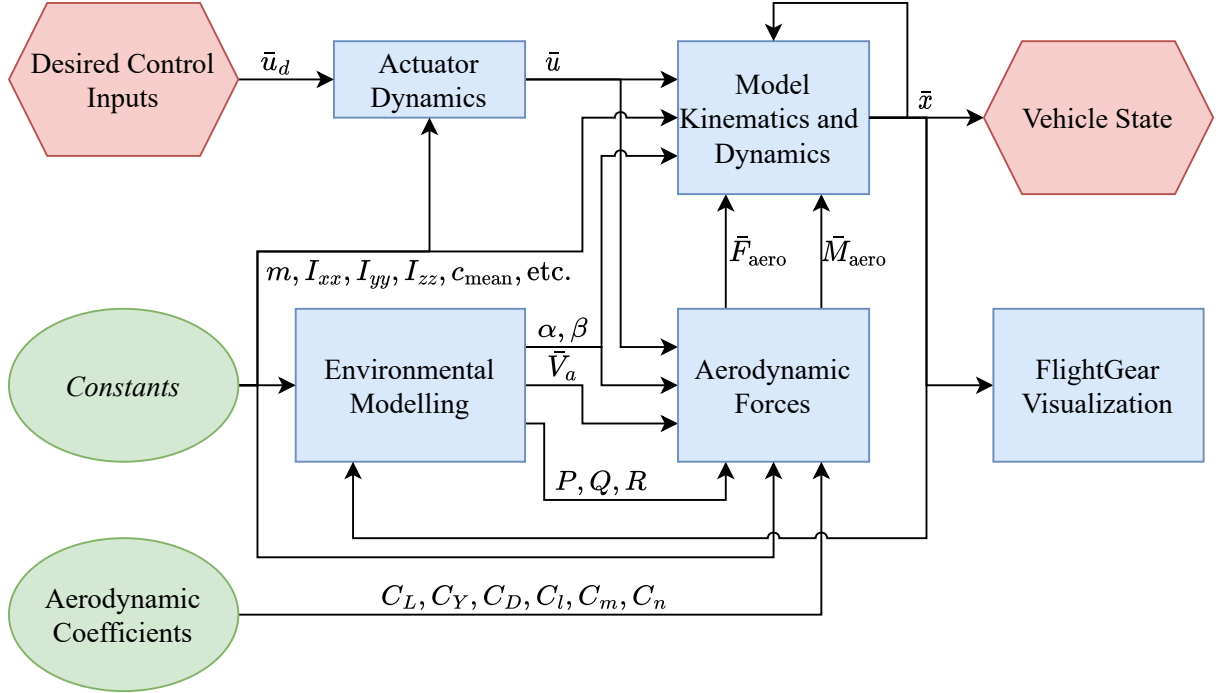


Figure 5.1: MUFASA Simulink simulation implementation.

Table 5.1: Simulation parameters.

Parameter	Value
Gravity ($\frac{\text{m}}{\text{s}^2}$)	9.81
Initial Longitude ($^\circ$)	-157.93
Initial Latitude ($^\circ$)	21.32
Initial State Vector (various)	\bar{x}
Initial Controls Vector (various)	\bar{u}

a file full of constant aircraft parameters and an aerodynamic coefficient array (shaded green ovals in Fig. 5.1) allows for various fixed-wing aircraft to be quickly simulated without requiring any changes to the base simulation framework. The simulation set up allows for an easier interface with the Flight Dynamics Model Exchange Standard (American Institute of Aeronautics and Astronautics, 2016) for vehicle simulation validation cases. The five main structural components of the Simulink model are presented as blue boxes in Fig. 5.1. Each of these five components and the information they transfer are described in the following

subsections.

5.1.1 Actuator Dynamics

Five actuators are used to control the SSUAV: four control surface actuators (i.e., two elevons and two vertical stabilizers) to control the aircraft’s attitude (Fig 1.2), and one motor to control the engine thrust. The actuator dynamics block (Fig. 5.1) receives the desired control inputs in the form of a desired control vector, \bar{u}_d , and outputs a control vector, \bar{u} , that is physically realizable. The actuator model takes into account the physical motor constraints by limiting the deflection rates and maximum deflection angles as specified in the *Constants* file. The aerodynamic control surface and engine model dynamics are modelled via Eqs. 4.10 and 4.23, respectively. MUFASA’s actuator deflection and rate limitations are provided in Section 6.2. It is important to note, while the commanded signals use elevator and aileron deflections, motion constraints have been applied to the elevon control surfaces of the delta-wing UAV. This switching requires the pitch and roll controls be continually mapped between the general aileron/elevator and elevon representations using Eq. 4.8.

5.1.2 Environmental Modelling

An environmental model was developed to calculate the aerodynamic forces and moments experienced by an aircraft in the Earth’s atmosphere. Based on the aircraft’s state, \bar{x} , physical constants such as atmospheric air density, temperature (t), and speed of sound (a) at various altitudes were calculated using the COESA Atmospheric model (MathWorks, 2021a; National Oceanic and Atmospheric Administration et al., 1976). Mach and Reynolds number changes associated with a vehicle’s altitude variation were calculated using Eqs. 5.1 (Anderson, 2011) and 5.2 (National Oceanic and Atmospheric Administration et al., 1976).

$$M = \frac{V_a}{a} \tag{5.1}$$

$$Re = \frac{\rho V_a c_{\text{mean}}}{2.791 \times 10^{-7} t^{0.7355}} \quad (5.2)$$

In this work atmospheric wind disturbances were set to zero, meaning the aircraft was effectively flying through a calm atmosphere. To facilitate future disturbance testing on the aircraft, an environmental wind model was implemented by combining a Dryden Turbulence model (Liepmann, 1952) with wind gust and shear models (Department of Defense, 1980) allowing for the creation of custom atmospheric conditions. The disturbances were incorporated into the simulation using a linear field approximation as the gust wavelength was constrained to be at least ten times larger than the UAV wingspan (Etele, 2006). The x , y , and z component of the wind velocity vector were aligned with positive components of the inertial coordinate frame.

The environmental model outputs the airspeed using Eq. 4.2, along with the required aerodynamic parameters such as AOA and sideslip angle. The aerodynamic parameters, as well as the generated angular rates are used as inputs to the aerodynamic forces block (Fig. 5.1).

5.1.3 Aerodynamic Forces

Aerodynamic coefficients are computed using environmental flight conditions from the environmental modelling block (Fig. 5.1), control surface deflections from the actuator dynamics block (Fig. 5.1), and aerodynamic coefficient inputs (Eqs. 4.8 to 4.20). Based on the aircraft's Mach Number the aerodynamic coefficients are obtained from lookup tables generated via CFD data. Such lookup tables are presented in Appendix A. If the needed coefficient value is not defined in the lookup table a linear interpolation process is used between the corresponding lookup table values. Interpolations are linearly computed in alignment with common practice (Stevens et al., 2015). Skin friction drag is then accounted for by considering the aircraft's Reynolds number per Eq. 4.20. The aerodynamic coefficients are then

used to calculate forces and moments in the aircraft’s body frame via Eqs. 4.28 and 4.29. These aerodynamic forces and moments are used in the model kinematics and dynamics block (Fig. 5.1).

5.1.4 Model Kinematics and Dynamics

The Model Kinematics and Dynamics block (Fig. 5.1) is used to calculate the aircraft’s change in state with respect to time represented by Eqs. 4.6, 4.7, 4.26, and 4.27. First the propulsion forces and moments (Eqs. 4.21 to 4.24) and gravitational forces (Eq. 4.25) are calculated using vehicle constants (i.e. engine constants, gravity, mass), aerodynamic parameters such as AOA and sideslip, and thrust input (i.e. δ_T). The calculated propulsion forces and moments are added with the body forces and moments calculated by the *Aerodynamic Forces* block in Fig. 5.1. The aircraft’s change in state is then computed using Eqs. 4.4 to 4.7. The new state of the aircraft is calculated by integrating the change in state over the 0.001s simulation time step via the Simulink integrator block (MathWorks, 2021d).

5.1.5 FlightGear

FlightGear Flight Simulator is used in the current work to both aid in debugging and visualize simulation results. Visualization software such as FlightGear assist with visual verification of manoeuvre correctness (Sagliano, 2021). FlightGear was chosen over other software tools such as XPlane and Microsoft AirSim which are not open source and at the time of this writing do not support fixed-wing aircraft (Craighead et al., 2007). FlightGear uses the JSBSim simulation environment (Berndt, 2004), however, this functionality is overridden in the current application such that all aircraft dynamics are computed in MATLAB/Simulink. Following the procedure presented by Sagliano (2021), the aircraft state vector is transferred to FlightGear from Simulink. A *set pace* block is used in Simulink (MathWorks, 2021e) to ensure that the simulation and FlightGear run together in real time. A visualization of the MUFASA UAV in flight within the FlightGear software environment is presented in Fig. 5.2.

To ease the analysis, the aircraft scene is overlaid with FlightGear's heads up display with variables transferred from Simulink pointed out.

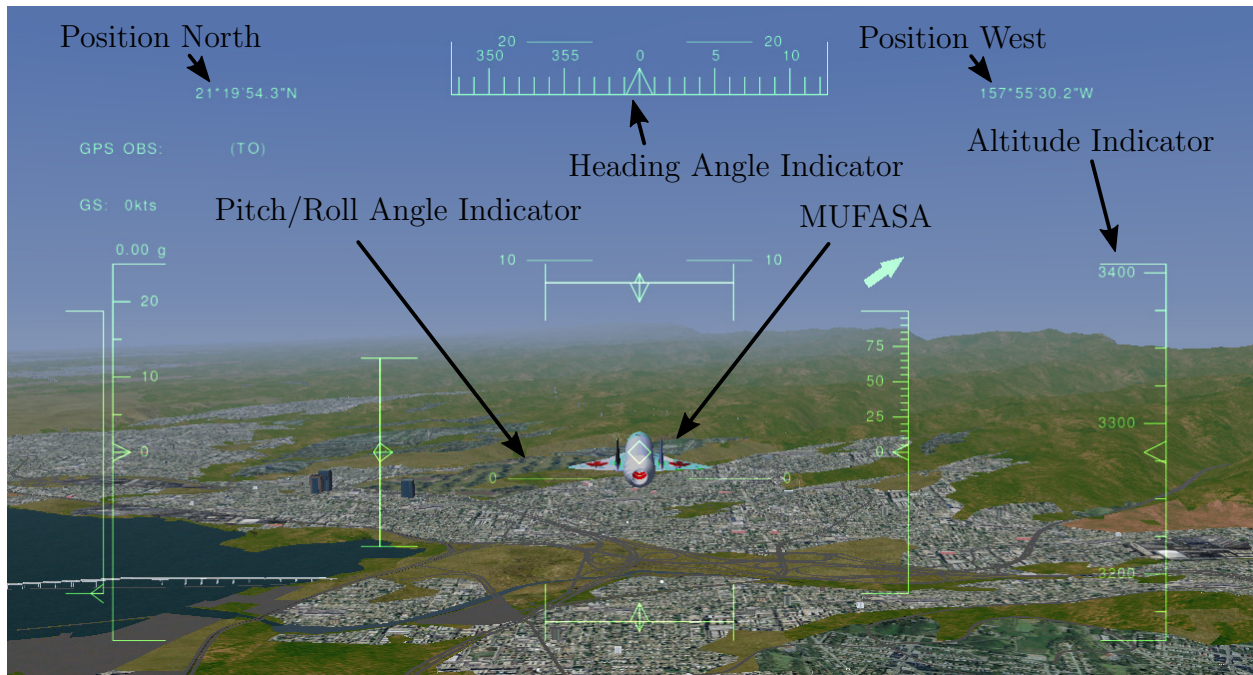


Figure 5.2: FlightGear visualization of the MUFASA model.

Chapter 6

Results

The flying and handling qualities of the MUFASA SSUAV are analyzed in this chapter. First the verification of the mathematical model developed is presented in Section 6.1. The constant parameters used to model the MUFASA SSUAV are presented in Section 6.2. Using Froude scaling, MUFASA is evaluated in Sections 6.3 and 6.4 using the MIL-STD-1797A standard to determine its quantitative flying and handling qualities. Based on the results obtained in Sections 6.3 and 6.4, MUFASA's stability is analyzed and discussed in Section 6.5. The qualitative handling qualities of the MUFASA SSUAV are compared to a range of full-scale and small-scale aircraft in Section 6.6. Sections 6.3 to 6.6 present results followed by a discussion of their relevance.

6.1 Model Verification

Verification of the mathematical model presented in Chapter 4 is presented in this section. Previous simulation verification work by Jackson et al. (2015) has highlighted that modelling even simple vehicles is challenging. Differences in interpretation of the scenario and initial conditions lead to equivalent simulations grouping together, but rarely agreeing with specific numbers (Jackson et al., 2015). To address such challenges three verification procedures were performed. Firstly, a mesh convergence study was performed as described in Section 6.1.1 to

verify the MUFASA CFD results. Secondly, the MUFASA model was subjected to an elevon deflection to evaluate its transient aircraft response as described in Section 6.1.2. Lastly, the flying quality parameters of an F-4 aircraft were calculated using the methodology described in Section 4.5 and compared against results from Heffley and Jewell (1972) and Roskam (2001) in Section 6.1.3.

6.1.1 CFD Case Verification

To verify the aerodynamic coefficient CFD results, a mesh convergence study was performed using the coefficient of drag (Ashton and Skaperdas, 2019) in accordance with the procedure laid out by Eça and Hoekstra (2014). Results were obtained at a cruise flight condition (Mach 1.05) with a zero AOA and zero sideslip angle, using scalable full-volume meshes (discussed in Section 4.3.3) ranging from four to twenty-four million elements. The processed mesh convergence data is presented in Fig. 6.1, with each mesh's grid spacing being normalized about the twenty-three million element mesh grid spacing.

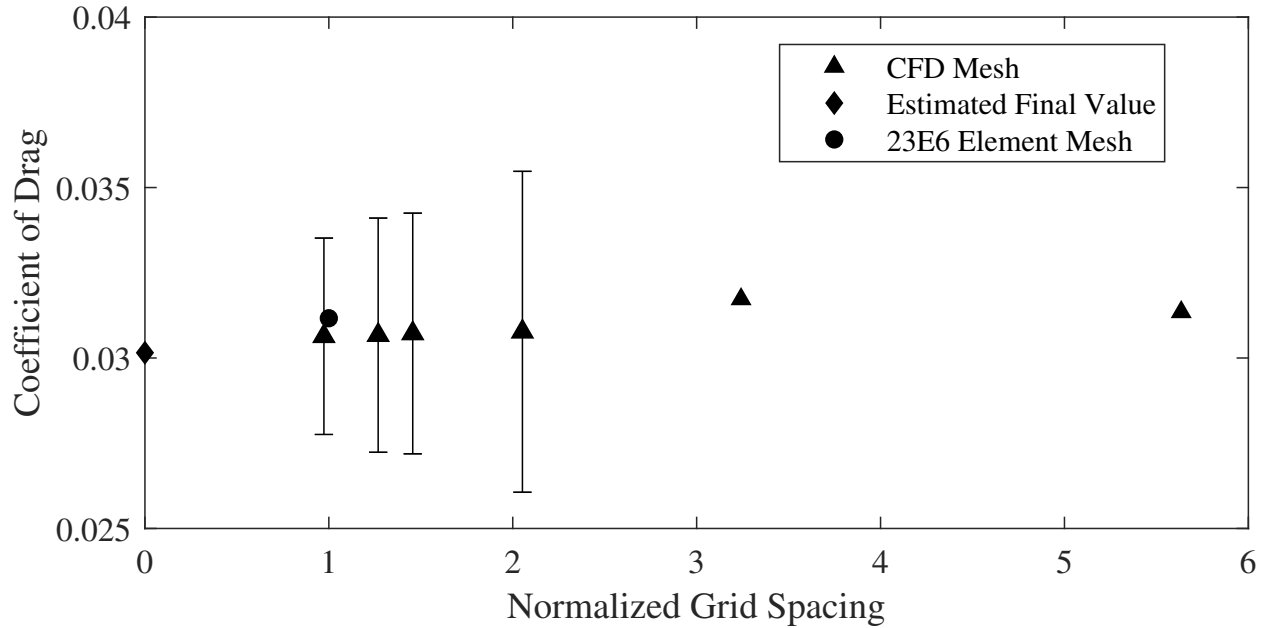


Figure 6.1: MUFASA UAV coefficient of drag mesh convergence study at Mach 1.05, based on the procedure by Eça and Hoekstra (2014).

Error bars in Fig. 6.1 represent the drag coefficient uncertainty for mesh results in the asymptotic range. The asymptotic range in the figure is the region where the mesh results provide a positive order of convergence that facilitates the estimation of a final coefficient of drag value (Eça and Hoekstra, 2014). As observed in the figure, the results of the twenty-three million element mesh for the drag coefficient exist within the uncertainty range of the asymptotic mesh elements. The verified twenty-three million element mesh was then used to obtain the remainder of the aerodynamic coefficients computed using SU2.

6.1.2 Transient Aircraft Response to Elevon Deflection

The mathematical model aircraft simulation based on Eqs. 4.6, 4.7, 4.26, and 4.27 was evaluated by comparing the transient aircraft response against documented generalized fixed-wing aircraft response tendencies identified by Berry and Powers (1970) and Katz (1999). This generalized response evaluation method was pursued as finding a modelled aircraft with associated experimental data using the same combination of vehicle parameters as used in this thesis (*Constants* and Aerodynamic Coefficients in Fig. 5.1) proved difficult due to literature cases having incomplete or different initial conditions or vehicle parameters. This observation is inline with conclusions by Jackson et al. (2015) who noted the non-trivial time required to reconcile vehicle models into a simulation and how they often lead to poor agreement without extensive adjustments to the initial conditions. Multiple runs were performed, and an example of this comparison method is presented in Fig. 6.2. An aerodynamically stable MUFASA model was trimmed for steady-state straight-and-level flight at $350 \frac{\text{m}}{\text{s}}$ (Mach 1.08) and at an altitude of 4km. At this trim state both elevons are negatively deflected. At 0.5s the port elevon was set to a deflection angle of zero (lowered), exposing only the starboard elevon to the airflow. Elevon deflection with time is presented in Fig. 6.2a, while a diagram of the final state is shown in Fig. 6.2d.

Intuitively a starboard elevon deflection should lead to a coupled longitudinal and lateral response causing a deviation in all aerodynamic forces and moments. As expected, positive roll

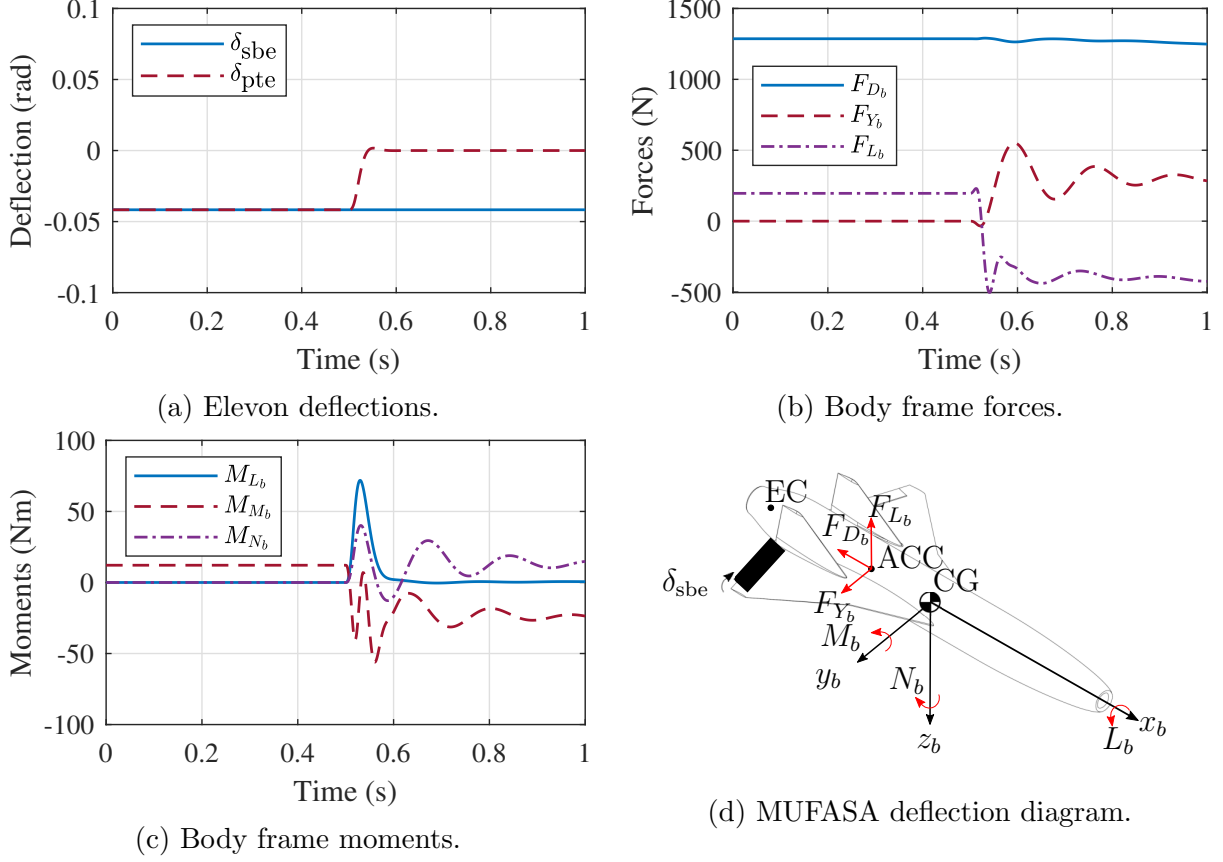


Figure 6.2: MUFASA aerodynamic body frame force and moment changes with respect to time in response to a single elevon deflection.

and yaw moments are observed (Fig. 6.2c) along with a sideforce due to the single starboard elevon deflection (Fig. 6.2b). Lowering of the port elevon reduces the control surface area rear of the CG exposed to the flow, thus reducing the pitching moment from its trimmed value (Fig. 6.2c) and also reducing the lifting force (Fig. 6.2b). The roll moment returning to zero following the initial deflection indicates that aerodynamic damping effects are present and that a constant equilibrium roll-rate was achieved. This equilibrium roll response aligns with the behaviour expected of a generic fixed-wing aircraft roll mode in subsonic or supersonic flight (Berry and Powers, 1970; Department of Defense, 1997; Weinacht and Sturek, 1996). The initial reactions at 0.5s are followed by an excitation of pitch and yaw moments (Fig. 6.2c) as the aircraft begins to transition from predominately rolling motion to a deep spin motion due to the influence of other aerodynamic variables such as coupling and aero-

dynamic damping (Katz, 1999). This simulation case indicates that control surfaces do not have absolute control, and that other aerodynamic influences such as damping can predominately influence the aircraft behaviour. The model’s representation of the MUFASA SSUAV cannot yet be compared to experimental data as the MUFASA airframe is still in development. The model will be indirectly verified in Section 6.1.3, however, in the absence of flight data, it is concluded that the model is setup and functioning properly as the simulated aircraft behaviour aligns with generalized fixed-wing aircraft tendencies identified by Berry and Powers (1970) and Katz (1999).

6.1.3 Flying Quality Parameter Verification

The aircraft mathematical model and flying quality evaluation procedure (Chapter 4) were verified together by comparing their results against flying quality parameters obtained by Heffley and Jewell (1972) and Roskam (2001). The verification case provided by Heffley and Jewell (1972) involved the inertial and aerodynamic data of a McDonnell Douglas F-4 aircraft flying at a Mach number of 0.9 and altitude of 35000ft (i.e., 10668m). The flight parameters were used as inputs to the mathematical model (Chapter 4) to generate predicted flying qualities of the F-4 aircraft via the Discrete model (Section 4.5). The flying qualities of the F-4 aircraft at these flight conditions were also previously calculated by Roskam (2001) via DAR Corporation’s Advanced Aircraft Analysis software program. Though no direct citations are shared between Heffley and Jewell (1972) and Roskam (2001), they both present the same F-4 inertial and aerodynamic data within rounding error. The flying quality parameters of the F-4 aircraft as stated by Heffley and Jewell (1972), and calculated by the Advanced Aircraft Analysis software (Roskam, 2001) and the Discrete model (Section 4.5) are presented in Table 6.1.

As presented in Table 6.1, neither the Advanced Aircraft Analysis software (Roskam, 2001), nor the Discrete model predict flying quality parameters identical to results from Heffley and Jewell (1972). The differing flying quality parameter values between analysis

methods are likely due to differences in setup of the scenario or initial trim conditions, however neither can be confirmed without knowing how the Advanced Aircraft Analysis software functioned. The Discrete model developed is assessed to provide comparable results as, but for Dutch-Roll natural frequency, it provides similar results to one, or both of the other methods.

Table 6.1: F-4 aircraft flying quality parameter comparison between Heffley and Jewell (1972), Roskam (2001), and the Discrete model procedure presented in Section 4.5.

F-4 Parameters	Heffley and Jewell (1972)	Roskam (2001)	Discrete Model
ω_{sp}	N/A	N/A	8.998
ζ_{sp}	N/A	N/A	0.461
ω_{ph}	N/A	N/A	0.048
ζ_{ph}	N/A	N/A	0.972
T_{ph_2}	15.200	N/A	14.774
ω_{dr}	2.366	2.396	3.731
ζ_{dr}	0.049	0.048	0.047
T_s	N/A	77.022	73.025
T_r	0.445	0.748	0.414

6.2 MUFASA SSUAV Physical Overview

The parameters used to simulate MUFASA in this thesis are detailed in this section. An overview of the physical characteristics of MUFASA are presented in Table 6.2. MUFASA's physical dimensions are derived from work by Dalman (2021). MUFASA's mass is set to 20kg to allow for regulatory classification as a small remotely piloted vehicle according to Transport Canada (2022). The MUFASA A.2 components of inertia are scaled from MUFASA A.1 as construction of MUFASA A.1 has been completed and the inertia measured. The UAV inertia was determined by employing bifilar pendulum testing following procedures outlined by Jardin and Mueller (2007) and Miller (1930). Key physical dimensions of the SSUAV are presented in Figs. 6.3 and 6.4. The main MUFASA wing is a NACA64-(0.3)05 A=0.5 airfoil, while the vertical stabilizers are NACA 0012 airfoils. MUFASA's CG, ACC

and EC exist on the aircraft centre line, with longitudinal location denoted in Table 6.2 and Fig. 6.3.

Table 6.2: MUFASA physical characteristics.

Parameter	MUFASA A.2
Length (m)	2.087
Mean Aerodynamic Chord (m)	0.595
Span (m)	1.070
Mass (kg)	20
I_{xx} (kg m ²)	0.210
I_{yy} (kg m ²)	1.022
I_{zz} (kg m ²)	1.206
I_{xz} (kg m ²)	0.014
Planform Area (m ²)	0.628
Wetted Area (m ²)	2.236

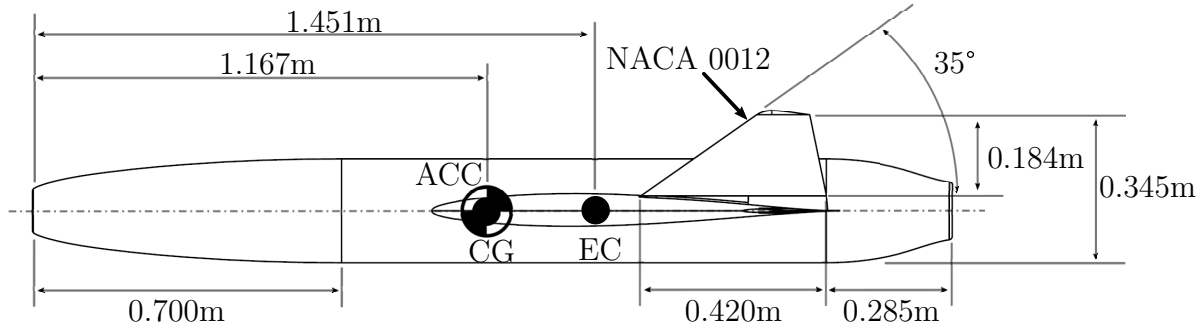


Figure 6.3: MUFASA side profile key dimensions.

6.2.1 MUFASA Aerodynamic Overview

The coefficients used to calculate aerodynamic forces and moments were acquired following the methods stated in Section 4.3.3. In addition to numerical aerodynamic coefficients, data about the fluid flow was generated by SU2 for every Mach number analyzed. Using flow data allowed for identification of the high-speed shock structure surrounding the MUFASA airframe and identification of aerodynamic coupling. An example Mach number contour for the UAV at nominal conditions, AOA and sideslip angle of zero, at a speed of Mach 1.1 is presented in Fig. 6.5 using the ParaView visualization program (Ahrens et al., 2005). As

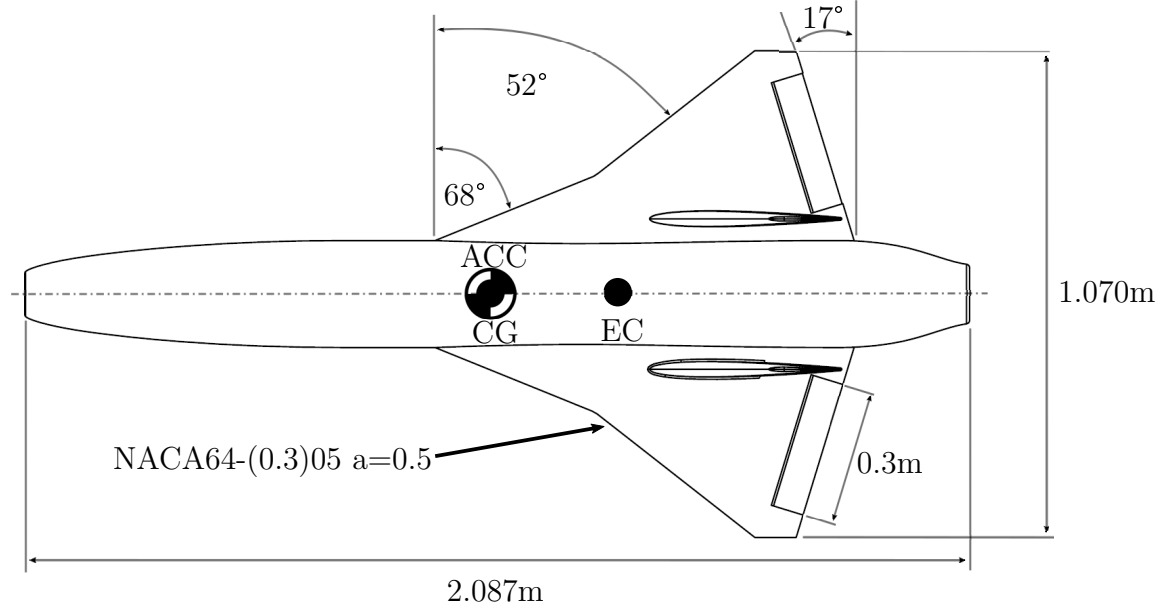


Figure 6.4: MUFASA top profile key dimensions.

expected for high-speed flight, multiple shocks are observed occurring along the UAV airframe. The expansion fan/shock interaction observed behind the vertical stabilizers suggests these control surfaces are aerodynamically coupled. This observation suggests that control surface constraints are present in the aircraft and will be discussed further in Section 6.2.2. The detached bow shock observed in Fig. 6.5 is likely due to the use of a blunt nose model without a pitot intake (Anderson, 1999, 2011).

In an effort to capture how MUFASA's aerodynamic coefficients change with speed the coefficient collection process described in Section 4.3.3 was repeated across a range of Mach numbers between 0.01 and 2.1. Aerodynamic coefficients were computed at the following sixteen Mach numbers: 0.01, 0.1, 0.3, 0.5, 0.7, 0.8, 0.9, 0.95, 1.05, 1.1, 1.2, 1.3, 1.5, 1.7, 1.9, and 2.1. The obtained coefficients were rotated from the CFD coordinate frame (seen in Fig. 6.5) to the body coordinate frame (seen in Fig. 4.1) and organized into a lookup table based on Mach number. The goal for the aerodynamic lookup table is to quantify the aircraft's aerodynamic behaviour across its entire flight regime. This lookup table is incorporated into the simulator developed in Chapter 5. A complete list of all MUFASA A.2 aerodynamic coefficients obtained are provided in Appendix A, Tables A.1 to A.3. Review of

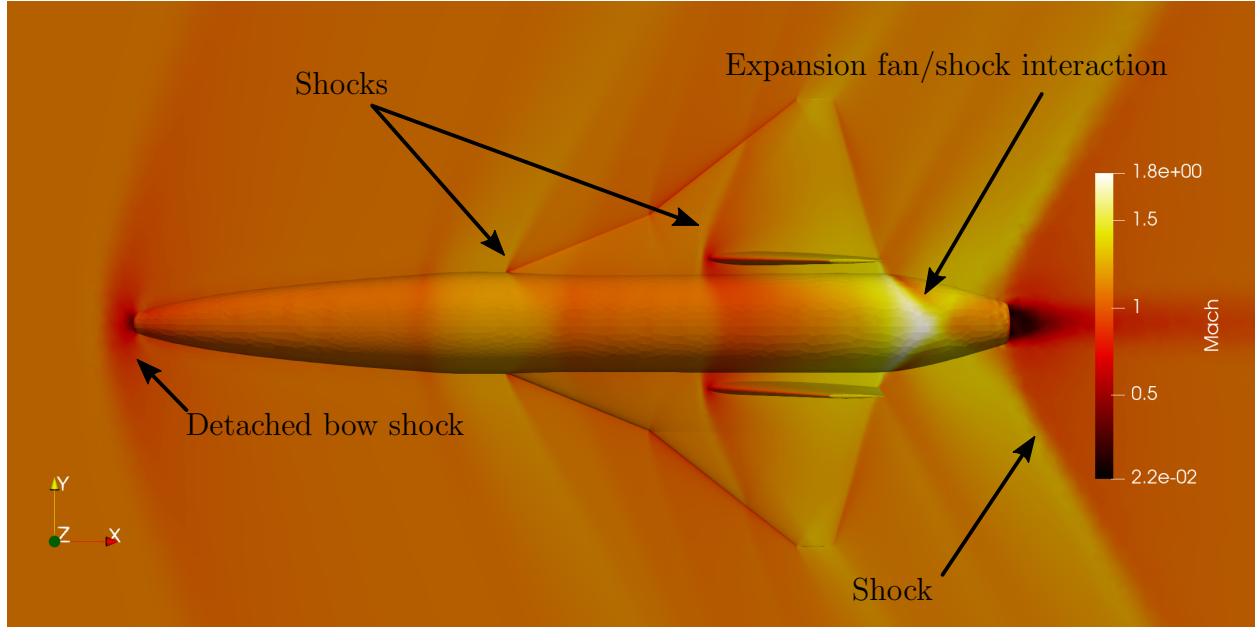


Figure 6.5: MUFASA Mach number contour at Mach 1.1 freestream conditions.

the aerodynamic coefficients obtained indicate that MUFASA is aerodynamically unstable. Further analysis is provided in Section 6.5.

6.2.2 MUFASA Actuator Overview

Physical hardware necessitates that input constraints be applied to the simulation input vector. MUFASA has four control surfaces, two vertical stabilators and two elevons, as highlighted in Fig. 1.2. All of the control surfaces are capable of moving independently of each other. Each elevon and vertical stabilator has a planform area of 0.023m^2 and 0.105m^2 , respectively. The control surfaces are constrained to be rigid, with infinitely powerful actuators, meaning they will not deflect unintentionally. Actuator motion constraints are based off of the physical constraints of the Futaba BLS172SV and BLS175SV servos earmarked for use in MUFASA A.2. The maximum deflection angle from nominal for the vertical stabilators is $\pm 5^\circ$ to avoid interference with MUFASA's fuselage. To avoid interference with the wing, the maximum deflection angle from nominal for the elevons is plus 34° and minus 44° following the sign convention presented in Fig. 4.4. Following procedures outlined by

Beard and McLain (2012), the elevon control surfaces were constrained to move in elevator and aileron combinations as related by Eq. 4.8. Additionally, the vertical stabilators were constrained to move in unison. The expansion fan/shock interaction observed trailing the vertical stabilators in Fig. 6.5 indicates that at high-speeds coupling exists between these vertical control surfaces. To avoid running CFD for every vertical stabilator port/starboard deflection state, the vertical stabilators were constrained to always maintain the same angle. This constraint, coupled with Eq. 4.9, implies that $\delta_{ptvs} = \delta_{sbvs} = \delta_r$.

Engine constraints are based off of the physical constraints of the KingTech K-160G2 engine earmarked for initial use in MUFASA A.2. Static testing indicated the KingTech engine maximum throttle ramp rate was $16 \frac{\%}{s}$. Previous work by Dalman (2021) has indicated the theoretical maximum flight regime for the MUFASA A.2 UAV is under 6km altitude and up to a Mach number of 0.99. As these estimates are preliminary, the MUFASA flight regime considered for this work will be up to an altitude of 10km and a Mach number of 1.5. These bounds allow for a factor of safety should future MUFASA UAV iterations achieve a larger flight regime. In order to facilitate analysis of the MUFASA SSUAV throughout the flight regime detailed it is assumed an equivalent engine exists capable of a maximum thrust output of 5000N. This 5000N engine is employed in the MUFASA model simulated and equates to engine constants k_0 and k_1 (from Eq. 4.22) of 0 and $6500 \left(\frac{m}{s}\right)^2$, respectively. A summary of MUFASA’s actuator characteristics is presented in Table 6.3.

6.3 Flying Qualities

Quantification of MUFASA’s cruise flying qualities are presented and discussed in this section. To facilitate the evaluation of MUFASA with the military flying quality specifications MIL-STD-1797A, MUFASA was scaled using Froude scaling. The damping and natural frequency of MUFASA’s aerodynamic modes were first computed from a steady-state trimmed and linearized state-space representation following the discrete modelling procedures pro-

Table 6.3: MUFASA actuator characteristics.

Parameter	MUFASA A.2
Motor Constant k_0 (unitless)	0
Motor Constant $k_1 \left(\frac{\text{m}}{\text{s}}\right)^2$	6500
Maximum Elevon Deflection ($^\circ$)	34
Minimum Elevon Deflection ($^\circ$)	-44
Maximum Elevon Deflection Rate ($\frac{\text{rad}}{\text{s}}$)	3.27
Maximum Vertical Stabilator Deflection ($^\circ$)	5
Minimum Vertical Stabilator Deflection ($^\circ$)	-5
Maximum Vertical Stabilator Deflection Rate ($\frac{\text{rad}}{\text{s}}$)	3.27
Minimum Throttle Setting (unitless)	0
Maximum Throttle Setting (unitless)	1
Maximum Throttle Ramp Rate ($\frac{1}{\text{s}}$)	0.16

vided in Section 4.5. Due to similarities in flight speeds and delta-wing design, MUFASA and its response frequencies were scaled to the size of a Lockheed SR-71 “Blackbird” aircraft. The SR-71 was chosen for comparison since it has a similar planform, is designed to maximize speed with limited manoeuvrability (Berry and Powers, 1970; Cox and Jackson, 1997), and has published mass and aerodynamic coefficient data (Moes and Iliff, 2002). A visual comparison of the two aircraft is presented in Fig. 6.6.

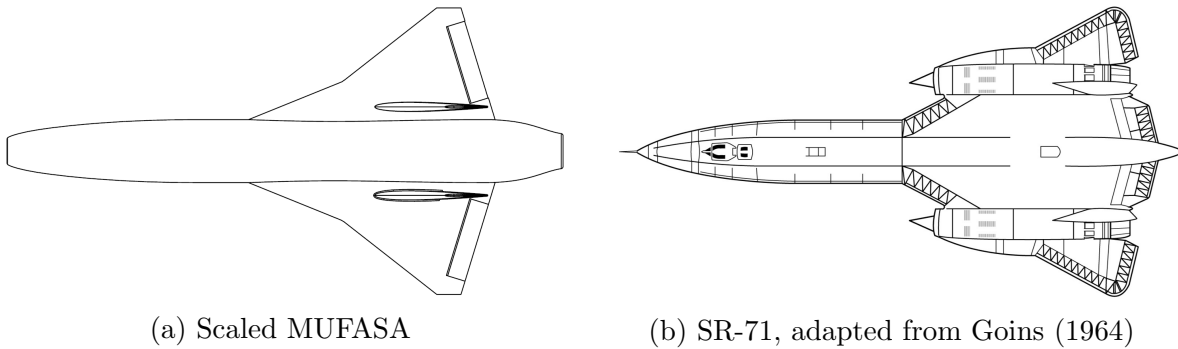


Figure 6.6: Proportionally scaled MUFASA and SR-71.

The Froude scaling number was determined by averaging the ratio between each aircraft’s wingspan (b) and mean aerodynamic chord as presented in Eq. 6.1 (Klyde et al., 2020a). In Eq. 6.1 subscript 1 and 2 denote whether the property belongs to the first or second aircraft being compared. The SR-71 wingspan and mean aerodynamic chord are 17.28m and 11.49m,

respectively (Moes and Iliff, 2002), yielding a scaling factor of $n = 17.5754$.

$$n = \frac{\frac{c_{\text{mean}_1}}{c_{\text{mean}_2}} + \frac{b_1}{b_2}}{2} \quad (6.1)$$

Work by Berry and Powers (1970), Berry (1978), and Cox and Jackson (1997), has determined that high-speed aircraft are best classified as class III aircraft in phase C flight according to the MIL-STD-1797A standard. As previously mentioned, according to the MIL-STD-1797A standard a class III aircraft is large, heavy, and has low-to-medium maneuverability while phase C flight denotes terminal flight phases where accurate flight-path control is required (Department of Defense, 2004). The supersonic SR-71 and scaled-up MUFASA SSUAV are evaluated against the MIL-STD-1797A class III, phase C requirements. The handling quality levels of the scaled-up MUFASA SSUAV were determined for each of the five flight modes (i.e., short period, phugoid, Dutch-Roll, roll subsidence, spiral) based on Table 2.4. MUFASA’s cruise conditions are set as $350 \frac{\text{m}}{\text{s}}$ (Mach 1.08) at 4.0km altitude. MUFASA’s scaled flying quality parameters at cruise, along with associated handling quality level, are presented in Table 6.4. Also included are the SR-71 flying and handling qualities evaluated at the same cruise conditions as MUFASA.

Table 6.4: MUFASA SSUAV cruise flying and handling qualities when scaled to the size of an SR-71.

Name	Flying Quality Parameter	Scaled MUFASA		SR-71	
		Value	Handling Level	Value	Handling Level
Short period	ζ_{sp}	0.294	2	0.931	1
Phugoid	T_{ph_2}	16.261 s	N/A	7.772 s	N/A
Dutch-Roll	ζ_{dr}	1	1	0.186	1
	ω_{dr}	$11.231 \frac{\text{rad}}{\text{s}}$		$2.341 \frac{\text{rad}}{\text{s}}$	
	$\zeta_{\text{dr}}\omega_{\text{dr}}$	$11.232 \frac{\text{rad}}{\text{s}}$		$0.436 \frac{\text{rad}}{\text{s}}$	
Roll subsidence	T_r	NaN s	N/A	0.507 s	1
Spiral	T_{s_2}	651.61 s	1	69.898 s	1

When compared to the MIL-STD-1797A standard, MUFASA at cruise conditions obtains satisfactory (level 1) handling qualities for Dutch-Roll and spiral modal responses. Short

period damping is rated as acceptable (level 2) while the phugoid response does not meet any of the military specification requirements. MUFASA’s roll subsidence time constant is Not a Number (NaN), denoting an unstable roll response. Because the MIL-STD-1797A standard does not specify how to treat modes not meeting any requirements, the phugoid and roll subsidence handling is set to N/A. The unstable roll response is discussed further in Section 6.5. MUFASA obtains equivalent or worse flying and handling qualities than calculated using the same method for the SR-71. The SR-71 results were calculated because the open-loop flying and handling qualities of the aircraft and its predecessor the YF-12 are confidential (Berry, 1978; Meyer et al., 1964). All of the SR-71’s flying quality parameters obtain satisfactory (level 1) handling qualities but for the phugoid mode which does not meet any handling requirements.

6.4 Flight Regime Flying Qualities

While supersonic cruise performance often drives optimization, acceptable transonic and subsonic flying qualities must also be accomplished (Luckring et al., 2017). This section analyzes the flying qualities of the scaled MUFASA SSUAV throughout it’s flight regime.

An alternative short period analysis of the scaled MUFASA’s response was performed by comparing the short period natural frequency against the load factor sensitivity parameter (Department of Defense, 2004). Load factor sensitivity ($\frac{n}{\alpha}$) denotes the forces experienced by an aircraft due to a change in AOA, and is defined by Eq. 6.2 (Klyde et al., 2020a):

$$\frac{n}{\alpha} = \frac{V_a}{g} \left(\frac{1}{T_{\theta_2}} \right) \quad (6.2)$$

where $\frac{1}{T_{\theta_2}}$ is the largest absolute stable zero in the transfer function describing the relationship between the pitch angle and elevator deflection. The short period natural frequency and load factor sensitivity were computed throughout MUFASA’s proposed flight regime at intervals of $25 \frac{\text{m}}{\text{s}}$ and 1km speed and altitude, respectively. The resulting flying quality data was overlaid

with the handling quality level requirements detailed by MIL-STD-1797A (Department of Defense, 2004) and is presented in Fig. 6.7.

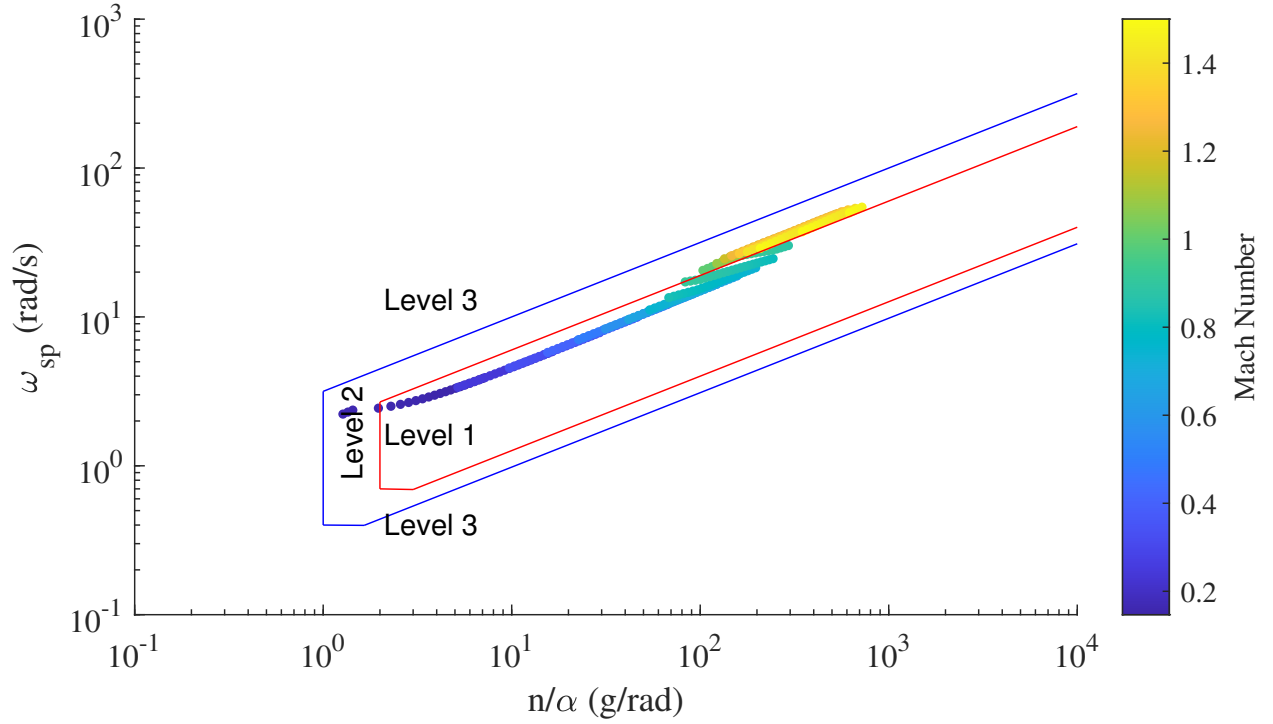


Figure 6.7: Scaled MUFASA longitudinal short period flying qualities evaluated against the MIL-STD-1797A standard class III, phase C requirements.

The majority of MUFASA’s subsonic flight is within the bounds defining satisfactory (level 1) flying qualities. Acceptable (level 2) flying qualities are observed at Mach numbers below Mach 0.2 and above Mach 1.0. MUFASA’s longitudinal short period natural frequency can be lowered in Fig. 6.7 by moving the CG of the airframe rearward (Foster and Bowman, 2005).

By performing the trim, linearization and scaling operation at multiple operating points throughout the flight regime a surface detailing handling quality levels was generated. Handling qualities level are evaluated as whole numbers, either level 1, 2 or 3 as shown in Table 2.4. The current discrete handling quality evaluation does not provide an indication to designers how close to optimal an aircraft is, whether it is solidly level 1 or barely level 1 for example. An alternative proposed in this thesis is the implementation of a continuous

flying quality evaluation metric based off the original MIL-STD-1797A standard. The proposed novel evaluation metric is presented in Table 2.4. The goal of continuous flying quality requirements is to generate smooth transitions between handling quality levels, allowing for the evaluation of how close to satisfactory (level 1) handling qualities an aircraft is. This new requirement is shown in Table 6.5 and evaluates handling quality performance on a continuous scale by linearly interpolating between the level ratings. Additionally a fourth handling level is added to quantify handling that is not satisfactory enough to be considered level 1, 2 or 3. Level 4 handling represents unstable or uncontrollable flight.

Table 6.5: Adapted flying quality requirements for a class III aircraft in phase C flight.

Mode	Handling			
	Level 1	Level 2	Level 3	Level 4
Short Period	$\zeta_{sp} = 0.825$	$\zeta_{sp} = 0.35$	$\zeta_{sp} = 0.25$	$\zeta_{sp} \leq 0.15$
Phugoid	$\zeta_{sp} = 0.825$	$\zeta_{sp} = 1.3$	$\zeta_{sp} = 2$	$\zeta_{sp} > 2$
	$\zeta_{ph} > 0.04$	$\zeta_{ph} = 0.04$	$\zeta_{ph} = 0$	
			$T_{ph_2} \geq 55 \text{ s}$	$T_{ph_2} < 55 \text{ s}$
Dutch-Roll	$\zeta_{dr} > 0.08$	$\zeta_{dr} = 0.08$	$\zeta_{dr} = 0.02$	$\zeta_{dr} \leq 0$
	$\zeta_{dr}\omega_{dr} > 0.10 \frac{\text{rad}}{\text{s}}$	$\zeta_{dr}\omega_{dr} = 0.10 \frac{\text{rad}}{\text{s}}$	$\zeta_{dr}\omega_{dr} = 0.05 \frac{\text{rad}}{\text{s}}$	$\zeta_{dr}\omega_{dr} < 0.05 \frac{\text{rad}}{\text{s}}$
	$\omega_{dr} \geq 0.4 \frac{\text{rad}}{\text{s}}$	$\omega_{dr} \geq 0.4 \frac{\text{rad}}{\text{s}}$	$\omega_{dr} \geq 0.4 \frac{\text{rad}}{\text{s}}$	$\omega_{dr} < 0.4 \frac{\text{rad}}{\text{s}}$
Roll Subsidence	$T_r = 0.0 \text{ s}$	$T_r = 1.4 \text{ s}$	$T_r = 3.0 \text{ s}$	$T_r \geq 10.0 \text{ s}$
Spiral				$T_r < 0.0 \text{ s}$
	$T_{s_2} > 12.0 \text{ s}$	$T_{s_2} = 12.0 \text{ s}$	$T_{s_2} = 8 \text{ s}$	$T_{s_2} \leq 4 \text{ s}$

As employed by Ammar et al. (2017), the handling qualities of the aircraft are plotted not just at cruise, but throughout the entire flight regime. The continuous handling qualities of the five modes were evaluated to provide a holistic view of the aircraft handling at points throughout the flight regime. The handling quality level of each modal parameter (short period, phugoid, Dutch-Roll, roll subsidence, and spiral) were averaged together and a mean handling quality level of the aircraft at each flight regime state determined. An overview of the scaled MUFASA SSUAV flying qualities throughout its outlined flight regime is presented in Fig. 6.8. This figure highlights at what conditions MUFASA handles best, and is a flying quality based tool for future flight trajectory optimization. The surface was generated using

velocity and altitude increments of $1\frac{\text{m}}{\text{s}}$ and 50m, respectively. Any area in Fig. 6.8 not covered in colour indicates a flight condition where insufficient lift is generated to produce steady-state cruise flight.

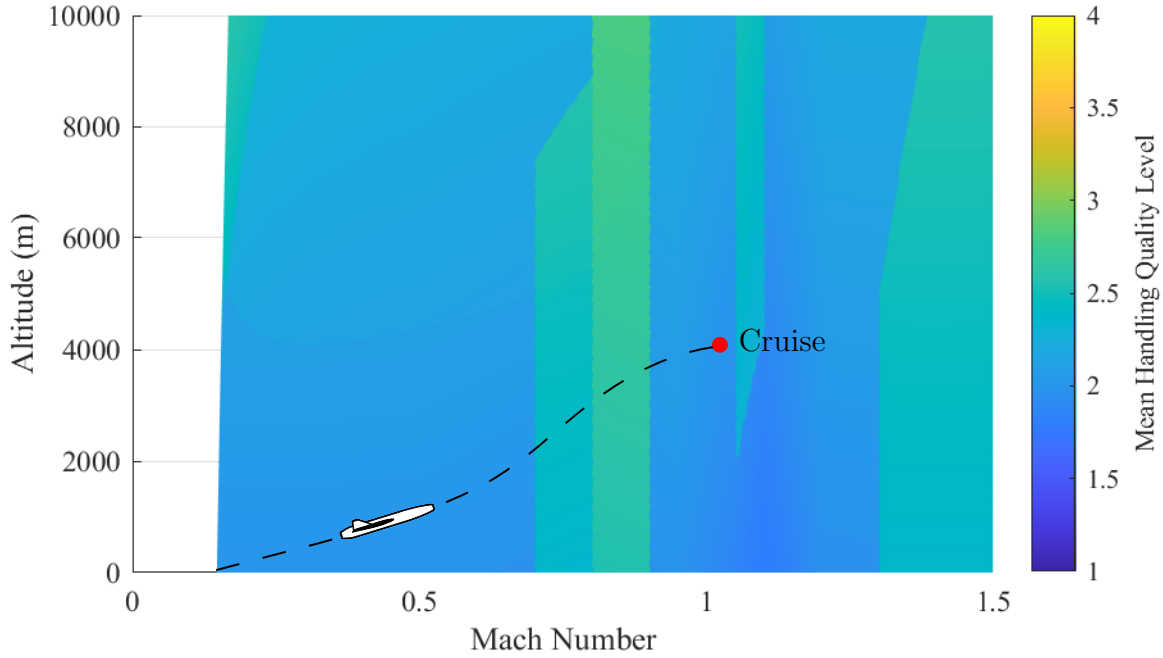


Figure 6.8: Scaled MUFASA flight regime mean handling quality level with a potential flight trajectory overlaid.

Figure 6.8 indicates MUFASA is most easily flown just above Mach 1.0, which is ideal as this is the designed cruise speed. Handling qualities of the MUFASA SSUAV do not degrade to near controllable (level 3) on average except at Mach numbers between 0.7 and 0.9, and at values above Mach 1.3. Based on MUFASA's handling qualities a potential flight trajectory from takeoff to cruise is overlaid in Fig. 6.8. The reason for flying quality variations observed are discussed in subsequent figures. How rapid changes in handling quality levels relate to the Mach numbers the aerodynamic coefficients were evaluated at was investigated via Fig. 6.9. Figure 6.9 overlays vertical lines on Fig. 6.8, indicating where aerodynamic coefficients were numerically determined via CFD, and interpolated between. The effect of dynamic pressure on flying quality changes were evaluated via Fig. 6.10. In Fig. 6.10 dynamic pressure contour

lines are overlaid on the mean flying qualities. The dynamic pressure values are presented in units of pascals.

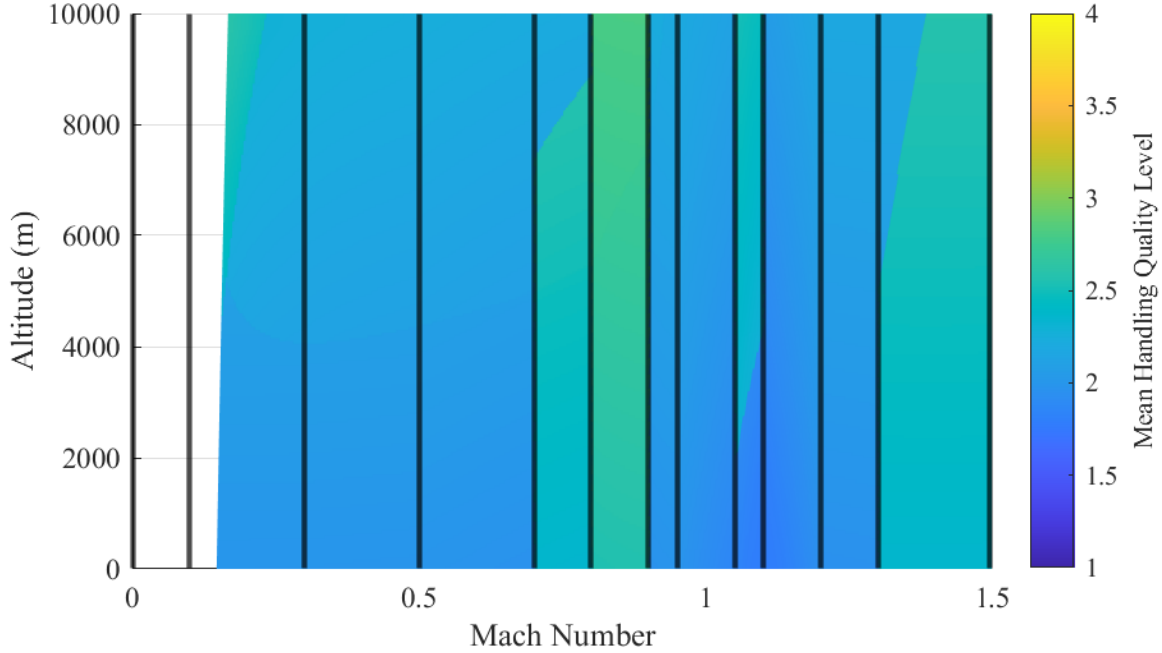


Figure 6.9: Scaled MUFASA flight regime mean handling qualities with aerodynamic coefficient evaluation Mach numbers overlaid.

Even though the goal of a continuous handling quality standard was to remove abrupt handling reclassification, as seen in Fig. 6.8, abrupt handling quality level transitions still occur. These transitions do exist with respect to the MUFASA model physics, as they correlate to behaviour observed in separate time response simulations. Sample non-linear time response simulations were run and the results were inline with the identified handling levels. Three potential causes of abrupt handling quality level transitions are discussed below.

Firstly, abrupt handling quality changes due solely to a change in Mach number are attributed to minor coefficient variation at each analysis point. In the interest of minimizing computation time 30 aerodynamic coefficients were evaluated at 13 Mach numbers between Mach 0.01 and 1.5. Linear interpolation was used to generate 30 aerodynamic coefficients

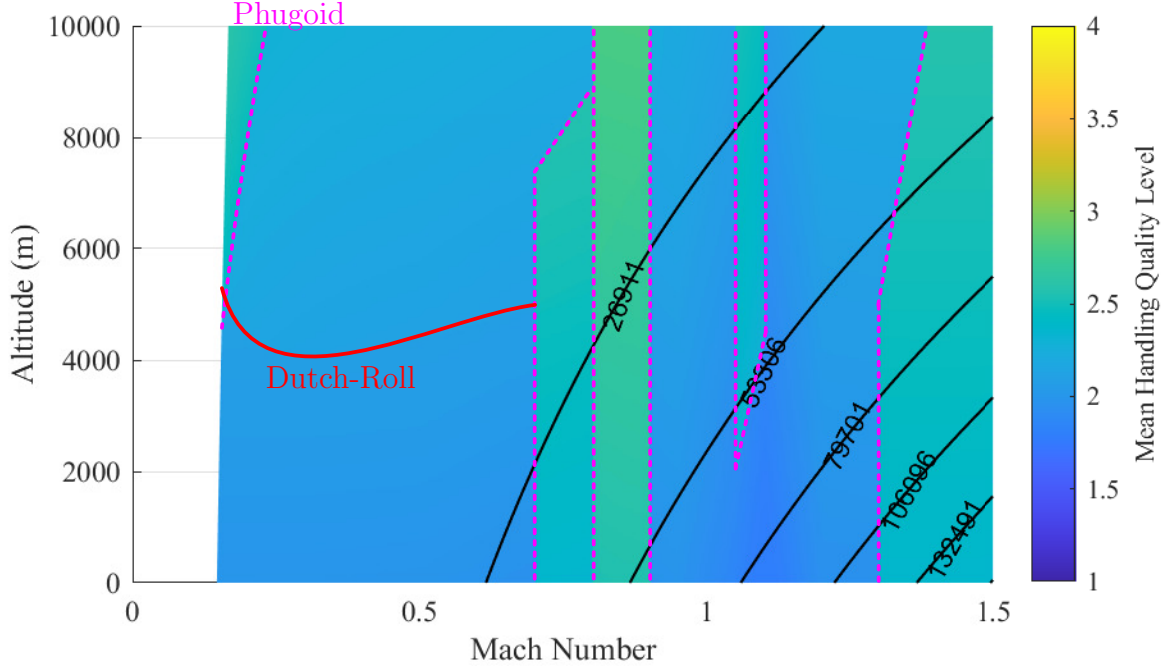


Figure 6.10: Scaled MUFASA flight regime mean handling qualities with dynamic pressure contour lines overlaid.

between each analyzed Mach number. The abrupt transitions at Mach numbers 0.7, 0.9, 1.05, 1.1, and 1.3 are caused by the phugoid mode changing from a satisfactory (level 1) to unstable (level 4) handling level, or vice-versa. This instability is caused by the phugoid eigenvalues having a non-oscillatory unstable configuration, which is a known phenomenon (Campos and Marques, 2021; Cook, 2012) and was presented in Section 4.5.3. Reviewing the MUFASA A.2 aerodynamic coefficients presented in Figs. A.1 to A.6 in Appendix A, no obvious coefficient discontinuities exist at Mach numbers 0.7, 0.9, 1.05, 1.1, or 1.3. The only discontinuities originating from the CFD results exist at/around Mach 1. It is well known that aerodynamic coefficient discontinuities exist around Mach 1 both in CFD and experimental data (Aprovitola et al., 2021; Rech and Leyman, 1980). The abrupt transitions at Mach numbers 0.7, 0.9, 1.05, 1.1, and 1.3 are thus attributed to slight aerodynamic coefficient changes at the Mach numbers evaluated. The phugoid mode in particular is influenced by all longitudinal (lift, drag, and pitch) aerodynamic coefficients (Cook, 2012) meaning small variations between the coefficients (C_L , C_D , and C_m) are capable of leading to rapid phugoid

response changes. Where the aerodynamic coefficients were obtained appears to lead to the abrupt vertical handling quality level transitions seen in Fig. 6.9.

Secondly, abrupt handling quality level transitions observed in Fig. 6.8 are attributed to the fact that not all parameters could be made continuous via Table 6.5. As seen in Table 2.4 and 6.5, parameters such as the phugoid mode experience a transition between level 2 and level 3 as the flying quality parameter being evaluated changes from damping ratio to time-to-double. Additionally, there is a transition once a flying quality parameter becomes unstable, generally characterized by a damping ratio of zero or less. The only modes to quantify acceptable levels of instability are the phugoid and spiral mode time-to-double.

Finally, changes in dynamic pressure were overlaid in Fig. 6.10 to evaluate if a relationship existed between dynamic pressure and SSUAV handling qualities. Non-vertical abrupt handling quality level transitions are highlighted in Fig. 6.10 and colour coded to the flying quality mode they are attributed to. The Dutch-Roll abrupt handling quality level transition is caused by unstable Dutch-Roll and roll subsidence flying quality parameters. When the Dutch-Roll handling is satisfactory (level 1), roll subsidence is unstable (level 4), and vice-versa. This coupled instability indicates MUFASA is laterally unstable and is discussed further in Section 6.5. Meanwhile, the phugoid mode shifts abruptly between satisfactory (level 1) and unstable (level 4) at multiple non-vertical points throughout MUFASA's flight regime. The cause of these abrupt phugoid shifts is attributed to the eigenvalues exhibiting an unstable non-oscillatory behaviour. The non-vertical abrupt handling quality level transitions do not coincide well with the slope of the dynamic pressure contour lines, thus, changing dynamic pressure is not a dominating affect on the aircraft's behaviour and flying quality parameters.

In summary, abrupt handling quality transitions do appear in non-linear time response simulations and are attributed to slight aerodynamic coefficient changes between coefficients at analyzed Mach numbers, and a lack of specifications to quantify instability.

6.5 Aerodynamic Stability

Flying quality analysis indicates the MUFASA SSUAV exhibits lateral instability. As mentioned with regards to Fig. 6.10, the Dutch-roll and roll subsidence modes exhibit coupled instability, where one of them exhibits unstable (level 4) handling quality behaviour while the other exhibits satisfactory (level 1) handling quality behaviour. The reason for this instability, along with MUFASA's unstable flying quality roll subsidence response in Table 6.4, is discussed in this section.

In conjunction with flying and handling qualities, aerodynamic stability was another method used to evaluate the MUFASA SSUAV. Vehicle aerodynamic static stability is determined based off of the sign (\pm) of its aerodynamic coefficients (Department of Defense, 1990). Reviewing the MUFASA aerodynamic coefficients in Appendix A obtained via the procedure presented in Section 4.3.3, the following aerodynamic coefficients have a sign which indicates an unstable aerodynamic response: C_{n_β} , C_{n_P} , $C_{n_{\delta_a}}$, and C_{l_R} . Of the four coefficients, the unstable directional stability coefficient (C_{n_β}) is the most impactful to the overall aircraft behaviour, causing any amount of sideslip to induce an unstable deviation from the desired flight direction. Perturbation simulations of MUFASA were performed to evaluate MUFASA's dynamic response. MUFASA was initially set at steady-state, straight-and-level flight. Multiple simulations were run where a perturbation was applied to the aircraft, originating from either an actuator deflection or environmental wind gust. MUFASA exhibited negative feedback behaviour to longitudinal perturbations and returned to its original flight trajectory (or close to). MUFASA exhibited positive feedback behaviour to lateral perturbations, resulting in an uncontrolled departure from the initial flying condition that grew exponentially. These simulations confirm MUFASA is aerodynamically unstable in the lateral plane based on the aerodynamic coefficients obtained. The MUFASA A aerodynamic profile is not an aerodynamically stable shape. Future work focusing on aircraft design should consider the stability and flying quality analysis presented in this work when designing the MUFASA B aerodynamic profile.

To facilitate MUFASA’s representation of all SSUAVs for the remainder of this thesis’ analysis it was assumed that MUFASA was redesigned to be aerodynamically stable and mimic the flight behaviour of an SR-71. This stability assumption was facilitated by attributing the aerodynamic behaviour of an SR-71 aircraft to the MUFASA aircraft. Thus the modified MUFASA A.2 (herein referred to as MUFASA-M) has the physical parameters of MUFASA A.2 (Tables 6.2 and 6.3) and the aerodynamic coefficients of the SR-71 obtained experimentally by Moes and Iliff (2002). This assumption means that MUFASA-M results are obtained using SR-71 aerodynamic coefficient data from Moes and Iliff (2002), and not the aerodynamic coefficients presented in Appendix A.

An abridged version of the analysis presented in Sections 6.3 and 6.4 is presented below for the MUFASA-M SSUAV. The flying and handling qualities of MUFASA-M at its cruise conditions of $350\frac{\text{m}}{\text{s}}$ (Mach 1.08) at 4.0km altitude are presented in Table 6.6. MUFASA-M obtains satisfactory (level 1) handling qualities for every modal response at cruise.

Table 6.6: MUFASA-M SSUAV cruise flying and handling qualities when scaled to the size of an SR-71.

Name	Flying Quality Parameter	Value	Handling Level
Short period	ζ_{sp}	0.483	1
Phugoid	ζ_{ph}	0.067	1
	ζ_{dr}	0.108	
Dutch-Roll	ω_{dr}	$9.993\frac{\text{rad}}{\text{s}}$	1
	$\zeta_{\text{dr}}\omega_{\text{dr}}$	$1.078\frac{\text{rad}}{\text{s}}$	
Roll subsidence	T_r	0.139 s	1
Spiral	T_{s_2}	148.78 s	1

Flight regime flying qualities were also calculated for MUFASA-M following the procedure outlined in Section 6.4. MUFASA-M’s mean handling quality level throughout its flight regime is presented in Fig. 6.11.

As per Fig. 6.11, MUFASA-M is most easily flown between Mach 0.8 and 1.05, or above Mach 1.3. Overall MUFASA-M obtains satisfactory (level 1) handling qualities, only dropping to controllable (level 3) around Mach 0.8 above 4km altitude. A potential flight trajec-

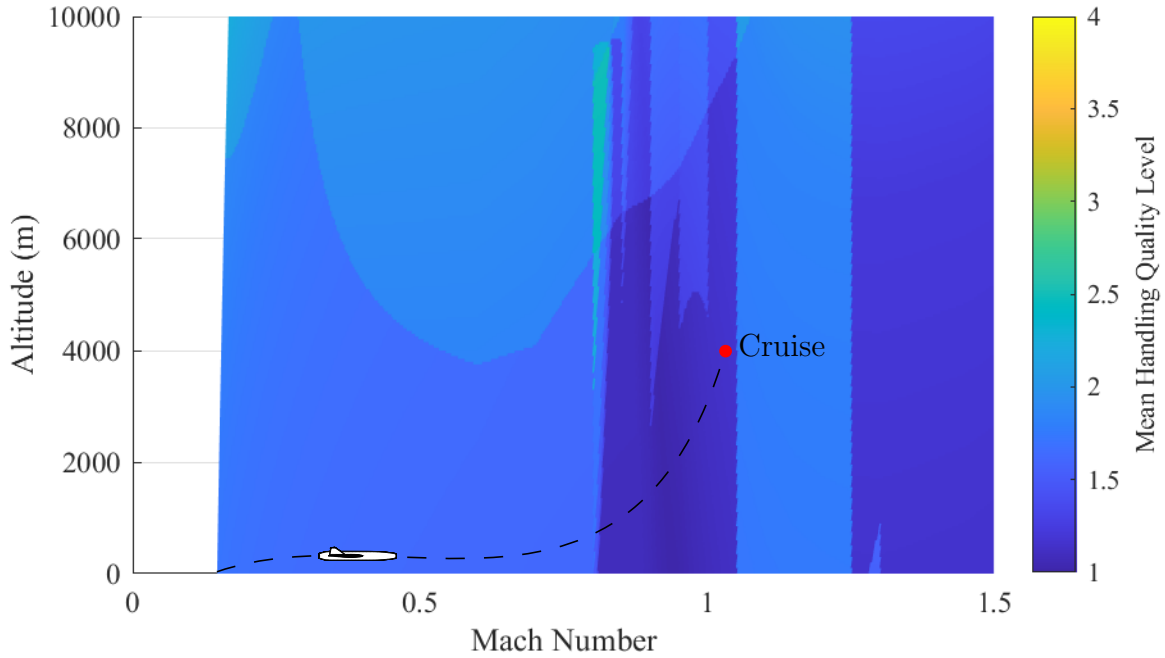


Figure 6.11: Scaled MUFASA-M flight regime mean handling quality level with potential trajectory overlaid.

tory from takeoff to cruise is presented in Fig. 6.11 and plotted along regions with the most optimal flying qualities. Abrupt handling quality level transitions are still present throughout this version of MUFASA's flight regime. The Mach numbers at which aerodynamic coefficients were obtained, along with the source of non-vertical abrupt handling quality level transitions, are overlaid in Fig. 6.12.

Similar to in Fig. 6.9, the vertical abrupt handling quality level transitions in Fig. 6.12 are correlated with where aerodynamic coefficients were evaluated at. Vertical abrupt handling quality level transitions align with aerodynamic coefficients computed at Mach 1.05 and Mach 1.3 at all altitudes. Another vertical abrupt handling quality level transition exists at Mach 0.9 and Mach 1, but only above 3km altitude. All vertical abrupt handling quality level transitions are attributed to the phugoid mode shifting between satisfactory (level 1) and unstable (level 4) due eigenvalues exhibiting unstable non-oscillatory behaviour. Non-vertical abrupt handling quality level transitions are attributed to one of three modes: phugoid, short

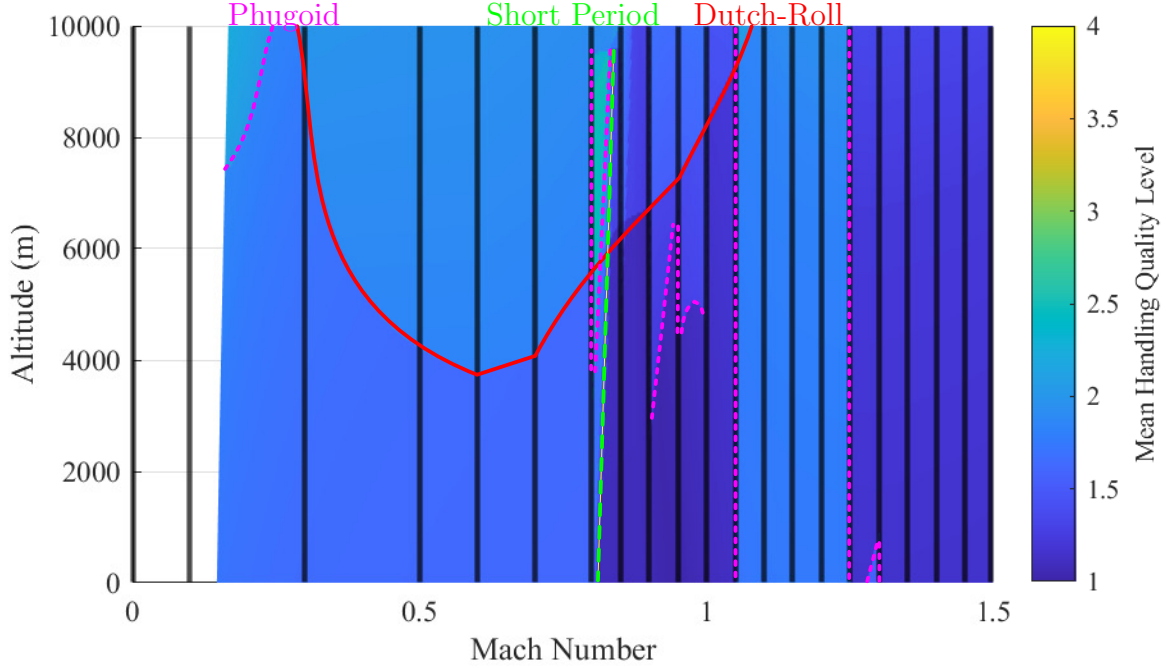


Figure 6.12: Scaled MUFASA-M flight regime mean handling qualities with aerodynamic coefficient evaluation Mach numbers overlaid.

period, or Dutch-Roll. The phugoid mode abruptly shifts between satisfactory (level 1) and unstable (level 3) at four non-vertical points: high altitude and low speed, just above Mach 0.9 at altitudes above 3km, at Mach 0.8 above 4km altitude, and a low altitude at Mach 1.255. The short period mode is unstable (level 4) below roughly Mach 0.8. This instability aligns with observations that the SR-71 was unstable longitudinally at subsonic speeds (Meyer et al., 1964; Moes and Iliff, 2002). Finally the Dutch-Roll mode abruptly transitions to acceptable (level 2) behaviour above 4km altitude at subsonic conditions. Inline with observations of Fig. 6.10, MUFASA-M's non-vertical abrupt handling quality level transitions do not correlate to changes in dynamic pressure and are instead attributed to variations of their respective modal responses mentioned above.

One limitation of the MIL-STD-1797A standard was observed when comparing MUFASA-M's cruise parameters to the flying quality requirements. As per Table 2.4, satisfactory (level 1) roll subsidence is characterized by a time constant less than or equal to 1.4s. The

scaled-up MUFASA-M roll subsidence time constant in Table 6.6 is equal to 0.139s, an order of magnitude smaller. It is presumed this deviation is not raised as an issue by the military specification because the standard was designed with crewed aircraft in mind (Mohamed et al., 2014). Thus, there was little incentive to bound the roll subsidence time constant as significantly fast responses were deemed unlikely in a crewed configuration. With regards to the un-scaled MUFASA-M roll subsidence time constant, it is even faster at a value of 0.033s. As noted by Bogos and Stroe (2012), small aircraft generally respond significantly faster than full-scale crewed aircraft. The impact of this faster response will be explored in Section 6.6.

6.6 Handling Qualities Time Response Comparison

In the absence of a UAV handling qualities standard, the response characteristics between six un-scaled aircraft were evaluated to contextualize SSUAV handling. While the MIL-STD-1797A standard and its predecessors are good resources for quantifying UAV flying qualities, they are not able to guarantee an aircraft’s handling qualities (Klyde et al., 2020b). Certain inequalities in Table 2.4, such as roll subsidence time constant, are not fully bounded. The response characteristics of MUFASA were compared to those of the SR-71, D-21, Simba (also known as MUFASA A.1), Trance, and Skywalker X8. These aircraft are presented in Fig. 6.13.

MUFASA-M was used in-place of MUFASA to represent the general performance expected of a stable delta-wing SSUAV. The SR-71 and D-21 represent the performance of previously flown supersonic aircraft. The SR-71 was a Mach 3 crewed reconnaissance aircraft, while the D-21 was a large-scale Mach 3 reconnaissance UAV (Geisler et al., 2007). The aerodynamic and inertial data needed to model the SR-71 was obtained from Moes and Iliff (2002). The D-21 was modelled using physical parameters obtained from Bradley et al. (1963) and Geisler et al. (2007). Aerodynamic coefficients for the D-21 could not be located within the

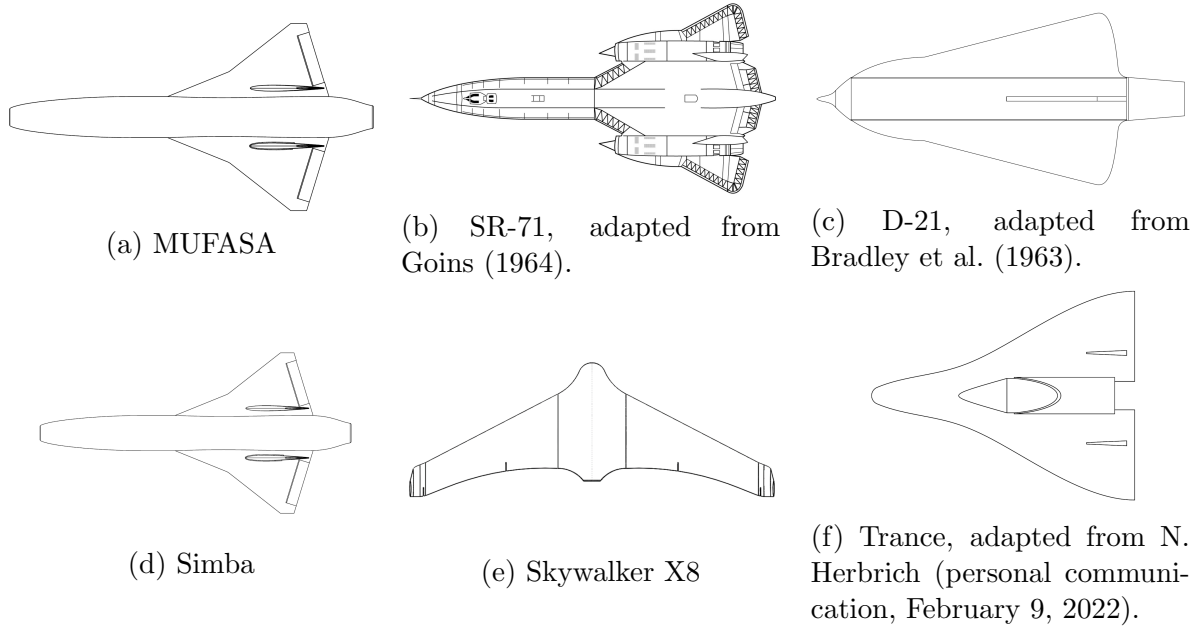


Figure 6.13: Drawings of aircraft modeled in the handling comparison study (not to scale).

public literature. Due to the similarity in shape and mission profile, the D-21 model utilizes the aerodynamic coefficients of the SR-71. Simba and Trance represent the performance of high-speed subsonic UAVs. Simba (also known as MUFASA A.1) is a high-speed, low-cost, scaled demonstrator of the MUFASA A aerodynamic profile. Because the MUFASA A aerodynamic profile is laterally unstable, so too is the Simba aircraft. To compare the vehicle response differences with aircraft scaling the Simba aerodynamic coefficients were modified. The modified Simba (herein referred to as Simba-M) uses the same assumption mentioned in Section 6.5, using SR-71 aerodynamic coefficients to simulate the UAV. Simba-M's mass and inertia were measured experimentally. The inertia was determined by employing bifilar pendulum testing following procedures outlined by Jardin and Mueller (2007) and Miller (1930). Trance is currently the fastest remote-controlled jet-powered model aircraft according to Guinness World Records (2017). With a top speed of 749km/h, Trance is currently the closest aircraft flown in size, speed, and capability to an SSUAV. The physical parameters of the Trance aircraft were determined from information provided by N. Herbrich (personal communication, February 9, 2022). Trance is 1.30m long with a wingspan of 1.04m. The

airfoil is a NACA 65006. The total wetted area of Trance is 0.65m^2 . The UAV weighs 7.5kg and uses a Behotec JB180 engine to generate 180N of thrust. The inertial values were estimated from a computer assisted design model generated of Trance based on discussions with the creator and publicly available images of the aircraft. Aerodynamic coefficients for Trance were evaluated using the procedure detailed in Section 4.3.3. Trance physical parameters and aerodynamic coefficients are provided in Appendix B. Finally, Skywalker X8 represents the performance of a standard small-scale subsonic UAV. The aerodynamic and inertial data needed to model the Skywalker X8 was taken from the publication by Gryte et al. (2018).

Each of these vehicles was simulated within MATLAB and Simulink throughout their respective flight regime. The aircraft were trimmed and linearized to obtain eigenvalues defining the aircrafts damping ratio and natural frequency. The sensitivity of each handling quality mode was indicated by the time constant of that mode. Natural frequency (excitability) and damping ratio (resistance to excitation) were combined using Eq. 2.1 (Saeed, 2008) to calculate the time constant. As stable time constants are generally small, the inverse of time constant is presented to provide visual context on the speed of a mode's response. To contextualize these inverse time constants the results from Trance, the SR-71, and MUFASA-M are overlaid in Fig. 6.14.

Inverse modal response times increase with Mach number as presented in Fig. 6.14. For MUFASA-M, the roll subsidence mode is the fastest throughout the Mach sweep, indicating it is the most excitable. MUFASA-M and Trance UAVs experience significantly faster time constants than the crewed SR-71. The most drastic difference between the full-scale and small-scale aircraft are seen when comparing the roll subsidence and short period mode time constants. Due to the similarity in physical (i.e., length, wingspan, mass, and inertia) and aerodynamic (i.e., delta-wing shape) properties between Trance and MUFASA-M their time constants follow a similar increase with Mach number. Due to MUFASA-M's greater flight speeds, it achieves shorter modal time constants than Trance. This result supports

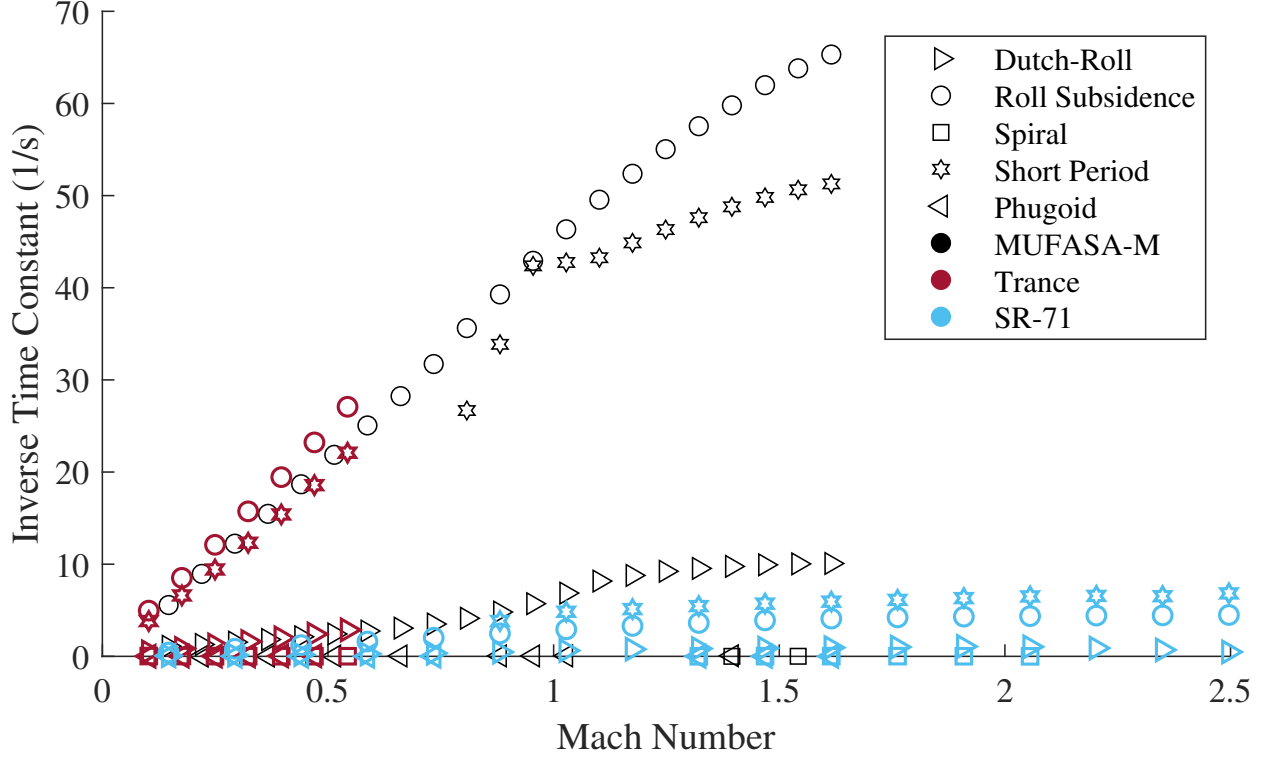


Figure 6.14: MUFASA-M, Trance, and SR-71 inverse time constant modal response comparison.

the notion that MUFASA-M and possibly all SSUAV's are unique in that they combine the handling quality challenges from both small-scale UAVs and supersonic delta-wing aircraft. MUFASA-M's modal time constants follow the trends of small-scale UAVs, however, a greater top speed due to its supersonic cruise conditions means MUFASA-M's time constants are significantly faster than achieved by a small-scale UAV or a supersonic aircraft.

To further evaluate the response characteristics of each airframe, the response to a perturbation at cruise conditions was observed. Each aircraft was set to its designed cruise conditions as outlined in Table 6.7. An equal elevon control surface perturbation was applied to each airframe and the vehicle's responses recorded. Aircraft attitude rate response to a 0.1° aileron (Fig. 6.15a) and elevator (Fig. 6.16a) deflection are presented in Figs. 6.15b and 6.16b, respectively. From the state derivative vector ($\dot{\vec{x}}$) the vehicle's roll and pitch attitude acceleration rate is presented in Figs. 6.17a and 6.17b, respectively.

Table 6.7: Cruise conditions of various aircraft.

Aircraft	Cruise Airspeed ($\frac{m}{s}$)	Cruise Altitude (km)
MUFASA	350	4.0
SR-71	885	29.0
D-21	885	27.0
Simba	59	0.5
Skywalker X8	18	0.5
Trance	160	0.5

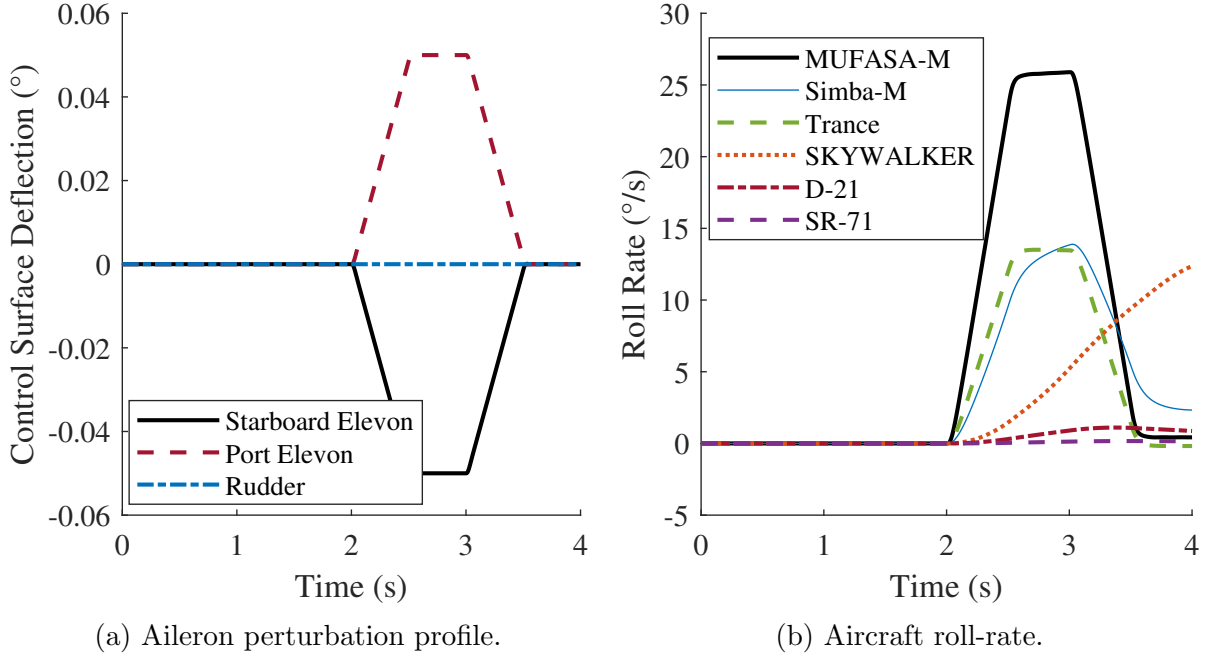
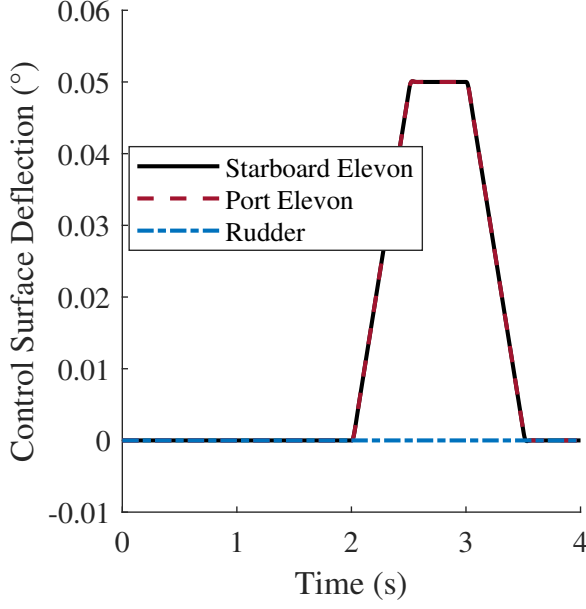
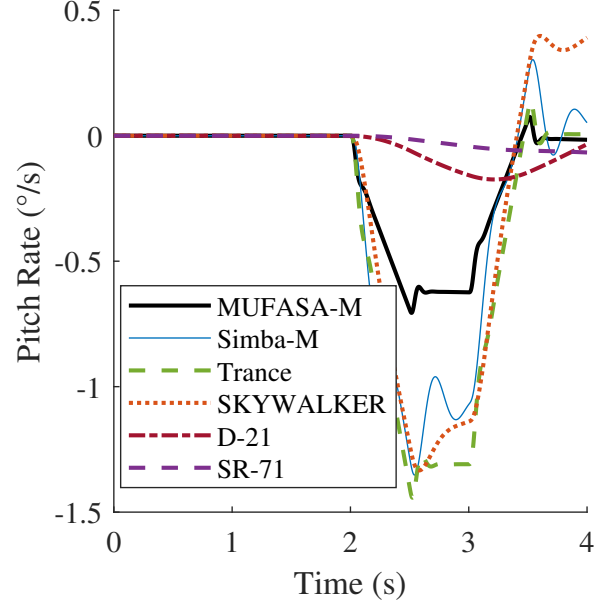


Figure 6.15: Aircraft response following a 0.1° aileron deflection at 2s.

With regard to Fig. 6.15, MUFASA-M reacts the fastest of all the aircraft in roll, and with the highest magnitude. The high roll acceleration in Fig. 6.17a following the control surface deflection aligns with previous observations that MUFASA-M has a very small roll subsidence time constant. MUFASA-M's roll-rate reaction is at least twice the other small-scale UAVs, and its reaction is an order of magnitude faster than that achieved by the SR-71 and D-21 supersonic aircraft. The Skywalker X8 small-scale UAV response lies between the high-speed UAVs and full-scale supersonic aircraft. The response of similarly classified aircraft (i.e., SSUAV, high-speed UAV, small-scale UAV, full-scale supersonic aircraft) thus group together in the roll-rate (Fig. 6.15b) and acceleration (Fig. 6.17a) response figures.

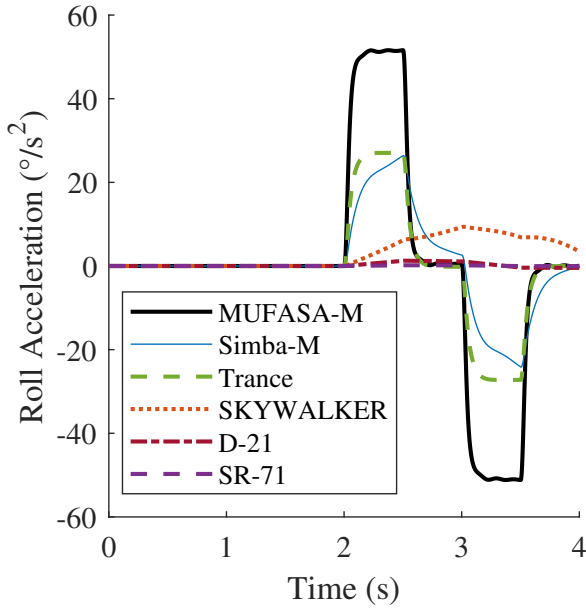


(a) Elevator perturbation profile.

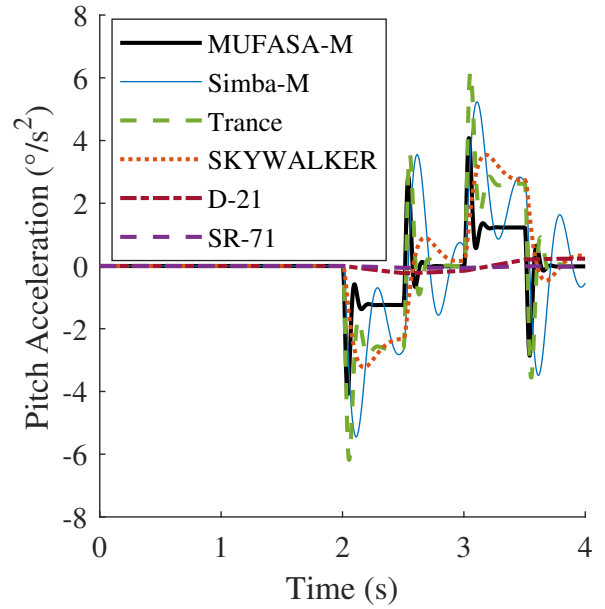


(b) Aircraft pitch-rate.

Figure 6.16: Aircraft response following a 0.1° elevator deflection at 2s.



(a) Aircraft roll acceleration to aileron perturbation.



(b) Aircraft pitch acceleration to elevator perturbation.

Figure 6.17: Aircraft attitude acceleration response following a 0.1° deflection at 2s.

Roll response hypersensitivity is a known issue with small-scale fixed-wing UAVs due to their low roll inertia (I_{xx}) (Mohamed et al., 2014; Panta et al., 2018). Small-scale UAV wings are generally made out of foam or a lightweight balsa/aluminum spar construction

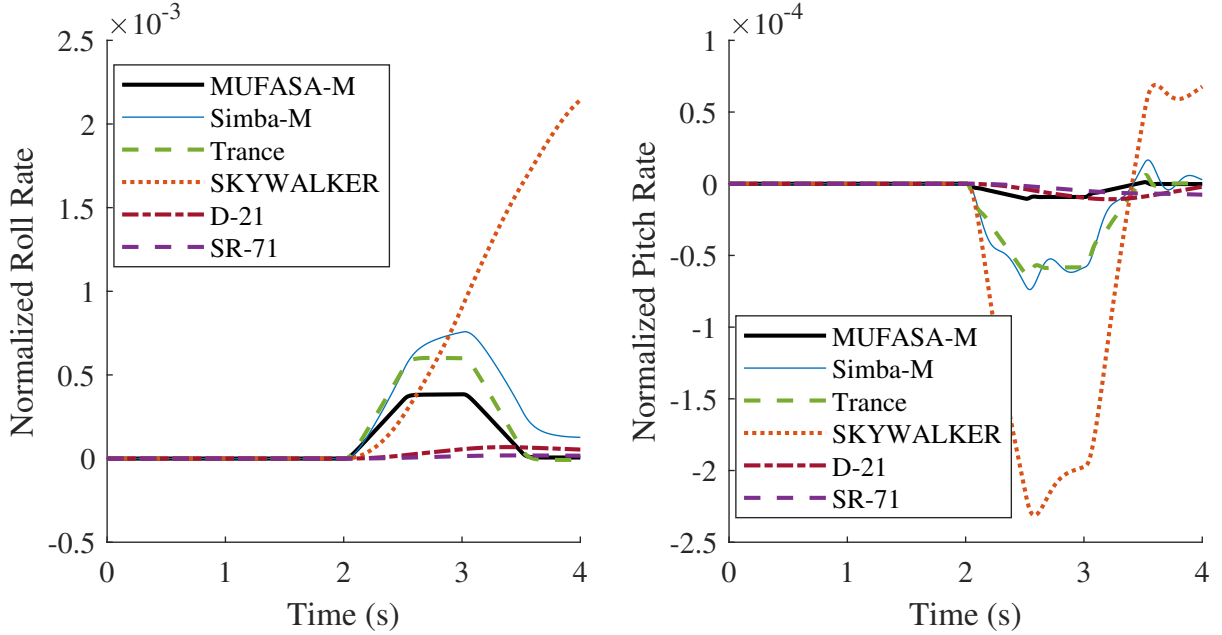
(Keane et al., 2017). Small-scale UAVs concentrate the majority of their mass around the centerline because the inertia advantages of placing components within the wings often do not outweigh the associated weight penalty of the increased structural requirements (Keane et al., 2017). Roll inertia is significantly increased by either adding mass or shifting mass away from the centreline (Mohamed et al., 2014). Adding mass to a small-scale aircraft would require a greater wingspan to maintain lift. Shifted mass is more effective the further from the centreline it is, also incentivizing a larger wingspan. Both ways to increase inertia provide a conundrum as they deviate from the design criteria of a small-scale aircraft. Without increasing roll axis inertia, the Fig. 6.15b and Fig. 6.17a results highlight potential future control challenges posed by SSUAVs. If a 0.1° equivalent aileron deflection causes at roughly $26^\circ/s$ roll-rate, extreme care must be taken implementing a rigid control surface, or a very fast robust controller must be developed.

With regards to Fig. 6.16, MUFASA-M's pitch rate is between the response of small-scale UAVs and full-scale supersonic aircraft. However, viewing pitch acceleration (Fig. 6.17b) MUFASA-M's response magnitude is larger than full-scale aircraft and more inline with small-scale UAVs. The Skywalker X8 and Trance pitch-rate magnitude exceed that of MUFASA-M likely due to a weaker opposing restoring force at their respective cruise speeds. The highest magnitude pitch-rate observed in Fig. 6.16b is significantly lower than the highest roll-rate observed in Fig. 6.15b. This difference in pitch-rate and roll-rate control surface effectiveness adds another layer of nuance because all of these aircraft rely on elevon control surfaces which mix the inputs of elevator and aileron commands into one deflection angle for each elevon. When performing a pure elevator deflection, any small deviation between the elevons will cause a rapid, unexpected rolling motion.

MUFASA-M's longitudinal and lateral response characteristics are further compared across aircraft types by normalizing the aircraft's pitch and roll rates. The aircraft's roll-rate responses were normalized using Eq. 6.3 (Stevens et al., 2015), where $\hat{\square}$ represents a normalized variable. A similar procedure was performed for pitch-rate by switching the roll-rate

variable for pitch-rate. These normalized plots are presented in Fig. 6.18.

$$\hat{P} = \frac{Pb}{2V_a} \quad (6.3)$$



(a) Aircraft normalized roll-rate to aileron perturbation.

(b) Aircraft normalized pitch-rate to elevator perturbation.

Figure 6.18: Normalized aircraft attitude rate response following a 0.1° deflection at 2s.

The normalized MUFASA-M SSUAV roll-rate in Fig. 6.18a falls between the response of small-scale high-speed UAVs and full-scale supersonic aircraft. It should be noted that the behaviour of the Skywalker X8 UAV following its initial 0.5s response is an outlier among the aircraft as it's roll-rate does not return to zero. Recent work by Reinhardt et al. (2022) indicates updates to the Skywalker X8 model developed by Gryte et al. (2018) are required due to unspecified issues observed. As the Skywalker X8 data was obtained from external sources commenting on why this behaviour occurs is outside the scope of this work.

The normalized MUFASA-M SSUAV pitch-rate in Fig. 6.18b follows a similar response to all of the full-scale supersonic aircraft. The small-scale UAVs have a larger normalized pitch rate response than the supersonic aircraft. The Skywalker X8 is once again an outlier which could

be caused by either an issue with coefficients obtained (Reinhardt et al., 2022) or because of its blended-wing-body design making it quite different than the highly-swept delta-wings characterizing the other aircraft. Two interesting results are extrapolated from these figures. Firstly, the MUFASA-M SSUAV behaves more similarly in roll-rate to small-scale UAVs than large-scale aircraft, even though all aircraft behave similarly in pitch-rate. Secondly, even when normalized, there still exists a order of magnitude difference between roll-rate and pitch-rate response magnitudes. Knowing this behaviour, future work can explore potential control system and physical design mitigation strategies.

Chapter 7

Conclusions

SSUAVs are envisioned as cost effective tools to aid in supersonic aircraft technology development (Eckstrom and Peele, 1975). These SSUAVs have the potential to be low cost, fast to produce, and safer than full-scale experimental aircraft. Multiple challenges still exist before SSUAVs take flight. A comprehensive overview of SSUAV flying qualities, along with a UAV standard to evaluate them, is critical for further development (Klyde et al., 2020a).

This thesis obtained SSUAV aerodynamic and flying quality data by modelling the MUFASA SSUAV concept. Aerodynamic coefficient data was coupled with inertial data to generate a 6-DOF nonlinear Newtonian flight mechanics model. Model implementation was kept modular to support future design revisions and analysis of additional aircraft. The MUFASA SSUAV was compared against the MIL-STD-1797A standard for full-scale aircraft via Froude scaling, and exhibited mostly acceptable (level 2) performance at the analyzed cruise conditions of 4km altitude and $350\frac{m}{s}$. MUFASA’s flying quality parameters were evaluated against a proposed continuous modification of MIL-STD-1797A. This evaluation was performed across MUFASA’s flight regime to generate a handling quality level surface that is a new tool for flying quality based flight trajectory optimization. Though the proposed modification to MIL-STD-1797A was designed to yield a continuous handling quality evaluation, abrupt transitions were still present. These abrupt handling quality level transitions are

attributed to slight aerodynamic coefficient changes occurring where data was collected and a lack of specifications to quantify instability.

It was determined that the MUFASA-M SSUAV, and possibly most SSUAV designs, are unique in that they combine handling quality challenges from both small-scale UAVs and supersonic delta-wing aircraft. When comparing each aircraft at its cruise conditions, MUFASA achieved a roll-rate at least twice as fast as small-scale UAVs, and an order of magnitude faster than full-scale supersonic aircraft. MUFASA exhibited roll-rate behaviour more similar to small-scale UAVs than full-scale supersonic aircraft when normalized. While the flying quality modal time constants of small-scale UAVs and MUFASA were similar, MUFASA's greater maximum speed meant that significantly shorter response times were achieved. With regards to pitch-rate, MUFASA's performance was inbetween that of small-scale UAVs and full-scale supersonic aircraft. Thus, when normalized MUFASA exhibits roll behaviour inline with a small-scale UAV, but pitch behaviour inline with a full-scale supersonic aircraft. Taken together, the MUFASA-M SSUAV poses unique handling quality challenges that combine elements of small-scale UAVs and large-scale supersonic aircraft.

7.1 Recommendations and Future Work

Due to the novelty of SSUAV development and UAV flying quality standards, multiple directions of future work exist for each. Recommendations for future UAV flying quality standard development are presented in Section 7.1.1. Next steps for SSUAV development, including the future of the MUFASA UAV are presented in Section 7.1.2.

7.1.1 UAV Flying Qualities

A lack of UAV flying quality data has been cited as a current roadblock in the development of a UAV specific flying quality standard (Holmberg et al., 2008; Klyde et al., 2020a). While this thesis work has contributed SSUAV data to the conversation, it has been limited to the

application of crewed standards to a single SSUAV. The flying quality evaluation of more SSUAVs and high-speed UAVs would provide additional data points to confirm if MUFASA or MUFASA-M are reasonably representative of all delta-wing SSUAV concepts. A further review and modelling of unique hobbyist UAV creations would provide an exciting wealth of UAV flying quality data.

How model parameters and initial conditions influence a UAV’s flying and handling qualities, and to what extent, is a potential future area of research. A sensitivity analysis comparing the impact of changing UAV model parameters (such as mass location, inertia, and aerodynamic coefficients) or initial conditions (velocity, AOA, sideslip, and altitude) on flying qualities could highlight parameters or flight states that dominate an aircraft’s behaviour.

This work has been limited to flying quality damping, natural frequency and time response parameters. Aircraft bandwidth coupled with MTE analysis is becoming a more popular way to evaluate flying and handling qualities (Klyde et al., 2018). While no specific standards exist yet for UAVs, a bandwidth evaluation should be performed on MUFASA. To facilitate a bandwidth flying quality evaluation a preliminary closed-loop control system will need to be implemented.

7.1.2 SSUAV Development

Experimental validation of the aerodynamic coefficients and the modelling approach presented in this thesis can be achieved by future flights of the Simba and MUFASA aircraft. This experimental data could then also contribute to flying quality standardization for SSUAVs.

With regards to MUFASA’s development, design, modelling, and evaluation improvements can be explored. The MUFASA A aerodynamic profile is laterally unstable. MUFASA must be redesigned in its next aerodynamic iteration (MUFASA B.1) to be aerodynamically stable with regards to sideslip. Directional stability could be improved by increasing MU-

FASA’s tail volume coefficient (Boisseau, 1955; Ciliberti et al., 2017) or via the addition of forebody strakes to the fuselage (Shah and Granda, 1998). This design process should be performed following delta-wing design best practices (Merlin, 2009; Morgan, 1972) and with consideration of the flying and handling quality procedures detailed in this thesis. A possible addition to the aircraft’s modelling is the inclusion of flexible airframe equations. As there is no experimental data to compare to, the constraint of a rigid airframe may not be valid for small-scale UAVs as suggested by Guimarães et al. (2022). Preliminary work by Guimarães et al. (2022) and Mai et al. (2019) indicates aeroelastic effects would not be negligible in SSUAV designs or during supersonic flight. Their preliminary work suggests that corrections via aeroelastic filtering might need to be performed once MUFASA’s aeroelastic behaviour becomes available. Additionally a control surface sizing and flutter analysis could determine if the sensitivities with respect to roll-rate observed in this work will cause instability in real world flight testing. The results of this sensitivity analysis could highlight further control requirements or inform the design process moving forward. The SSUAV design process must maintain a balance between controllability, manufacturing, and aerodynamic performance. It may be that SSUAVs require specific design considerations, such as an additional set of control surfaces, to apply and facilitate satisfactory lateral roll control.

Further research into SSUAV roll-rate sensitivity should be undertaken via aerodynamic design or mass distribution. Work could examine methods to reduce directional instability via aerodynamic changes like the addition of chines (McMaster and Schenkt, 1974), or implementation of a gull-wing design (Morgan, 1972). Alternatively, roll inertia could be increased by distributing UAV mass in the y_b axis away from the aircraft centreline. This weight redistribution could be accomplished by employing a lower mass propulsion system, such as the proposed Atlantis Intake System (Wilson et al., 2015), and redistributing the weight saved to the wingtips. Additionally, the flying and handling quality feasibility of various vehicle scales could be evaluated. Response results in Section 6.6 often saw the MUFASA-M SSUAV exhibiting behaviours similar to small-scale UAVs or full-scale aircraft

depending on whether the perturbation occurred in pitch or roll. An aircraft scale optimization based on flying qualities could add to the mechanical aircraft scale optimization performed by Dalman (2021). Finally, a control system should be implemented to evaluate the feasibility of controlling the optimized aerodynamic configuration and size. This control system should be capable of controlling the UAV not just at one point, but throughout its flight regime.

Bibliography

Aerion Supersonic (2021). Aerion AS2. <https://www.aerionsupersonic.com/>.

Ahrens, J., Geveci, B., and Law, C. (2005). Paraview: An end-user tool for large data visualization. *The visualization handbook*, 717(8).

Air Registration Board and Secrétariat Général a l’Aviation Civile (1969). TSS standards, part 3 - flying qualities. Technical report, Air Registration Board (England) or Secrétariat Général a l’Aviation Civile (France).

American Institute of Aeronautics and Astronautics (2016). Standard: Flight dynamics model exchange standard (ANSI/AIAA S-119-2011(2016)). Technical report, American Institute of Aeronautics and Astronautics, Reston, Virginia.

Ammar, S., Legros, C., and Trépanier, J.-Y. (2017). Conceptual design, performance and stability analysis of a 200 passengers blended wing body aircraft. *Aerospace Science and Technology*, 71:325–336.

Anderson, J. (1999). *Aircraft performance and design*, volume 1. WCB/McGraw-Hill, Boston.

Anderson, J. (2011). *Fundamentals of aerodynamics (SI units)*. McGraw-Hill, 5 edition.

Aprovitola, A., Di Nuzzo, P. E., Pezzella, G., and Viviani, A. (2021). Aerodynamic analysis of a supersonic transport aircraft at landing speed conditions. *Aerospace*, 14(20):6615.

- Ashton, N. and Skaperdas, V. (2019). Verification and validation of OpenFOAM for high-lift aircraft flows. *Journal of Aircraft*, 56(4):1641–1657.
- Barbosa, L. M. F., Maciel, F. M. O., and de Barros, J. E. M. (2014). Study of unmanned supersonic aircraft configuration. In *23rd SAE Brasil International Congress and Display*, pages 1–10. SAE.
- Beard, R. W. and McLain, T. W. (2012). *Small unmanned aircraft: Theory and practice*. Princeton University Press, Princeton.
- Berndt, J. (2004). JSBSim: An open source flight dynamics model in C++. In *AIAA Modeling and Simulation Technologies Conference and Exhibit*, pages 1–27, Providence, Rhode Island. American Institute of Aeronautics and Astronautics.
- Berry, D. T. (1978). A summary of YF-12 handling qualities. In *YF-12 Experiments Symposium*, pages 95–96, Edwards, California. National Aeronautics and Space Administration.
- Berry, D. T. and Powers, B. G. (1970). Flying qualities of a large, supersonic aircraft in cruise and landing approach. In *Propulsion and ASW Meeting*, pages 1–11, Tullahoma, Tennessee. American Institute of Aeronautics and Astronautics.
- Bertolin, R., Chaves Barbosa, G., Cunis, T., Kolmanovsky, I. V., and Cesnik, C. E. (2022). Gust rejection of a supersonic aircraft during final approach. In *AIAA SCITECH 2022 Forum*, pages 1–19, San Diego, California. American Institute of Aeronautics and Astronautics.
- Bogos, S. and Stroe, I. (2012). Similarity criteria for “full” and “scale” aircraft on the lateral stability analysis. *UPB Scientific Bulletin, Series D: Mechanical Engineering*, 74(4):13–26.
- Boisseau, P. C. (1955). Investigation in the Langley free-flight tunnel of the low-speed stability and control characteristics of a 1/10-scale model simulating the convair F-102A

- airplane. Technical report NACA-RM-SL55B21, National Advisory Committee for Aeronautics, Langley Field, Va.
- Boom Technology (2022). Overture. <https://boomsupersonic.com/>.
- Bradley, A., Boehme, R. F., and Johnson, C. L. (1963). Manufacturer’s model specification. Technical report SP-582, Lockheed Aircraft Corporation, Burbank, California.
- Burk, S. M. and Wilson, C. F. (1975). Radio-controlled model design and testing techniques for stall/spin evaluation of general-aviation aircraft. Technical report NASA-TM-80510, National Aeronautics and Space Administration, Hampton, Virginia.
- Burnashev, V. and Zbrutsky, A. (2019). Robust controller for supersonic unmanned aerial vehicle. *Aviation*, 23(1):31–35.
- Cai, G., Dias, J., and Seneviratne, L. (2014). A survey of small-scale unmanned aerial vehicles: Recent advances and future development trends. *Unmanned Systems*, 02(02):175–199.
- Campos, L. M. B. C. and Marques, J. M. G. (2021). On the handling qualities of two flying wing aircraft configurations. *Aerospace*, 8(3):77.
- Candel, S. (2004). Concorde and the future of supersonic transport. *Journal of Propulsion and Power*, 20(1):59–68.
- Capello, E., Guglieri, G., Marguerettaz, P., and Quagliotti, F. (2012). Preliminary assessment of flying and handling qualities for mini-UAVs. *Journal of Intelligent & Robotic Systems*, 65(1-4):43–61.
- Ciliberti, D., Della Vecchia, P., Nicolosi, F., and De Marco, A. (2017). Aircraft directional stability and vertical tail design: A review of semi-empirical methods. *Progress in Aerospace Sciences*, 95(November):140–172.

- Collard, D. (1991). Concorde airframe design and development. *Journal of Aerospace*, 100:2620–2641.
- Cook, M. V. (2012). *Flight dynamics principles: A linear systems approach to aircraft stability and control*. Butterworth-Heinemann.
- Cooper, G. E. and Harper, R. P. (1969). The use of pilot rating in the evaluation of aircraft handling qualities. Technical report NASA TN D-5153, National Aeronautics and Space Administration, Washington, D.C.
- Cotting, M. (2009). An initial study to categorize unmanned aerial vehicles for flying qualities evaluation. In *47th AIAA Aerospace Sciences Meeting including The New Horizons Forum and Aerospace Exposition*, pages 1–12, Orlando, Florida. American Institute of Aeronautics and Astronautics.
- Cotting, M. (2010a). Proposed longitudinal flying qualities criterion for unpiloted autonomous aircraft, starting the conversation. In *AIAA Atmospheric Flight Mechanics Conference*, pages 1–26, Toronto, Ontario Canada. American Institute of Aeronautics and Astronautics.
- Cotting, M. C. (2010b). *Evolution of flying qualities analysis: Problems for a new generation of aircraft*. [Doctoral dissertation, Virginia Polytechnic Institute and State University].
- Cox, T. and Jackson, D. (1997). Supersonic flying qualities experience using the SR-71. In *22nd Atmospheric Flight Mechanics Conference*, pages 1–13, Edwards, California. National Aeronautics and Space Administration, American Institute of Aeronautics and Astronautics.
- Craighead, J., Murphy, R., Burke, J., and Goldiez, B. (2007). A survey of commercial & open source unmanned vehicle simulators. In *Proceedings 2007 IEEE International Conference on Robotics and Automation*, pages 852–857, Rome, Italy. IEEE.

- Dalman, B. (2021). Conceptual design methods for small-scale supersonic uncrewed aerial vehicles. [Master’s thesis, University of Calgary].
- Dalman, B., Korobenko, A., Ziade, P., Ramirez-Serrano, A., and Johansen, C. T. (2021). Validation and verification of a conceptual design tool for evaluating small-scale, supersonic, unmanned aerial vehicles. In *AIAA AVIATION 2021 FORUM*, pages 1–31, Virtual Event. American Institute of Aeronautics and Astronautics.
- De Marco, A., Duke, E. L., and Berndt, J. S. (2007). A general solution to the aircraft trim problem. In *AIAA Modeling and Simulation Technologies Conference and Exhibit*, volume 2, pages 1–40, Hilton Head, South Carolina.
- Department of Defense (1980). Military specification: Flying qualities of piloted airplanes. Technical report MIL-F-8785C, U.S. Military.
- Department of Defense (1990). Lateral-directional static stability. In *Flying Qualities Phase*, volume II, chapter 7, pages 1–108. Defense Technical Information Center, Edwards, California.
- Department of Defense (1997). Flying qualities of piloted aircraft. Technical report MIL-HDBK-1797, U.S. Military, Washington, D.C.
- Department of Defense (2000). Aeronautical design standard performance specification handling qualities requirements for military rotorcraft. Technical report ADS-33E-PRF, U.S. Military, Redstone Arsenal, Alabama.
- Department of Defense (2002). Unmanned aerial vehicle roadmap. Technical report, U.S. Military, Washington, D.C.
- Department of Defense (2004). Flying qualities of piloted aircraft. Technical report MIL-STD-1797A, U.S. Military.

- Department of Defense (2009). FY2009–2034 unmanned systems integrated roadmap. Technical report, U.S. Military.
- Department of Defense (2011). Mishap notification, investigation, reporting, and record keeping. Technical report 6055.07, U.S. Military, Washington, D.C.
- Duke, E. L., Antoniewicz, R., and Krambeer, K. (1994). Derivation and definition of a linear aircraft model. Technical report 1207, National Aeronautics and Space Administration, Edwards, California.
- Durante, B. J., Gair, S. R., Ramirez-Serrano, A., Morton, C., and Johansen, C. T. (2022). Development and controllability evaluation of a small-scale supersonic UAV. In *AIAA AVIATION 2022 Forum*, pages 1–18, Chicago, IL & Virtual. American Institute of Aeronautics and Astronautics.
- Eça, L. and Hoekstra, M. (2014). A procedure for the estimation of the numerical uncertainty of CFD calculations based on grid refinement studies. *Journal of Computational Physics*, 262:104–130.
- Eckstrom, C. V. and Peele, E. L. (1975). Flight assessment of a large supersonic drone aircraft for research use. Technical report NASA TM X-3259, National Aeronautics and Space Administration, Hampton, Virginia.
- Economou, T. D., Palacios, F., Copeland, S. R., Lukaczyk, T. W., and Alonso, J. J. (2016). SU2: An open-source suite for multiphysics simulation and design. *AIAA Journal*, 54(3):828–846.
- Etele, J. (2006). Overview of wind gust modelling with application to autonomous low-level UAV control. Technical report, Defence Research and Development Canada.
- Exosonic (2022). Exosonic. <https://www.exosonic.com/>.

- Foster, T. and Bowman, J. (2005). Dynamic stability and handling qualities of small unmanned- aerial vehicles. In *43rd AIAA Aerospace Sciences Meeting and Exhibit*, pages 1–12, Reno, Nevada. American Institute of Aeronautics and Astronautics.
- Franke, U. E. (2014). The global diffusion of unmanned aerial vehicles (UAVs), or ‘drones’. In Aaronson, M., Aslam, W., Dyson, T., and Rauxloh, R., editors, *Precision strike warfare and international intervention: Strategic, ethico-legal and decisional implications*, chapter 3, pages 52–72. Routledge, Abingdon, United Kingdom.
- Franke, U. E. (2018). *The unmanned revolution: How drones are revolutionising warfare*. [Doctoral dissertation, New College, Oxford].
- Gabaldo, M., Barros, J. E., Guerra, M. D., and Oliveira, E. (2016). Aerothermodynamic simulation model for new hypersonic propulsion: Rocket ignited supersonic combustion ram jet. In *AIAA SPACE 2016*, pages 1–13, Long Beach, California. American Institute of Aeronautics and Astronautics.
- Geisler, R. L., Moore, T. L., Rohrbaugh, E. M., and Pignoli, C. R. (2007). Unlocking the mystery of the D-21B solid rocket boosted air-launched Mach-3 UAV. In *Collection of Technical Papers - 43rd AIAA/ASME/SAE/ASEE Joint Propulsion Conference*, volume 8, pages 7411–7424, Cincinnati, Ohio.
- Geuzaine, C. and Remacle, J.-F. (2009). Gmsh: A 3-d finite element mesh generator with built-in pre- and post-processing facilities. *International Journal for Numerical Methods in Engineering*, 79(11):1309–1331.
- Goins, J. (1964). SR-71A blackbird. <https://www.af.mil/News/Art.aspx?igphoto=2000791546>.
- Grauer, J. A. and Morelli, E. A. (2015). Generic global aerodynamic model for aircraft. *Journal of Aircraft*, 52(1):13–20.

- Greene, K. M., Kunz, D. L., and Cotting, M. C. (2014). Toward a flying qualities standard for unmanned aircraft. In *AIAA Atmospheric Flight Mechanics Conference*, pages 1–19, Atlanta, Georgia. American Institute of Aeronautics and Astronautics.
- Gryte, K. (2015). High angle of attack landing of an unmanned aerial vehicle. [Master’s thesis, Norwegian University of Science and Technology].
- Gryte, K., Hann, R., Alam, M., Rohac, J., Johansen, T. A., and Fossen, T. I. (2018). Aerodynamic modeling of the Skywalker X8 fixed-wing unmanned aerial vehicle. In *2018 International Conference on Unmanned Aircraft Systems, ICUAS 2018*, pages 826–835, Dallas.
- Guillermo-Monedero, D. (2020). A comparison of euler finite volume and supersonic vortex lattice methods used during the conceptual design phase of supersonic delta wings. [Master’s thesis, Ohio State University].
- Guimarães, T. A., Cesnik, C. E., and Kolmanovsky, I. V. (2022). An integrated low-speed aeroelastic-flight-dynamics framework for modeling supersonic aircraft. In *AIAA SCITECH 2022 Forum*, pages 1–15, San Diego, California. American Institute of Aeronautics and Astronautics.
- Guinness World Records (2017). Fastest remote-controlled (RC) jet-powered model aircraft. [https://www.guinnessworldrecords.com/world-records/fastest-remote-controlled-jet-powered-model-aircraft-\(rc\)](https://www.guinnessworldrecords.com/world-records/fastest-remote-controlled-jet-powered-model-aircraft-(rc)).
- Gupta, S. G., Ghonge, M. M., and Jawandhiya, P. (2013). Review of unmanned aircraft system (UAS). *International Journal of Advanced Research in Computer Engineering & Technology (IJARCET)*, 2(4):1–23.
- Harper, R. P. and Cooper, G. E. (1986). Handling qualities and pilot evaluation. *Journal of Guidance, Control, and Dynamics*, 9(5):515–529.

- Harris, J. J. and Stanford, J. R. (2018). F-35 flight control law design, development and verification. In *2018 Aviation Technology, Integration, and Operations Conference*, pages 1–18, Atlanta, Georgia.
- Hassanalian, M. and Abdelkefi, A. (2017). Classifications, applications, and design challenges of drones: A review. *Progress in Aerospace Sciences*, 91:99–131.
- Heffley, R. K. and Jewell, W. T. (1972). Aircraft handling qualities data. Technical report NASA CR-2144, American Institute of Aeronautics and Astronautics, Hawthorne, California.
- Hildmann, H. and Kovacs, E. (2019). Review: Using unmanned aerial vehicles (UAVs) as mobile sensing platforms (MSPs) for disaster response, civil security and public safety. *Drones*, 3(3):59.
- Holmberg, J., Leonard, J., King, D., and Cotting, M. (2008). Flying qualities specifications and design standards for unmanned air vehicles. In *AIAA Atmospheric Flight Mechanics Conference and Exhibit*, pages 1–14, Honolulu, Hawaii. American Institute of Aeronautics and Astronautics.
- Hussain, M. M., Siddiqui, B. A., and Memon, A. (2019). Design and analysis of rocket assisted take-off high-speed UAV. In *6th International Conference on Aerospace Science and Engineering*, pages 1–8, Islamabad, Pakistan. IEEE.
- Iwamiya, T. (2002). A computational study on unmanned scaled supersonic experimental airplane. In *32nd AIAA Fluid Dynamics Conference and Exhibit*, pages 1–9, St. Louis, Missouri. American Institute of Aeronautics and Astronautics.
- Jackson, B., Madden, M. M., Shelton, R., Castro, M. P., Noble, D. M., and Zimmerman, C. (2015). Further development of verification check-cases for six-degree-of-freedom flight vehicle simulations. In *AIAA Modeling and Simulation Technologies Conference*, pages 1–34, Kissimmee, Florida. American Institute of Aeronautics and Astronautics.

- Jacob, S. M., Burgess, J., Watson, C., Compton, J., Jalan, G., Park, M., Schroeder, B., and Vallabhaneni, S. (2021). Proposed design of a transonic unmanned aircraft system as a platform for understanding supersonic flight design. In *AIAA AVIATION 2021 FORUM*, pages 1–12, Virtual Event. American Institute of Aeronautics and Astronautics.
- Japan Aerospace Exploration Agency (2012). D-SEND database. https://d-send.jaxa.jp/d_send_e/index.html.
- Jardin, M. and Mueller, E. (2007). Optimized measurements of UAV mass moment of inertia with a bifilar pendulum. In *AIAA Guidance, Navigation and Control Conference and Exhibit*, volume 5, pages 1–23, Hilton Head, South Carolina. American Institute of Aeronautics and Astronautics.
- Katz, J. (1999). Wing/vortex interactions and wing rock. *Progress in Aerospace Sciences*, 35(7):727–750.
- Kawaguchi, J., Suzuki, H., Ninomiya, T., and Tomita, H. (2017). Post-flight evaluation of the guidance and control for D-SEND#2 2nd drop test. In *AIAA Atmospheric Flight Mechanics Conference*, pages 1–12, Grapevine, Texas. American Institute of Aeronautics and Astronautics.
- Keane, A. J., Sóbester, A., and Scanlan, J. P. (2017). *Small unmanned fixed-wing aircraft design: A practical approach*. John Wiley & Sons.
- Kim, C. S., Ji, C. H., and Kim, B. S. (2020). Development of flight control law for improvement of uncommanded lateral motion of the fighter aircraft. *International Journal of Aeronautical and Space Sciences*, 21(4):1059–1077.
- Klyde, D. H., Schulze, C. P., Miller, J. P., Manriquez, J. A., Kotikalpudi, A., Mitchell, D. G., Seiler, P. J., Regan, C., Taylor, B., and Olson, C. (2020a). Defining handling qualities of unmanned aerial systems: Phase II final report. Technical Report NASA/CR–2020–220564, National Aeronautics and Space Administration, Hawthorne, California.

- Klyde, D. H., Schulze, P. C., Mitchell, D. G., and Alexandrov, N. (2018). Development of a process to define unmanned aircraft systems handling qualities. In *2018 AIAA Atmospheric Flight Mechanics Conference*, pages 1–16, Kissimmee, Florida. American Institute of Aeronautics and Astronautics.
- Klyde, D. H., Schulze, P. C., Mitchell, D. G., Sizoo, D., Schaller, R., and McGuire, R. (2020b). Mission task element development process: An approach to FAA handling qualities certification. In *AIAA AVIATION 2020 FORUM*, pages 1–15, Virtual Event. American Institute of Aeronautics and Astronautics.
- Langston, S., Nelson, C. P., and Livne, E. (2016). Low-speed stability and control of a reduced scale long-range supersonic configuration with reduced-size or no vertical tail. In *AIAA Atmospheric Flight Mechanics Conference*, pages 1–44, San Diego, California. American Institute of Aeronautics and Astronautics.
- Lensi, M. (2000). Estimating open-loop stability and control derivatives for the Tu-144LL supersonic transport from flight data. In *Atmospheric Flight Mechanics Conference*, Denver, Colorado. American Institute of Aeronautics and Astronautics.
- Liepmann, H. W. (1952). On the application of statistical concepts to the buffeting problem. *Journal of the Aeronautical Sciences*, 19(12):793–800.
- Livne, E. (2017). Integrated research/education university aircraft design program development. Technical report AFRL-AFOSR-VA-TR-2017-0077, University of Washington.
- Livne, E. and Nelson, C. (2012). From blank slate to flight ready new small research UAVs in twenty weeks - undergraduate airplane design at the University of Washington. In *50th AIAA Aerospace Sciences Meeting including the New Horizons Forum and Aerospace Exposition*, pages 1–39, Nashville, Tennessee. American Institute of Aeronautics and Astronautics.

- Lockheed Martin (2016). Quick and quiet: Supersonic flight promises to hush the sonic boom. <https://www.lockheedmartin.com/en-us/news/features/2016/webt-supersonic-flight-hush-sonic-boom.html>.
- Loschke, R. (2003). Development of the F-117 flight control system. In *AIAA Guidance, Navigation, and Control Conference and Exhibit*, pages 1–12, Austin, Texas. American Institute of Aeronautics and Astronautics.
- Luckring, J. M., Park, M. A., Hitzel, S. M., Jirásek, A., Lofthouse, A. J., Morton, S. A., McDaniel, D. R., Rizzi, A., and Tomac, M. (2017). Synthesis of hybrid computational fluid dynamics results for F-16XL aircraft aerodynamics. *Journal of Aircraft*, 54(6):2100–2114.
- MacDonald, T., Botero, E., Vegh, J. M., Variyar, A., Alonso, J. J., Orra, T. H., and Ilario da Silva, C. R. (2017). SUAVE: An open-source environment enabling unconventional vehicle designs through higher fidelity. In *55th AIAA Aerospace Sciences Meeting*, pages 1–14, Grapevine, Texas. American Institute of Aeronautics and Astronautics.
- Machida, S., Yoshida, K., and Ohnuki, T. (2007). Supersonic flight testing of unmanned experimental airplane for next-generation SST. In *45th AIAA Aerospace Sciences Meeting and Exhibit*, pages 1–7, Reno, Nevada. American Institute of Aeronautics and Astronautics.
- Magee, T. E., Hayes, P. J., Dorgan, A. J., and Khodadoust, A. (2022). Dynamic stability characteristics for commercial supersonic configurations at low-speed flight conditions. In *AIAA SCITECH 2022 Forum*, pages 1–38, San Diego, California. American Institute of Aeronautics and Astronautics.
- Mai, H., Nitzsche, J., Saitoh, K., and Yoshimoto, N. (2019). Control surface dynamics at transonic airspeeds. In *International Forum on Aeroelasticity and Structural Dynamics 2019, IFASD 2019*, pages 1–17, Savannah, Georgia. International Forum on Aeroelasticity and Structural Dynamics.

- Mandal, T. and Gu, Y. (2016). Analysis of pilot-induced-oscillation and pilot vehicle system stability using UAS flight experiments. *Aerospace*, 3(4):42.
- MathWorks (2021a). COESA atmosphere model. <https://www.mathworks.com/help/aeroblks/coesaatmospheremodel.html>.
- MathWorks (2021b). Exact linearization algorithm. <https://www.mathworks.com/help/slcontrol/ug/exact-linearization-algorithm.html>.
- MathWorks (2021c). findop. <https://www.mathworks.com/help/slcontrol/ug/findop.html>.
- MathWorks (2021d). Integrator. <https://www.mathworks.com/help/simulink/slref/integrator.html>.
- MathWorks (2021e). Simulation Pace. <https://www.mathworks.com/help/aeroblks/simulationpace.html>.
- Mavriplis, N., Ting, K.-Y., Moustafa, A., Hill, C., Soltani, R., Nelson, C. P., and Livne, E. (2022). Supersonic configurations at low speeds (SCALOS): Test / simulation correlation studies. In *AIAA SCITECH 2022 Forum*, pages 1–13, San Diego, California. American Institute of Aeronautics and Astronautics.
- McCrink, M. H. and Gregory, J. W. (2021). Design and development of a high-speed UAS for beyond visual line-of-sight operations. *Journal of Intelligent and Robotic Systems: Theory and Applications*, 101(2):1–16.
- Mcmaster, J. R. and Schenkt, F. L. (1974). Development of the F-12 aircraft flight control system. *Journal of Aircraft*, 11(4):225–231.
- Merlin, P. (2009). Design and development of the blackbird: Challenges and lessons learned. In *47th AIAA Aerospace Sciences Meeting including The New Horizons Forum*

- and Aerospace Exposition*, pages 1–38, Orlando, Florida. American Institute of Aeronautics and Astronautics.
- Mettler, B., Tischler, M. B., and Kanade, T. (1999). System identification of small-size unmanned helicopter dynamics. In *Annual Forum Proceedings - American Helicopter Society*, volume 2, pages 1706–1717, Montreal, Canada. American Helicopter Society, Inc.
- Meyer, J., McMaster, J., and Moody, R. (1964). Handling qualities of the SR-71. Technical report SP-508, Lockheed Advanced development Company, Burbank, California.
- Meyer, R. and Husband, E. (1990). Large aircraft flying qualities revisited. In *17th Atmospheric Flight Mechanics Conference*, pages 456–464, Portland, OR. American Institute of Aeronautics and Astronautics.
- Michailidis, M. G., Rutherford, M. J., and Valavanis, K. P. (2020). A survey of controller designs for new generation UAVs: The challenge of uncertain aerodynamic parameters. *International Journal of Control, Automation and Systems*, 18(4):801–816.
- Miller, M. (1930). An accurate method of measuring the moments of inertia of airplanes. Technical report 351, Langley Memorial aeronautical Laboratory, Washington.
- Mills, S. (2019). *The dawn of the drone: From the back-room boys of World War One*. Casemate.
- Mitchell, D. G., Doman, D. B., Key, D. L., Klyde, D. H., Leggett, D. B., Moorhouse, D. J., Mason, D. H., Raney, D. L., and Schmidt, D. K. (2004). Evolution, revolution, and challenges of handling qualities. *Journal of Guidance, Control, and Dynamics*, 27(1):12–28.
- Mitchell, D. G., Hoh, R. H., Aponso, B. L., and Klyde, D. H. (1994). Proposed incorporation of mission-oriented flying qualities into MIL-STD-1797A. Technical report WL-TR-94-3162, Systems Technology, Inc., Hawthorne, California.

- Mitchell, D. G., Klyde, D. H., Pitoniak, S., Schulze, P. C., Manriquez, J. A., Hoffler, K. D., and Jackson, E. B. (2020). NASA’s flying qualities research contributions to MIL-STD-1797C. Technical report NASA/CR-2020-5002350, National Aeronautics and Space Administration, Long Beach, California.
- Mizobata, K., Minato, R., Higuchi, K., Ueba, M., Takagi, S., Nakata, D., Higashino, K., and Tanatsugu, N. (2014). Development of a small-scale supersonic flight experiment vehicle as a flying test bed for future space transportation research. *Transactions of the Japan Society for Aeronautical and Space Sciences, Aerospace Technology Japan*, 12(29):1–10.
- Mizobata, K., Minato, R., Kimura, H., Sugiyama, H., Tanatsugu, N., and Arai, T. (2005). Development study on a small-scale supersonic flight experiment vehicle with air-breathing propulsion. In *AIAA/CIRA 13th International Space Planes and Hypersonics Systems and Technologies Conference*, pages 1–6, Capua, Italy.
- Moes, T. R. and Iliff, K. (2002). Stability and control estimation flight test results for the SR-71 aircraft with externally mounted experiments. Technical report NASA/TP-2002-210718, National Aeronautics and Space Administration.
- Mohamed, A., Massey, K., Watkins, S., and Clothier, R. (2014). The attitude control of fixed-wing MAVS in turbulent environments. *Progress in Aerospace Sciences*, 66:37–48.
- Morgan, M. (1972). A new shape in the sky. *The Aeronautical Journal*, 76(733):1–18.
- Moritz, H. (1980). Geodetic reference system 1980. *Bulletin géodésique*, 54(3):395–405.
- Murakami, Y., KWAK, D.-Y., and NAKAHATA, K. (2008). Flight test verification of the guidance and navigation systems design for an unmanned scaled supersonic experimental airplane NEXST-1. In *AIAA Guidance, Navigation and Control Conference and Exhibit*, pages 1–14, Honolulu, Hawaii. American Institute of Aeronautics and Astronautics.

National Aeronautics and Space Administration (2022). Quesst. <https://www.nasa.gov/X59>.

National Oceanic and Atmospheric Administration, National Aeronautics and Space Administration, and United States Air Force (1976). *US standard atmosphere, 1976*. U.S. Government Printing Office.

Nelson, C. P., Ting, K.-Y., Mavriplis, N., Soltani, R., and Livne, E. (2022). Supersonic configurations at low speeds (SCALOS): Project background and progress at University of Washington. In *AIAA SCITECH 2022 Forum*, pages 1–32, San Diego, California. American Institute of Aeronautics and Astronautics.

Ninomiya, T., Suzuki, H., and Kawaguchi, J. (2018). Dynamic inversion controller design for balloon-launched supersonic aircraft. *Transactions of the Japan Society for Aeronautical and Space Sciences*, 61(6):248–257.

North Atlantic Treaty Organization (2016). Unmanned aircraft systems airworthiness requirements. Technical report AJP-3.3, North Atlantic Treaty Organization, Brussels, Belgium.

North Atlantic Treaty Organization (2019). Unmanned aircraft systems airworthiness requirements. Technical report AEP-4671, North Atlantic Treaty Organization, Brussels, Belgium.

Ozyetis, E. and Alemdaroglu, N. (2014). Design and manufacturing of a high speed jet powered UAV. In *2014 International Conference on Unmanned Aircraft Systems (ICUAS)*, pages 974–983, Orlando, Florida. IEEE.

Palacios, F., Alonso, J., Duraisamy, K., Colonno, M., Hicken, J., Aranake, A., Campos, A., Copeland, S., Economon, T., Lonkar, A., Lukaczyk, T., and Taylor, T. (2013). Stanford University Unstructured (SU2): An open-source integrated computational environment for

- multi-physics simulation and design. In *51st AIAA Aerospace Sciences Meeting including the New Horizons Forum and Aerospace Exposition*, pages 1–60, Grapevine, Texas. American Institute of Aeronautics and Astronautics.
- Pamadi, B., Brauckmann, G., Ruth, M., and Fuhrmann, H. (2001). Aerodynamic characteristics, database development and flight simulation of the X-34 vehicle. *Journal of Spacecraft and Rockets*, 38(3):334–344.
- Panta, A., Mohamed, A., Marino, M., Watkins, S., and Fisher, A. (2018). Unconventional control solutions for small fixed wing unmanned aircraft. *Progress in Aerospace Sciences*, 102(May):122–135.
- Prasad B., B. and Pradeep, S. (2007). Automatic landing system design using feedback linearization method. In *AIAA Infotech@Aerospace 2007 Conference and Exhibit*, volume 1, pages 1–20, Rohnert Park, California. American Institute of Aeronautics and Astronautics.
- Prosser, C. F. and Wiler, C. D. (1976). RPV flying qualities design criteria. Technical report AFFDL-TR-76-125, Rockwell International Corporation, Columbus, Ohio.
- Rech, J. and Leyman, C. (1980). *Case Study by Aerospatiale and British Aerospace on the Concorde*. American Institute of Aeronautics and Astronautics, New York.
- Reed, D. (2021). The collapse of Aerion Supersonic shows that aviation advances must be as affordable as they are amazing. <https://tinyurl.com/AerionCollapseForbes2021-06-02>.
- Reinhardt, D., Gryte, K., and Arne Johansen, T. (2022). Modeling of the skywalker X8 fixed-wing UAV: Flight tests and system identification. In *2022 International Conference on Unmanned Aircraft Systems (ICUAS)*, pages 506–515, Dubrovnik, Croatia. IEEE.
- Roskam, J. (2001). *Airplane flight dynamics and automatic flight controls*. DARcorporation.
- Saeed, S. H. (2008). *Automatic control system*. Seagull Books Pvt Ltd.

- Sagliano, M. (2021). Open-source visualization of reusable rockets motion: Approaching simulink - FlightGear co-simulation. In *AIAA Scitech 2021 Forum*, pages 1–20, Virtual Event. American Institute of Aeronautics and Astronautics.
- Sato, Y., Imai, R., Nakata, D., Minato, R., and Uchiumi, M. (2020). Study on propellant supply system for small-scale supersonic flight experiment vehicle (development of design technology for LOX supply system). *International Journal of Microgravity Science and Application*, 37(1):1–10.
- Sebbane, Y. B. (2015). *Smart autonomous aircraft: Flight control and planning for UAV*. CRC Press, Universite d’Evry, France.
- Sepulveda, E. and Smith, H. (2017). Technology challenges of stealth unmanned combat aerial vehicles. *The Aeronautical Journal*, 121(1243):1261–1295.
- Shah, G. and Granda, J. (1998). Application of forebody strakes for directional stability and control of transport aircraft. In *23rd Atmospheric Flight Mechanics Conference*, pages 1–9, Boston, Massachusetts. American Institute of Aeronautics and Astronautics.
- Shakhatreh, H., Sawalmeh, A. H., Al-Fuqaha, A., Dou, Z., Almaita, E., Khalil, I., Othman, N. S., Khreishah, A., and Guizani, M. (2019). Unmanned aerial vehicles (UAVs): A survey on civil applications and key research challenges. *IEEE Access*, 7:48572–48634.
- Sheetz, M. (2020). Virgin Galactic’s supersonic jet would go from NYC to London in 2 hours, shattering Concorde record. <https://www.cnbc.com/2020/08/03/virgin-galactics-supersonic-jet-would-go-nyc-to-london-in-2-hours.html>.
- Sheetz, M. (2021). Aerion Supersonic shuts down, ending plans to build silent high speed business jets. <https://www.cnbc.com/2021/05/21/aerion-supersonic-shuts-down-ending-plans-for-silent-business-jets.html>.

- Snyder, C. T. (1976). Advanced control technology and airworthiness flying qualities requirements. In *Advanced Control Technol. and its Potential for Future Transport Aircraft*, pages 707–733. National Aeronautics and Space Administration.
- Sobron, A., Lundström, D., and Krus, P. (2021). A review of current research in subscale flight testing and analysis of its main practical challenges. *Aerospace*, 8(3):74.
- Spike Aerospace (2022). The Spike S-512 supersonic jet. <https://www.spikeaerospace.com/>.
- Stansbury, R. S., Rigby, K., Clifford, J., and Rudolph, D. (2015). An alternative UAS classification and analysis approach for integration into the national airspace system. In *AIAA Infotech @ Aerospace*, pages 1–19, Kissimmee, Florida. American Institute of Aeronautics and Astronautics.
- Steer, A. J. (2004). Supersonic transport aircraft longitudinal flight control law design. *Aeronautical Journal*, 108(1084):319–329.
- Steer, A. J. and Cook, M. V. (1999). Control and handling qualities considerations for an advanced supersonic transport aircraft. *The Aeronautical Journal*, 103(1024):265–272.
- Stengel, R. F. (2015). *Flight dynamics*. Princeton University Press.
- Stevens, B. L., Lewis, F. L., and Johnson, E. N. (2015). *Aircraft control and simulation: Dynamics, controls design, and autonomous systems*. John Wiley & Sons.
- Stöcker, C., Bennett, R., Nex, F., Gerke, M., and Zevenbergen, J. (2017). Review of the current state of UAV regulations. *Remote Sensing*, 9(5):1–26.
- Stoldt, H. H., Korobenko, A., Ziade, P., and Johansen, C. T. (2021). Verification and validation of high-fidelity open-source simulation tools for supersonic aircraft aerodynamic analysis. *Journal of Verification, Validation and Uncertainty Quantification*, 6(4):1–11.

- Sun, Y. and Smith, H. (2017). Review and prospect of supersonic business jet design. *Progress in Aerospace Sciences*, 90:12–38.
- Sun, Y. and Smith, H. (2020). Low-boom low-drag solutions through the evaluation of different supersonic business jet concepts. *The Aeronautical Journal*, 124(1271):76–95.
- The Mach Initiative (2023). The mach initiative. <https://themachinitiative.com/>.
- Transport Canada (2022). Aeronautical information manual.
- Tyan, M., Kim, M., Pham, V., Choi, C. K., Nguyen, T. L., and Lee, J.-W. (2018). Development of advanced aerodynamic data fusion techniques for flight simulation database construction. In *2018 Modeling and Simulation Technologies Conference*, pages 1–10, Atlanta, Georgia. American Institute of Aeronautics and Astronautics.
- Ueba, M., Kamata, T., Nakajima, S., and Maeda, Y. (2021). Verification of fully autonomous flight from takeoff to landing of a low-speed model airplane with application to a small unmanned supersonic airplane. *Transactions of the Japan Society for Aeronautical and Space Sciences, Aerospace Technology Japan*, 19(5):667–675.
- Vicroy, D. D., Huber, K. C., Schütte, A., Rein, M., Irving, J. P., Rigby, G., Löser, T., Hübner, A.-R., and Birch, T. J. (2018). Experimental investigations of a generic swept unmanned combat air vehicle with controls. *Journal of Aircraft*, 55(2):475–501.
- Virgin Galactic (2020). Virgin Galactic supersonic aircraft. <https://www.virgingalactic.com/>.
- Viviani, A., Aprovitola, A., Pezzella, G., and Rainone, C. (2021). CFD design capabilities for next generation high-speed aircraft. *Acta Astronautica*, 178(April 2020):143–158.
- Walter, S. and Starkey, R. P. (2012). GoJett: Design and optimization of a lightweight supersonic unmanned aerial flight system. In *12th AIAA Aviation Technology, Integration*

- and Operations (ATIO) Conference and 14th AIAA/ISSMO Multidisciplinary Analysis and Optimization Conference*, pages 1–13, Indianapolis, Indiana.
- Wanner, J. and Carlson, J. (1972). Comparison of french and united states flying qualities requirements. In *AGARD Conference Proceedings No. 106 on Handling Qualities Criteria*.
- Weinacht, P. and Sturek, W. B. (1996). Computation of the roll characteristics of a finned projectile. *Journal of Spacecraft and Rockets*, 33(6):769–775.
- Weissman, B. (1966). A handling qualities theory for precise flight-path control. Technical report AFFDL-TR-65-198, U.S. Air Force Flight Dynamics Lab, Wright–Patterson AFB, Ohio.
- Wienke, F. (2011). Implementation of a flight dynamics model and inner loop control system for the GOJETT aircraft. [Master’s thesis, Technical University of Munich].
- Williams, W. (2003). UAV handling qualities You must be joking. Technical report, Aerospace Sciences Corporation Pty. Ltd., Elizabeth, Australia.
- Wilson, S. J., Johansen, C. T., and Mravcak, V. (2015). Performance analysis of the atlantis intake system. In *53rd AIAA Aerospace Sciences Meeting*, pages 1–12, Kissimmee, Florida. American Institute of Aeronautics and Astronautics.
- Wolowicz, C. H. and Bowman, J. S. (1979). Similitude requirements and scaling relationships as applied to model testing. Technical report 1435, National Aeronautics and Space Administration, Edwards, California.
- Yamazaki, Y., Mizobata, K., and Higashino, K. (2019). Drag reduction on the basis of the area rule of the small-scale supersonic flight experiment vehicle being developed at muroran institute of technology. *Transactions of the Japan Society for Aeronautical and Space Sciences, Aerospace Technology Japan*, 17(2):127–133.

- Yang, Z., Huang, R., Zhao, Y., and Hu, H. (2017). Design of an active disturbance rejection control for transonic flutter suppression. *Journal of Guidance, Control, and Dynamics*, 40(11):2905–2916.
- Yoshida, K. (2009). Supersonic drag reduction technology in the scaled supersonic experimental airplane project by JAXA. *Progress in Aerospace Sciences*, 45(4-5):124–146.
- Yoshida, K., Yoshikazu, M., and Shimbo, Y. (2002). An experimental study on unmanned scaled supersonic experimental airplane. In *32nd AIAA Fluid Dynamics Conference and Exhibit*, pages 1–12, St. Louis, Missouri. American Institute of Aeronautics and Astronautics.

Appendix A

MUFASA A Aerodynamic Coefficients

Tables A.1 to A.3 provide the aerodynamic coefficients describing the behaviour of the MUFASA A SSUAV aerodynamic profile. The nominal and partial derivatives of each aerodynamic coefficient from Tables A.1 to A.3 are grouped together and presented in Figs. A.1 to A.6 to aid in discontinuity visualization as discussed in Section 6.4.

Table A.1: MUFASA A.2 control surface dependant partial derivative coefficients.

Mach	$C_{Y_{\delta_a}}$	$C_{l_{\delta_a}}$	$C_{n_{\delta_a}}$	$C_{Y_{\delta_r}}$	$C_{l_{\delta_r}}$	$C_{n_{\delta_r}}$	$C_{L_{\delta_e}}$	$C_{D_{\delta_e^2}}$	$C_{m_{\delta_e}}$
0.01	-0.0375	0.1224	0.0292	0.2908	0.0075	-0.2224	0.3084	0.00047	-0.1876
0.10	-0.0376	0.1227	0.0293	0.2658	0.0083	-0.1806	0.3092	0.00047	-0.1883
0.30	-0.0387	0.1248	0.0302	0.2608	0.0082	-0.1729	0.3158	0.00049	-0.1938
0.50	-0.0410	0.1296	0.0323	0.2643	0.0072	-0.1749	0.3310	0.00053	-0.2066
0.70	-0.0456	0.1390	0.0364	0.2752	0.0043	-0.1837	0.3615	0.00062	-0.2333
0.80	-0.0496	0.1472	0.0401	0.2834	0.0006	-0.1893	0.3889	0.00070	-0.2580
0.90	-0.0561	0.1611	0.0461	0.3330	-0.0145	-0.2322	0.4379	0.00085	-0.3041
0.95	-0.0614	0.1738	0.0509	0.3784	0.0114	-0.2897	0.4856	0.00101	-0.3505
1.05	-0.1009	0.2208	0.0984	0.3476	0.0030	-0.2793	0.5378	0.00227	-0.4559
1.10	-0.0987	0.1949	0.0877	0.3349	0.0018	-0.2711	0.3977	0.00211	-0.3400
1.20	-0.0717	0.1800	0.0669	0.3178	0.0090	-0.2578	0.3689	0.00186	-0.3195
1.30	-0.0251	0.1680	0.0236	0.2961	0.0156	-0.2392	0.3161	0.00169	-0.2746
1.50	-0.0121	0.1258	0.0113	0.2461	0.0229	-0.1920	0.2216	0.00129	-0.2021
1.70	-0.0120	0.1019	0.0137	0.2195	0.0262	-0.1659	0.1776	0.00110	-0.1566
1.90	-0.0096	0.0877	0.0115	0.1987	0.0271	-0.1467	0.1529	0.00098	-0.1318
2.10	-0.0030	0.0774	0.0042	0.1800	0.0270	-0.1309	0.1344	0.00087	-0.1161

Table A.2: MUFASA A.2 angular rate dependant partial derivative coefficients.

Mach	C_{Y_P}	C_{l_P}	C_{n_P}	C_{L_Q}	C_{D_Q}	C_{m_Q}	C_{Y_R}	C_{l_R}	C_{n_R}
0.01	0.1198	-0.5597	-0.0467	3.7186	0.0072	-1.7877	1.2264	-0.0071	-0.4329
0.10	0.1202	-0.5604	-0.0468	3.7264	0.0072	-1.7930	1.2276	-0.0073	-0.4335
0.30	0.1236	-0.5661	-0.0483	3.7921	0.0075	-1.8376	1.2383	-0.0081	-0.4382
0.50	0.1311	-0.5784	-0.0514	3.9403	0.0081	-1.9401	1.2619	-0.0101	-0.4489
0.70	0.1442	-0.6001	-0.0569	4.2230	0.0094	-2.1426	1.3048	-0.0136	-0.4689
0.80	0.1541	-0.6163	-0.0609	4.4612	0.0105	-2.3206	1.3393	-0.0162	-0.4855
0.90	0.1674	-0.6388	-0.0662	4.8493	0.0125	-2.6252	1.3914	-0.0195	-0.5118
0.95	0.1758	-0.6536	-0.0693	5.1821	0.0143	-2.9010	1.4320	-0.0203	-0.5335
1.05	0.2537	-0.7359	-0.1048	6.0044	0.0014	-4.0335	1.1167	-0.0914	-0.6368
1.10	0.3089	-0.7745	-0.1204	7.7174	0.0024	-5.0442	1.1731	-0.0820	-0.6757
1.20	0.3240	-0.8641	-0.1367	4.8215	0.0010	-3.3313	1.2558	-0.0687	-0.7480
1.30	0.2044	-0.8928	-0.0787	4.4164	0.0010	-3.1970	1.3022	-0.0098	-0.7960
1.50	0.3039	-0.9131	-0.1166	4.0250	0.0009	-2.9592	1.4691	0.0241	-0.9340
1.70	0.3093	-0.9065	-0.1224	3.4597	0.0009	-2.7606	1.5988	0.0726	-1.0770
1.90	0.2555	-1.1740	0.0096	3.0290	0.0008	-2.5557	1.6628	0.0760	-1.1079
2.10	0.2555	-0.9886	-0.0964	2.6881	0.0006	-2.3262	1.4820	0.0689	-1.0418

Table A.3: MUFASA A.2 nominal, AOA, and sideslip dependant partial derivative coefficients.

Mach	C_{L_0}	C_{D_0}	C_{Y_0}	C_{l_0}	C_{m_0}	C_{n_0}	C_{L_α}	$C_{D_{\alpha^2}}$	C_{m_α}	C_{Y_β}	C_{l_β}	C_{n_β}
0.01	0.0192	0.0245	0	0	-0.0174	0	2.2683	0.0264	-0.4237	-0.3197	0	-0.1605
0.10	0.0219	0.0050	0	0	-0.0202	0	2.2101	0.0191	-0.4508	-0.2336	0	-0.1448
0.30	0.0226	0.0031	0	0	-0.0209	0	2.2430	0.0203	-0.4694	-0.2303	0	-0.1420
0.50	0.0241	0.0028	0	0	-0.0226	0	2.3290	0.0243	-0.5087	-0.2346	0	-0.1409
0.70	0.0280	0.0029	0	0	-0.0268	0	2.4105	0.0291	-0.5388	-0.2413	0	-0.1438
0.80	0.0325	0.0030	0	0	-0.0317	0	2.5204	0.0316	-0.5932	-0.2470	0	-0.1469
0.90	0.0590	0.0066	0	0	-0.0622	0	2.8058	0.0377	-0.8011	-0.2797	0	-0.1279
0.95	0.0221	0.0122	0	0	-0.0400	0	3.1023	0.0421	-1.0570	-0.3379	0	-0.0654
1.05	-0.0007	0.0312	0	0	-0.0186	0	3.0551	0.0470	-1.1071	-0.3181	0	-0.0688
1.10	-0.0061	0.0312	0	0	-0.0109	0	3.0450	0.0473	-1.1513	-0.3242	0	-0.0556
1.20	-0.0074	0.0307	0	0	-0.0055	0	2.8954	0.0451	-1.1334	-0.3321	0	-0.0437
1.30	-0.0059	0.0302	0	0	-0.0047	0	2.7197	0.0422	-1.0586	-0.3391	0	-0.0350
1.50	-0.0042	0.0293	0	0	-0.0043	0	2.3983	0.0381	-0.8890	-0.3231	0	-0.0568
1.70	-0.0054	0.0283	0	0	-0.0016	0	2.1459	0.0352	-0.7490	-0.3028	0	-0.0904
1.90	-0.0067	0.0270	0	0	0.0009	0	1.9464	0.0327	-0.6429	-0.2916	0	-0.1158
2.10	-0.0071	0.0257	0	0	0.0022	0	1.7798	0.0304	-0.5566	-0.2858	0	-0.1351

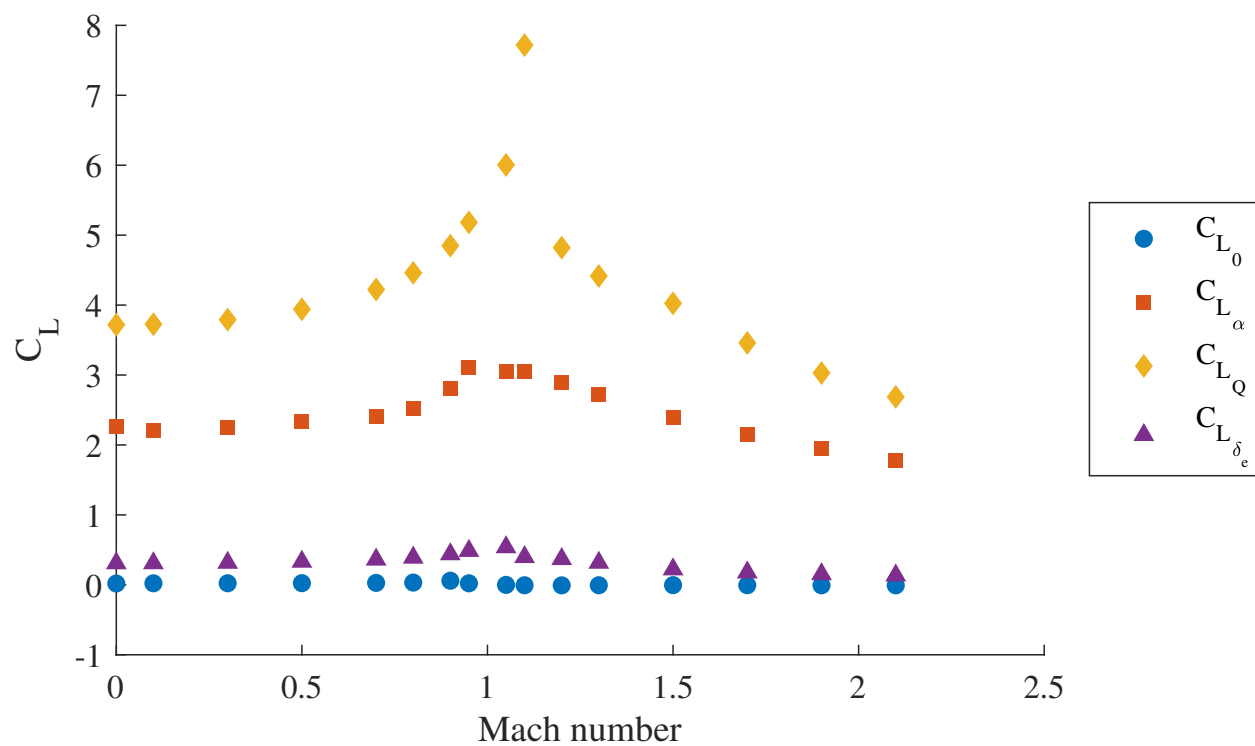


Figure A.1: MUFASA lift aerodynamic coefficients.

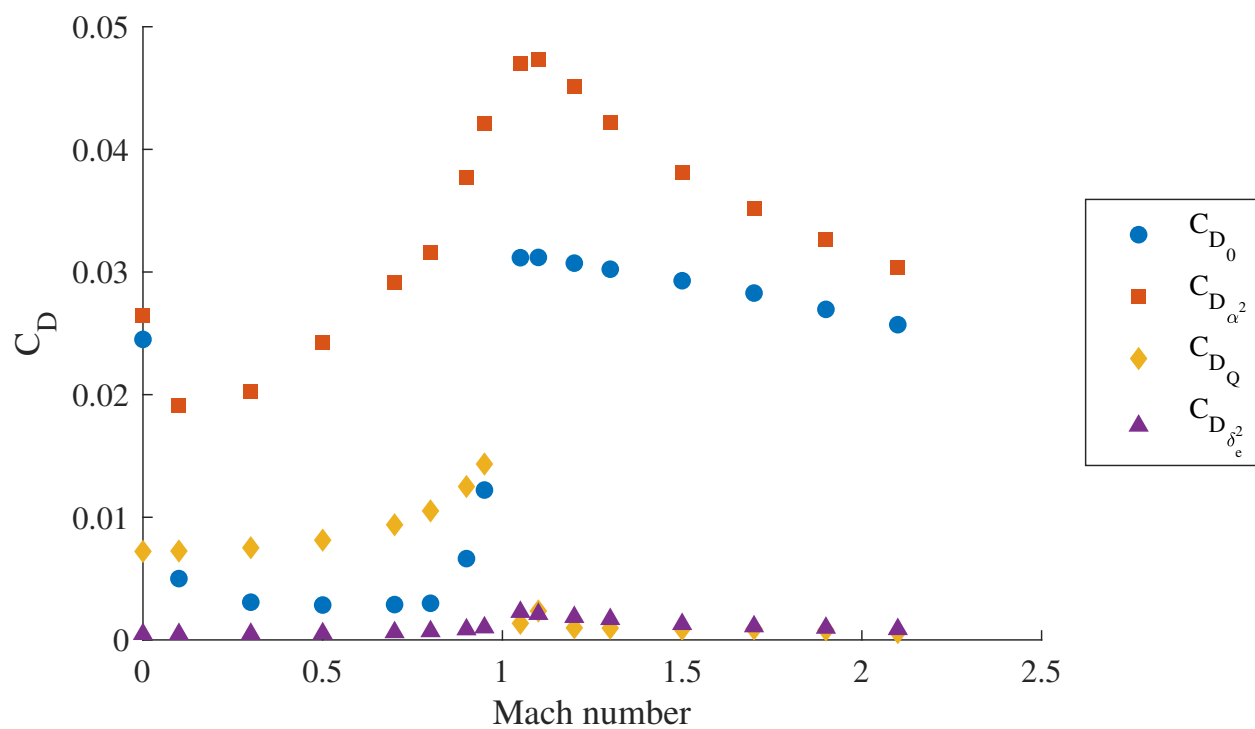


Figure A.2: MUFASA drag aerodynamic coefficients.

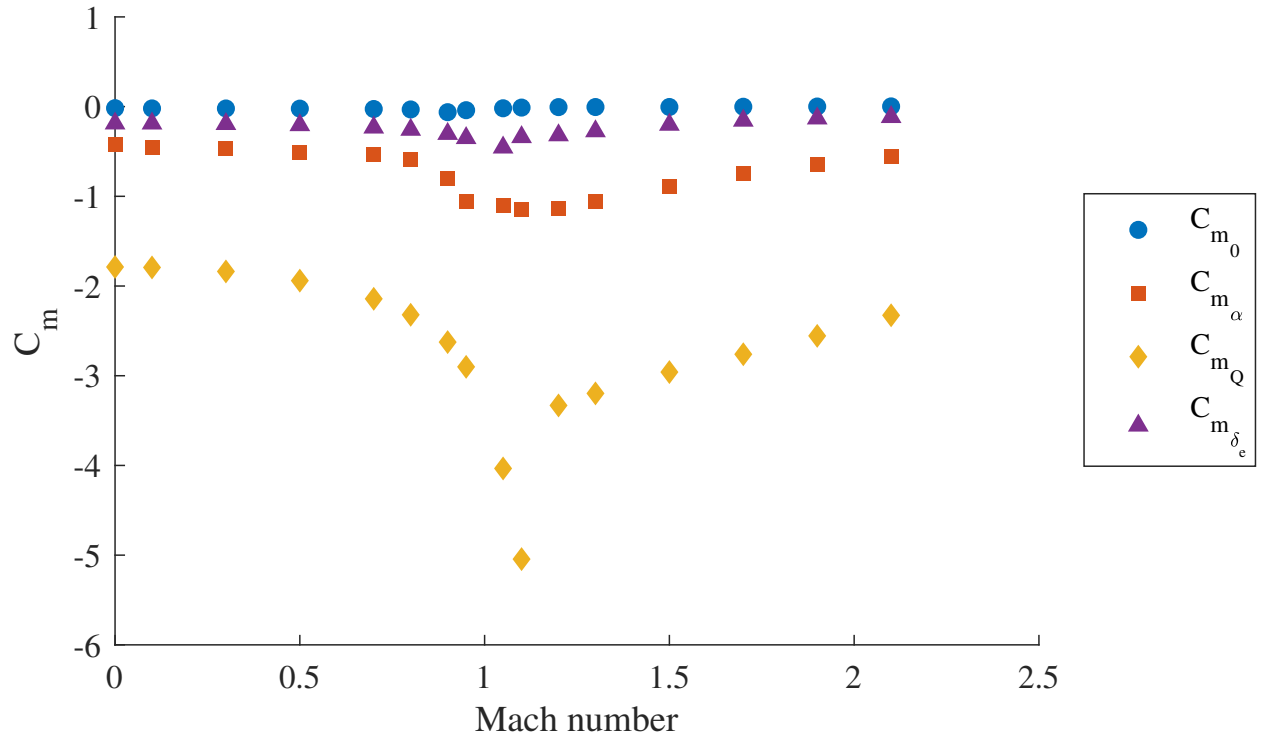


Figure A.3: MUFASA pitch aerodynamic coefficients.

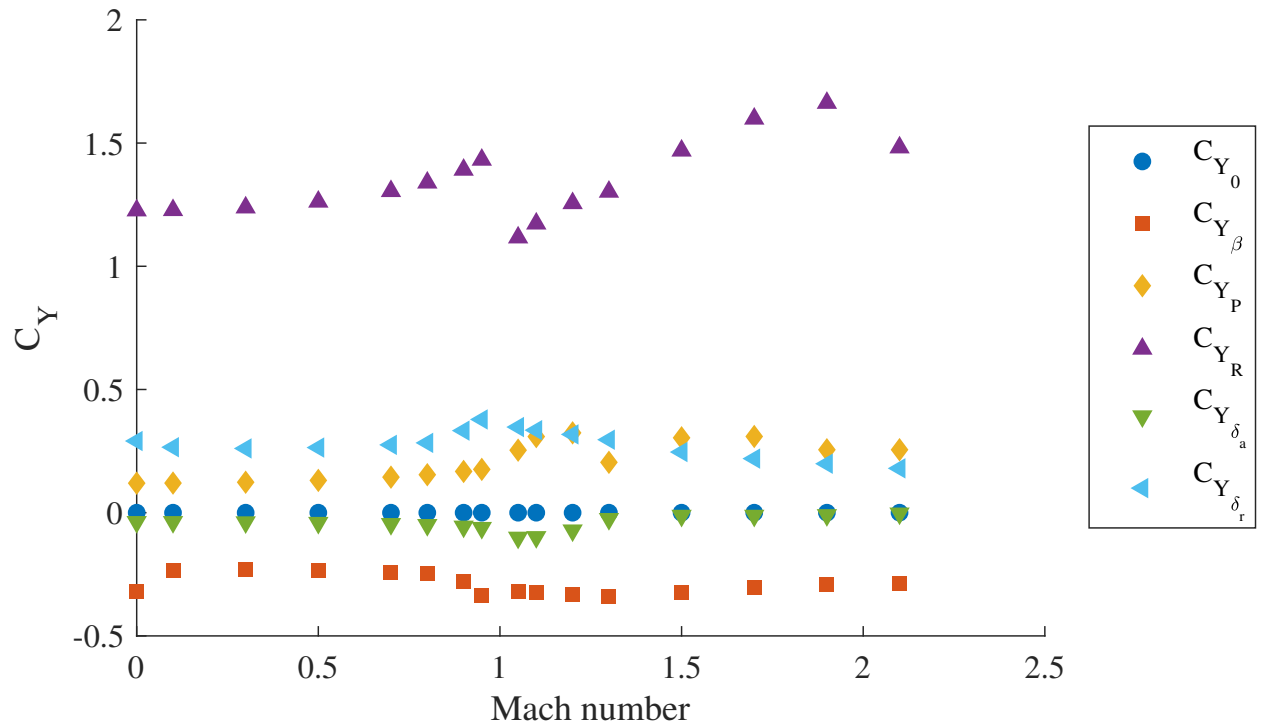


Figure A.4: MUFASA sideforce aerodynamic coefficients.

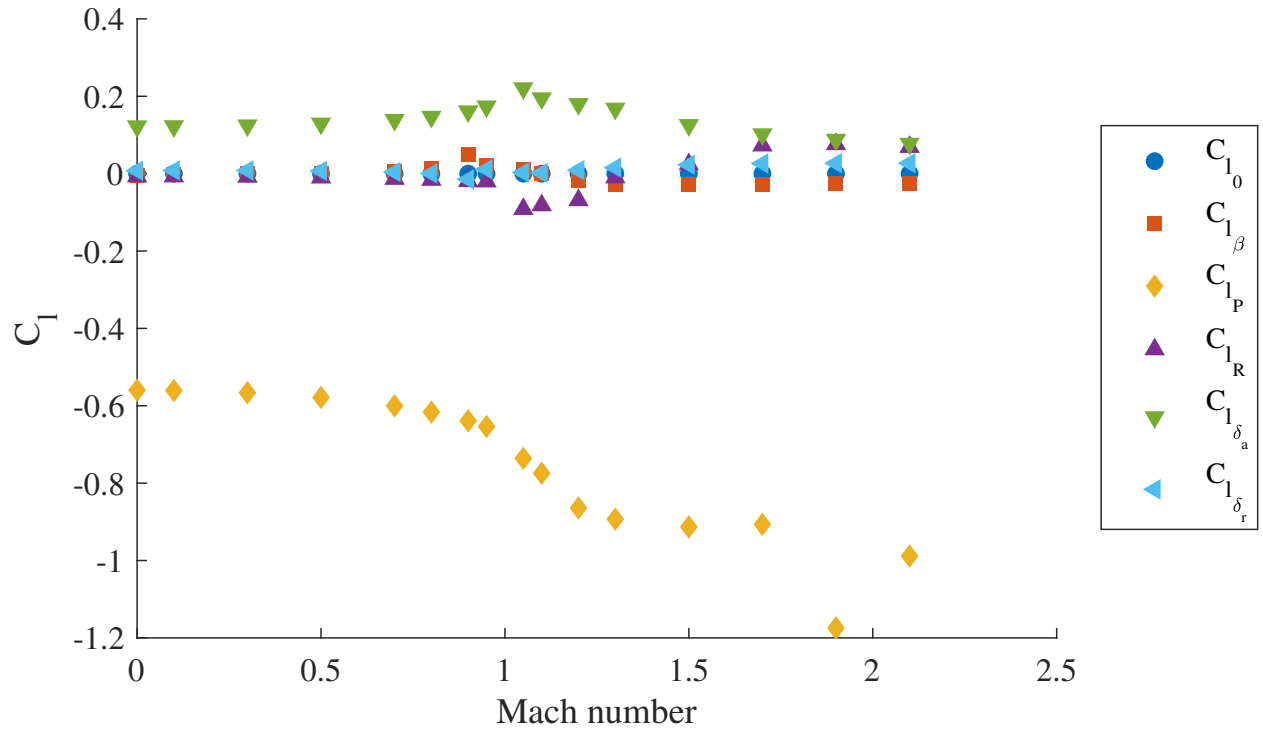


Figure A.5: MUFASA roll aerodynamic coefficients.

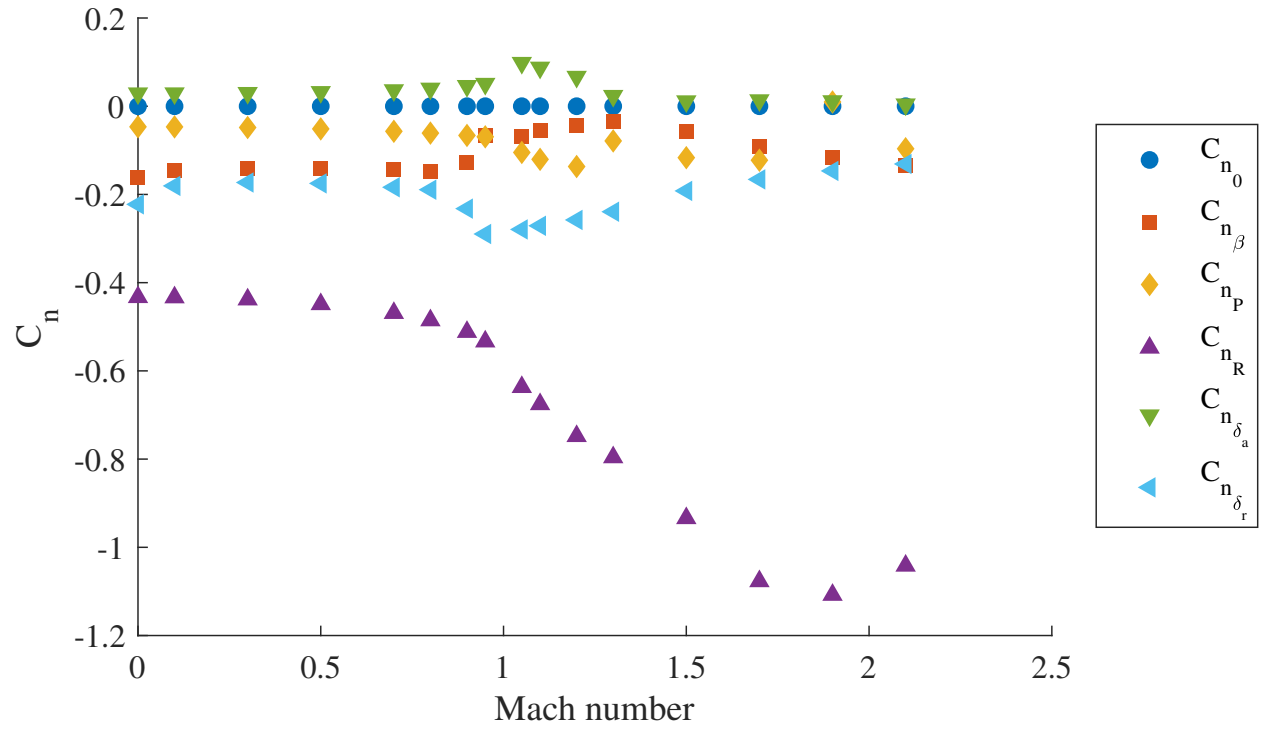


Figure A.6: MUFASA yaw aerodynamic coefficients.

Appendix B

Trance Constants

Information provided by N. Herbrich (personal communication, February 9, 2022) was used to inform and approximate the Trance parameters presented in Table B.1. Trance’s actuator characteristics were assumed similar to MUFASA’s (Table 6.3) but for the motor constant k_1 which was set to $226\left(\frac{\text{m}}{\text{s}}\right)^2$.

Table B.1: Trance modelled characteristics.

Parameter	Trance
Length (m)	1.03
Mean Aerodynamic Chord (m)	0.817
Span (m)	1.04
Mass (kg)	7.5
I_{xx} (kg m ²)	0.238
I_{yy} (kg m ²)	0.612
I_{zz} (kg m ²)	0.842
I_{xz} (kg m ²)	0.005
Planform Area (m ²)	0.65
Wetted Area (m ²)	1.506
r_{CG}^T (m)	$\begin{bmatrix} 0.900 & 0 & 0 \end{bmatrix}$
r_{ACC}^T (m)	$\begin{bmatrix} 0.861 & 0 & 0 \end{bmatrix}$
r_{EC}^T (m)	$\begin{bmatrix} 1.200 & 0 & 0 \end{bmatrix}$

Tables B.2 to Table B.5 provide the aerodynamic coefficients describing the Trance high-speed UAV. All aerodynamic coefficients were obtained via the procedure detailed in Sec-

tion 4.3.3. An aerodynamic model was generated using information provided by N. Herbrich (personal communication, February 9, 2022) and scaling of publicly available images of the aircraft.

Table B.2: Trance control surface dependant partial derivative coefficients.

Mach	$C_{Y_{\delta_a}}$	$C_{l_{\delta_a}}$	$C_{n_{\delta_a}}$	$C_{Y_{\delta_r}}$	$C_{l_{\delta_r}}$	$C_{n_{\delta_r}}$	$C_{L_{\delta_e}}$	$C_{D_{\delta_e^2}}$	$C_{m_{\delta_e}}$
0.10	-0.0103	0.0845	0.0039	0.1374	-0.0190	-0.0599	0.3298	0.000479	-0.0985
0.30	-0.0108	0.0864	0.0041	0.1410	-0.0201	-0.0617	0.3386	0.000501	-0.1028
0.50	-0.0121	0.0908	0.0046	0.1498	-0.0225	-0.0661	0.3597	0.000557	-0.1133
0.70	-0.0150	0.1005	0.0059	0.1689	-0.0278	-0.0761	0.4079	0.000693	-0.1387

Table B.3: Trance angular rate dependant partial derivative coefficients.

Mach	C_{Y_P}	C_{l_P}	C_{n_P}	C_{L_Q}	C_{D_Q}	C_{m_Q}	C_{Y_R}	C_{l_R}	C_{n_R}
0.10	0.011301	-0.2530	-0.0024	1.4442	0.0017	-0.4245	0.3288	-0.0525	-0.0836
0.30	0.012781	-0.2555	-0.0028	1.4770	0.0018	-0.4364	0.3351	-0.0546	-0.0854
0.50	0.016192	-0.2605	-0.0037	1.5534	0.0020	-0.4648	0.3493	-0.0595	-0.0897
0.70	0.022762	-0.2679	-0.0055	1.7123	0.0024	-0.5270	0.3755	-0.0685	-0.0977

Table B.4: Trance nominal partial derivative coefficients.

Mach	C_{L_0}	C_{D_0}	C_{Y_0}	C_{l_0}	C_{m_0}	C_{n_0}
0.10	0.0081	0.0007	0	0	-0.0032	0
0.30	0.0085	0.0004	0	0	-0.0034	0
0.50	0.0096	0.0004	0	0	-0.0040	0
0.70	0.0117	0.0007	0	0	-0.0051	0

Table B.5: Trance AOA and sideslip dependant partial derivative coefficients.

Mach	C_{L_α}	$C_{D_{\alpha^2}}$	C_{m_α}	C_{Y_β}	C_{l_β}	C_{n_β}
0.10	2.0949	0.0160	-0.0048	-0.2423	0	0.0566
0.30	2.1199	0.0164	-0.0090	-0.2425	0	0.0567
0.50	2.1973	0.0183	-0.0238	-0.2511	0	0.0591
0.70	2.3458	0.0222	-0.0532	-0.2710	0	0.0650